



MAX PLANCK INSTITUTE FOR
BIOLOGY OF AGEING



University of Cologne



Mechanisms of aging-mediated loss of stem cell potency through changes in niche architecture and chromatin accessibility

In a u g u r a l - D i s s e r t a t i o n

zur

Erlangung des Doktorgrades

der Mathematisch-Naturwissenschaftlichen Fakultät

der Universität zu Köln

vorgelegt von

Janis Koester

aus Leverkusen

2020

Berichterstatter: Dr. Sara A. Wickström
Prof. Dr. Mirka Uhlirova
Prüfungsvorsitzender: Prof. Dr. Ulrich Baumann

Tag der mündlichen Prüfung: 10.12.2020

Table of Contents

ABSTRACT	7
ZUSAMMENFASSUNG.....	8
1. INTRODUCTION	9
1.1 AGING.....	9
1.1.1 AGING THEORIES AND FACTORS	9
1.1.1.1 Reactive oxygen and nitrogen species damage and the oxidative stress theory of aging	10
1.1.1.2 Mitochondrial theory of aging	11
1.1.1.3 Senescence.....	11
1.1.1.4 Telomere length.....	12
1.1.1.5 Nutrient sensing and metabolism	12
1.1.1.6 Protein homeostasis	14
1.1.1.7 Genomic Instability	15
1.1.2 STEM CELL THEORY OF AGING	16
1.1.3 AGING AND THE STEM CELL NICHE	17
1.2 CHROMATIN ARCHITECTURE AND EPIGENETIC REGULATION OF GENE EXPRESSION	19
1.2.1 CHROMATIN.....	19
1.2.2 THE HISTONE CODE	20
1.2.3 PROMOTERS, ENHANCERS AND REGULATION OF TRANSCRIPTION BY RNA POLYMERASE II	22
1.2.4 BIVALENCY MAINTAINS GENES “READY TO BE TRANSCRIBED”	23
1.2.5 AGING AND EPIGENETICS	25
1.3 MECHANOTRANSDUCTION AND ITS ROLE IN EPIGENETIC - AND STEM CELL -REGULATION	26
1.4 MAMMALIAN SKIN.....	29
1.4.1 HAIR FOLLICLE MORPHOGENESIS AND CYCLING	30
1.4.2 HAIR FOLLICLE STEM CELLS	32
1.4.3 SIGNALING DURING HF CYCLE.....	34
1.4.4 THE EXTRACELLULAR MATRIX.....	36
1.4.5 ECM STRUCTURES IN THE DERMIS	38
1.4.6 THE SKIN BASEMENT MEMBRANE	39
1.4.7 AGING IN THE SKIN	39
2 AIM OF THE THESIS.....	42
3 MATERIALS AND METHODS.....	43
3.1 CHEMICALS AND REAGENTS.....	43
3.2 MICE	43
3.3 ISOLATION OF PRIMARY EPIDERMAL CELLS	43
3.4 HFSC ORGANOIDs AND HYDROGELS.....	44
3.4.1 3C HFSC ORGANOIDs.....	44
3.4.2 COLLAGEN HYDROGELS.....	44
3.5 siRNA KNOCKDOWN AND COLONY FORMING ASSAY	45
3.6 CHEMICAL TREATMENTS	46
3.7 DEPILATION AND EDU INJECTIONS	46
3.8 FLOW CYTOMETRY	46
3.9 IMMUNOFLUORESCENCE AND CONFOCAL MICROSCOPY	48

3.9.1	PARAFFIN SECTIONS.....	48
3.9.2	CRYO-SECTIONS	49
3.9.3	HYDROGELS.....	51
3.9.4	EDU STAINING	51
3.9.5	H&E STAINING	52
3.9.6	CONFOCAL MICROSCOPY	52
3.9.7	IMAGE ANALYSES.....	53
3.10	ATOMIC FORCE MICROSCOPY.....	53
3.10.1	ATOMIC FORCE INDENTATION SPECTROSCOPY OF HYDROGELS	53
3.10.2	ATOMIC FORCE INDENTATION SPECTROSCOPY OF HAIR FOLLICLE BASEMENT MEMBRANES	54
3.11	RNA ISOLATION	54
3.12	RNA SEQUENCING AND ANALYSIS.....	55
3.12.1	RNA-SEQ LIBRARY CONSTRUCTION	55
3.12.2	BIOINFORMATIC ANALYSIS	55
3.13	ATAC SEQUENCING AND ANALYSIS	56
3.13.1	ATAC-LIBRARY CONSTRUCTION	56
3.13.2	BIOINFORMATIC ANALYSIS	57
3.14	qPCR.....	57
3.15	NASCENT RNA ANALYSIS.....	59
3.16	CHROMATIN IMMUNOPRECIPITATION.....	60
3.17	MASS SPECTROMETRY.....	63
3.17.1	PROTEIN AND PEPTIDE SAMPLE PREPARATION.....	63
3.17.2	TMT LABELING, MASS SPECTROMETRY AND ANALYSIS.....	63
3.18	SKIN DECELLULARIZATION	64
3.19	STATISTICS AND REPRODUCIBILITY	65
3.20	DATA AVAILABILITY	65
4	<u>RESULTS</u>	<u>66</u>
4.1	AGEING INDUCES HFSC EXHAUSTION	66
4.2	MINOR DIFFERENCES IN THE TRANSCRIPTOMES OF YOUNG AND AGED HFSCs	68
4.3	ATAC-SEQ REVEALS REDUCED CHROMATIN ACCESSIBILITY IN AHFSCs	70
4.4	MAJORITY OF DIFFERENTIAL INTERGENIC PEAKS ARE MOST LIKELY PRIMED ENHANCERS.....	72
4.5	CPG ENRICHED PROMOTERS ARE LESS ACCESSIBLE IN AHFSCs	75
4.6	AGE-INDUCED DECREASED CHROMATIN ACCESSIBILITY SPECIFICALLY AT BIVALENT PROMOTERS.....	78
4.7	AGING LEADS TO COMPROMISED ACTIVATION OF POISED GENES AND LOSS OF SC POTENTIAL.....	80
4.8	SYNTHETIC NICHE RESTORES STEM CELL POTENTIAL OF AHFSCs	82
4.9	MASS SPECTROMETRY ANALYSIS OF AGED SKIN REVEALS CHANGES IN ECM COMPOSITION	83
4.10	HFSC NICHE IS STIFFER IN AGED MICE	85
4.11	ALTERED BM COMPOSITION, MECHANICS, OR BOTH INFLUENCES HFSC POTENCY.....	86
4.12	ACTIVATION OF THE POISED SC SELF-RENEWAL AND DIFFERENTIATION GENES IS ATTENUATED IN STIFF HYDROGELS	87
4.13	BM STIFFENING INDUCED HFSC LOSS CAN BE RECAPITULATED <i>IN VIVO</i>	88
4.14	NICHE STIFFENING TRIGGERS MECHANICAL STRESS.....	90
4.15	GLOBAL TRANSCRIPTION IS REDUCED IN HFSCs OF AGED- AND TNX-DEFICIENT-MICE	92
4.16	REDUCTION OF GLOBAL TRANSCRIPTION LEADS TO INCREASED H3K27ME3 OCCUPANCY AT POISED GENES..	93
5	<u>DISCUSSION</u>	<u>96</u>
5.1	AGE-INDUCED HFSC EXHAUSTION IS ASSOCIATED WITH DECREASED CHROMATIN ACCESSIBILITY	97
5.2	DECREASED CHROMATIN ACCESSIBILITY SPECIFICALLY AT BIVALENT PROMOTERS.....	99

5.3	AGING LEADS TO NICHE-DEPENDENT COMPROMISED ACTIVATION OF POISED GENES AND LOSS OF SC POTENTIAL	100
5.4	WIDESPREAD BIOCHEMICAL ALTERATIONS IN THE EXTRACELLULAR MATRIX INDUCE SC NICHE STIFFENING TO CONTROL SC POTENTIAL	102
5.5	MECHANICAL STRESS SUPPRESSES TRANSCRIPTION TO SILENCE BIVALENT PROMOTERS.....	104
	REFERENCES	108
	ABBREVIATIONS	128
	ACKNOWLEDGEMENTS.....	131
	PUBLICATION	133
	ERKLÄRUNG	134
	LEBENS LAUF	135

Abstract

All multicellular organisms undergo a decline in tissue and organ function as they age. Loss in stem cell number or activity over time is one possible explanation for this decline. However, little is known about mechanisms leading to stem cell exhaustion in aged tissues. This study reveals a mechanism explaining stem cell exhaustion in the hair follicle. Genome-wide analyses revealed that aged hair follicle stem cells displayed widespread reduction of chromatin accessibility, specifically at crucial self-renewal and differentiation genes that were characterized by bivalent promoters occupied by both active and repressive chromatin marks. Aged hair follicle stem cells showed reduced self-renewing capacity and attenuated ability to activate the expression of these bivalent genes upon regeneration. These functional defects were niche-dependent as transplantation of aged hair follicle stem cells into synthetic niches restored stem cell functions and transcription of poised genes. Mechanistically, the old hair follicle stem cell niche displayed widespread alterations in extracellular matrix composition and mechanics, resulting in mechanical stress and concomitant transcriptional repression, shifting these bivalent promoters to a silenced state. Tuning tissue mechanics *in vivo* and *in vitro* recapitulated age-related stem cell changes implicating niche mechanics as a central regulator of chromatin state, which, when altered, leads to age-dependent stem cell exhaustion.

Zusammenfassung

Alle mehrzelligen Organismen erleiden mit zunehmendem Alter einen Rückgang der Gewebe- und Organfunktionen. Eine mögliche Erklärung für diesen Rückgang ist der Verlust der Stammzellenzahl oder -aktivität im Laufe der Zeit. Über die Mechanismen, die zur Erschöpfung der Stammzellen in gealterten Geweben führen, ist jedoch wenig bekannt. Diese Studie enthüllt einen Mechanismus, der die Erschöpfung der Stammzellen im Haarfollikel erklärt. Genomweite Analysen ergaben, dass gealterte Haarfollikel-Stammzellen eine weit verbreitete Reduktion der Chromatinzugänglichkeit zeigten, insbesondere bei wichtigen Selbsterneuerungs- und Differenzierungsgenen. Diese waren durch bivalente Promotoren gekennzeichnet, die sowohl aktive als auch repressive Chromatinmarken haben. Gealterte Haarfollikel-Stammzellen zeigten bei der Regeneration eine verminderte Selbsterneuerung und eine abgeschwächte Expression der bivalenten Gene. Diese funktionellen Defekte waren nischenabhängig, da durch die Transplantation gealterter Haarfollikel-Stammzellen in synthetische Nischen die Stammzellfunktionen und die Transkription der bivalenten Gene wiederhergestellt wurden. Mechanistisch gesehen zeigte die alte Haarfollikel-Stammzellnische Veränderungen in der Zusammensetzung und Mechanik der extrazellulären Matrix, was zu mechanischem Stress und damit einhergehender Unterdrückung der Transkription führte und die bivalenten Promotoren in einen stillgelegten Zustand versetzte. Veränderung der Gewebemechanik, *in vivo* und *in vitro*, rekapitulierte altersbedingte Stammzellveränderungen. Wir zeigen somit, dass die Mechanik der Stammzellennische ein zentraler Regulator des Chromatinzustands ist, der, wenn er verändert wird, zur Stammzellerschöpfung führt.

1. Introduction

Aging is an unavoidable outcome of life characterized by a progressive decline in tissue and organ function in addition to an increased mortality risk [1]. It is also the primary risk factor for major human pathologies, including cancer, diabetes, cardiovascular disorders, and neurodegenerative diseases. The process of aging has fascinated, attracted curiosity and excited imagination throughout the history of humankind. Although it is a very familiar, it is one of the least well-understood aspect of human biology. The next sections will unroll in more detail some factors that underlie and associate with aging, mainly focusing on epigenetics, stem cell exhaustion, and the niche, before talking about the model system used in this thesis: the hair follicle stem cells.

1.1 Aging

30 years ago, a new era in aging research was initiated by the isolation of the first long-lived strains in *Caenorhabditis elegans* [2]. Although a lot of progress has been made, the complexity of aging and its causes remain a significant challenge for human kind. Aging has been linked, at the molecular level, with DNA damage, epigenetic alterations, telomere shortening, protein aggregation, and accumulation of aberrant mitochondria and lysosomes. At the cellular and organismal level, aging includes cellular senescence, deregulated nutrient sensing, chronic low-grade inflammation, and stem cell exhaustion [3-5].

1.1.1 Aging theories and factors

In recent decades, aging research entered the realm of molecular and cellular biology, and many factors have been identified to contribute to this process (Fig. 1).

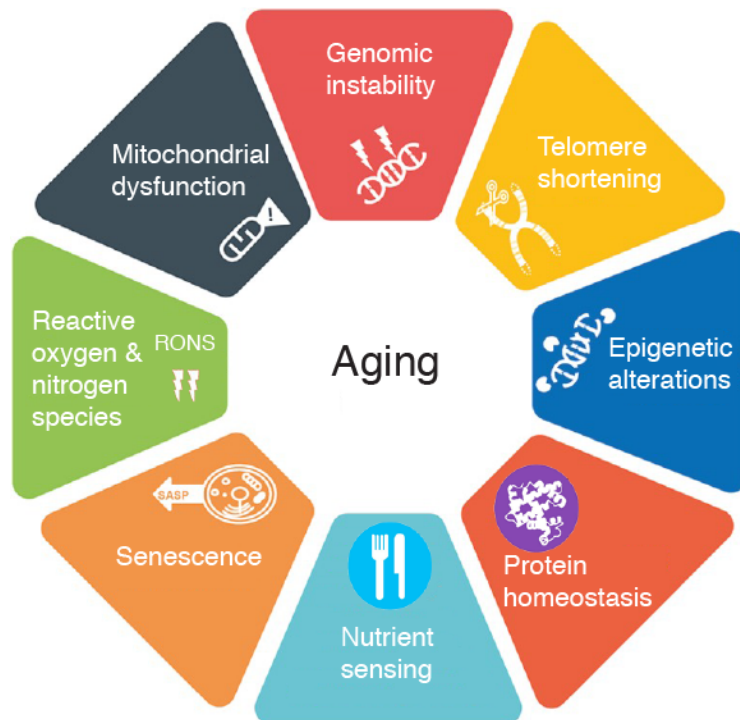


Fig. 1. Factors involved in aging

This diagram highlights multiple factors involved in aging: Genomic instability, Telomere shortening, Epigenetic alterations, Senescence, Mitochondrial dysfunction, Reactive oxygen and nitrogen species, Nutrient sensing, Protein homeostasis. Adapted from [3, 6]

1.1.1.1 Reactive oxygen and nitrogen species damage and the oxidative stress theory of aging

With age, damage to macromolecules (lipids, DNA, and proteins) accumulates and is associated with loss of functionality. A prime candidate that causes this damage is the accumulation of oxidative stress by reactive oxygen and nitrogen species (RONS) [7]. However, the exact mechanisms of oxidative stress-induced aging are still unclear. One proposed probability is that increased RONS levels lead to cellular senescence, a physiological mechanism described in more detail below (s. 1.1.1.3) [8]. Interestingly, although RONS in high doses have the potential to damage the majority of cellular macromolecules, balanced RONS signaling may contribute to longevity by initiating an adaptive response [9]. An extension of this theory is the oxidation-inflammatory theory of aging. This theory proposes that chronic oxidative stress disturbs regulatory systems, such as the nervous, endocrine, and immune systems. Immune system

activation induces an inflammatory state that creates a vicious circle in which chronic oxidative stress and inflammation feed each other, and consequently, increases the age-related morbidity and mortality [10].

1.1.1.2 Mitochondrial theory of aging

Several reports have shown that mitochondrial function has a profound impact on the aging process and mitochondrial dysfunction can accelerate aging in mammals [11, 12]. Accumulating evidence from the last three decades shows that mitochondrial DNA (mtDNA) mutations, like point mutations or large-scale deletions, increase with age in humans and mammalian model organisms. The original mitochondrial theory of aging concentrates on mitochondria as the main producer of reactive oxygen species (ROS), and oxidative damage as a source for mtDNA mutations [13]. However, new data suggests that most mammalian mtDNA mutations originate as replication errors made by the mtDNA polymerase γ [14, 15]. These mutations may polyclonally expand and cause respiratory chain dysfunction in different tissues [16] [17]. Mice deficient in mitochondrial DNA polymerase γ display several aspects of premature aging and a reduced lifespan in addition to an increase of point mutations and mtDNA linear deletions [11, 12, 17]. Furthermore, mtDNA mutations have been linked with stem cell dysfunction, contributing to the age-associated decrease in homeostasis and regenerative potential. [18, 19]. Therefore, evidence suggests mtDNA mutations might be implicated in the aging process.

1.1.1.3 Senescence

Cellular senescence is a permanent exit from the cell cycle, triggered by multiple factors such as DNA damage, oncogenic mutations, oxidative stress. Thus, senescent cells cannot contribute to tissue homeostasis because of their lack of replicative capacity [20, 21]. However, they remain metabolically active and obtain an irreversible senescence-associated secretory phenotype (SASP). This involves secretion of soluble factors (interleukins, chemokines, and growth factors), degradative enzymes like matrix metalloproteases (MMPs), and insoluble proteins/extracellular matrix (ECM) components [8, 22, 23]. Cellular senescence can be caused by multiple factors,

including, short telomeres, overexpression of oncogenes, and DNA damage [24]. Mice that were engineered to eliminate senescent cells showed rejuvenation or delayed aging, thereby demonstrating an essential role of cellular senescence in aging [25, 26].

1.1.1.4 Telomere length

Telomeres are nucleoprotein caps flanking DNA. They are shortened by cell division and oxidative stress and are lengthened by the enzyme telomerase and DNA exchange during mitosis. When telomeres reach a critical length, cells become senescent [27, 28]. Telomere shortening also explains the limited proliferative capacity of some types of in-vitro-cultured cells, the so-called Hayflick limit [29]. Notably, telomere shortening can also be observed during normal aging both in humans and in mice [30]. Mice with shortened or lengthened telomeres show decreased or increased lifespans, respectively [31, 32], and activating telomerase can revert aging phenotypes [33, 34]. Furthermore, meta-analyses in humans support the existence of a strong relationship between short telomeres and mortality risk [35]. However, other large-scale epidemiological studies showed that telomere length has only a weak negative association with other markers of biological age and life expectancy [28, 36, 37]. These findings indicate that telomere length might be one of several factors of aging and might function independently of others.

1.1.1.5 Nutrient sensing and metabolism

Metabolic homeostasis is a major constituent of cellular and organismal homeostasis. Metabolic homeostasis involves the coordinated response of distinct cells and tissues [38]. Cell signaling pathways that sense the availability of nutrients and the energy status of the cells communicate coordinately with hormonal and growth factor signaling pathways to regulate whole-body metabolic homeostasis. The four associated key protein groups are Insulin/Insulin-like growth factor (IGF-1), mechanistic Target Of Rapamycin (mTOR), sirtuins, and AMP-activated kinase (AMPK) [38]. During aging, metabolic homeostasis declines, which likely contributes to the general aging of the whole organism [39]. Several interventions, genetic and pharmacological, affecting the activity of metabolic pathways also affect the rate of aging. Indeed, the Insulin/IGF-1

Signalling (IIS) pathway and the mTOR pathway are among the most extensively studied pathways shown to regulate life- and health span in several organisms [40, 41]. Similar to insulin, IGF-1 takes part in glucose sensing [42] IGF-1 inhibits the secretion of other growth hormones by binding to its cell surface receptor [42]. mTOR is composed of the mTORC1 and mTORC2 protein complexes and senses amino acids and it is related with nutrient abundance [43]. mTOR and IIS are both part of the anabolic metabolism. Calorie restriction, the most potent environmental intervention shown to extend lifespan and healthspan in many species, is accompanied by changes in the insulin/IGF-1 circulating levels, while inhibition of the mTOR pathway has mutual and distinct effects with calorie restriction [44, 45]. The Sirtuin protein family acts as nicotinamide adenine dinucleotide (NAD⁺) dependent histone deacetylases [46, 47]. Sirtuins sense low energy levels by detecting the simultaneously increase of NAD⁺ and help to control catabolic metabolism. In addition to histones, they also deacetylate transcription factors and other cellular proteins affecting gene expression activity. Sirtuins mediate various beneficial effects on metabolic tissues, e.g., visceral fat and liver. They are involved in reduced glycolysis and increased fatty acid oxidation in liver and muscle, reduced hepatic lipogenesis, adipose tissue browning, and fat mobilization [46]. Various lines of evidence support the notion that sirtuins mediate the effects of calorie restriction to a large extent [48]. The lifespan-extending of worms, flies, and mice through sirtuin activation is still uncertain, but the improvements in healthspan seem to be robust [47]. AMPK senses adenosine monophosphate (AMP) and adenosine diphosphate (ADP) [49]. These molecules are present in higher amounts when nutrients are low. Therefore, AMPK is a sensor of fasted or calorie-restricted states and catabolism. Similar to sirtuins, higher activity of AMPK seems to have longevity-promoting effects [49]. AMPK inhibits mTORC1 directly, by phosphorylating Raptor, which functions as a scaffold for recruiting mTORC1 substrates, and indirectly, by activating TSC2, which in turn regulates further downstream kinases [50-52]. At the same time, by reprogramming metabolism away from anabolic pathways, AMPK relieves the pressure on mitochondrial respiration and reduces the chances of cellular damage from the generation of reactive oxygen species [53]. Calorie restriction can also increase the activity of AMPK. On the other hand, less AMPK sensitivity due to cellular stress results in oxidative stress, reduced autophagy, metabolic syndrome, more fat disposition, and inflammation [54]. Taken

together, the main cell signaling pathways in metabolic regulation also seem to play a dominant role in the modulation of the rate of aging. From the current point of research, finetuning these pathways might be the best option to expand life- and healthspan in humans as seen in model organisms already.

1.1.1.6 Protein homeostasis

Most proteins fold into well-defined 3D structures and remain folded throughout their lifetime to perform their biological functions. Moreover, the abundance of each of the thousands of different proteins in a mammalian cell must be carefully controlled [55]. A complex protein homeostasis network, comprising molecular chaperones and proteolytic machinery and their regulators, operates to ensure the maintenance of protein homeostasis [56]. These factors, most prominently the heat-shock family of proteins, coordinate protein synthesis with polypeptide folding, the conservation of protein conformation [57]. Beyond regulation of folding, this network also ensures that misfolded protein species are removed, either by autophagy, lysosome, or by degradation mediated by the proteasome [58]. Together, these mechanisms avoid the accumulation of potentially toxic protein aggregates. Nonetheless, sustaining proteome balance is challenging when facing various external and endogenous stresses that accumulate during aging [59]. These stresses lead to the decline of protein homeostasis network capacity and proteome integrity. The resulting accumulation of misfolded and aggregated proteins affects, in particular, postmitotic cell types such as neurons, which in turn manifests in disease [60, 61]. The age-dependent decline in the ability of cells to maintain a functional proteome is a significant driver of age-related cellular dysfunction and degenerative diseases [62, 63]. During aging, the protein homeostasis network becomes increasingly burdened by increasing loads of misfolded proteins and proteins damaged by oxidative stress, especially in nondividing, long-lived cells such as neurons [64-66]. Interestingly, stem cells seem to be more resistant to age-dependent protein homeostasis network decline than differentiated cells. Human embryonic stem cells exhibit elevated levels of proteasome activity for degrading misfolded proteins, while human pluripotent stem cells have increased capacity to assist protein folding [67, 68]. Furthermore, the asymmetrical division of stem cells might also help to maintain a balanced proteome, with the

differentiating cell inheriting the damaged proteins [69, 70]. These mechanisms may contribute to the maintenance of stem cells throughout the animal lifespan.

1.1.1.7 Genomic Instability

Under physiological conditions, DNA is continuously damaged by both endogenous and environmental factors, including DNA replication errors, spontaneous hydrolytic reactions, and RONS. A highly conserved system of genome maintenance mechanisms provides most of the DNA stability [71]. Genetic lesions resulting from extrinsic or intrinsic damages are highly diverse. They include point mutations, translocations, chromosomal gains and losses, telomere shortening, and gene disruption caused by the integration of viruses or transposons [72]. These forms of DNA alterations may affect crucial genes and transcriptional pathways, and consequently result in dysfunctional cells. If these cells are not eliminated by regulated cell death such as apoptosis or senescence, they may endanger tissue and organismal homeostasis. Therefore, DNA damage may impact the functional competence of stem cells, thus compromising their role in tissue renewal [73, 74]. Extensive data from humans and animal models show increased markers of genome instability with age, thereby establishing the association between DNA damage and aging [72, 75]. Cells have established ways to repair damage, decrease damaging molecules before damage can appear, or to remove cells that have accumulated too much damage. Repair enzymes reverse the damage and return the DNA to its intact state. These repair mechanisms are highly conserved and can be classified into the following pathways: direct reversal, base excision repair, nucleotide excision repair, double-strand break repair, and interstrand crosslink repair. Direct reversal repair tries to correct single-base methylation incidents. Mutations in these enzymes have been linked with increased brain, lung, and bladder cancer risk [76, 77]. Base excision repair fixes single-base lesions, e.g., guanine oxidation. Defects in this process have been linked with neurodegeneration and cancer [78]. Mismatch DNA repair solves misincorporated bases during replication or as part of other DNA repair pathways. It is linked to Lynch syndrome and colon cancer development [79].

Nucleotide excision repair deals with bulky or helix-distorting lesions, e.g., 6–4 photoproducts or cyclopyrimidine dimers, which are often caused by UV irradiation. Patients with defects in nucleotide excision repair suffer from sun sensitivity and increased risk of skin cancer development [80]. Interstrand crosslink repair corrects covalently linked DNA strands, while double-strand break repair deals with breaks in both strands. These repair pathways are also linked to numerous age-related diseases [72]. In total, more than 50 DNA repair disorders have been described with various degrees of overlapping phenotypes with aging [81, 82]. Since most of these syndromes recapitulate only some aspects of aging, their relevance to normal aging remains unsolved. However, DNA repair capacity may decrease with age [83, 84]. If the repair fails and damage accumulates, three outcomes can occur: cells can transform and become cancerous, cells can enter senescence, or die through apoptosis. Aging may also alter these outcomes, e.g., the incidence of cancer increases [85, 86].

1.1.2 Stem cell theory of aging

Tissues undergo continuous cell renewal in a process termed homeostasis. This process depends on the dynamic activity of tissue-resident stem cells. Stem cells can self-renew and differentiate along multiple lineages. These same stem cells are also called into action to regenerate damaged tissue following an injury to repair and prevent tissue overgrowth. They are rare cells located in specialized niches, which contribute to the proper control of stem cell self-renewal and differentiation. As all multicellular organisms undergo a decline in tissue and organ function as they age, the stem cell theory of aging postulates that a loss in stem cell number or activity over time causes this decline [87]. Several stem cell lineages show this decline: Neural progenitors show a decrease in number and impaired proliferative potential with aging and telomere dysfunction [88]. Melanocyte SCs are significantly depleted, possibly due to impaired melanocyte maintenance and melanoblast senescence. In the case of specific mouse models of hair greying, melanocyte SCs accumulate ectopic pigments [89, 90]. Hematopoietic SCs (HSCs) display altered function for mobilization, homing, and lineage choice and are skewed towards a myeloid fate at the cost of lymphoid fate, suggesting a decline of fully functional HSCs with age [91-93]. Muscle SC precursors, called satellite cells, show a markedly impaired tendency to proliferate and to produce

myoblasts necessary for muscle regeneration. This impairment is due to a reduced expression of the notch ligand delta and, therefore, an aberrant differentiation towards a fibrogenic fate, giving rise to fibrotic muscles during aging [94-96]. A decline in stem cell number and function has also been reported in the forebrain and bone [97, 98]. Stem cell exhaustion is also frequently observed in human age-related diseases and rare genetic disorders. As an example, patients with Hutchinson-Gilford progeria syndrome [99], Werner syndrome [100], and Fanconi anemia [101] show premature depletion of mesenchymal stem cells (MSCs). Neural stem cells (NSCs) show defects in neuronal differentiation and DNA repair in patients with Parkinson's disease [102] and xeroderma pigmentosum [103].

The mechanisms underlying stem cell senescence and exhaustion during organismal aging include genomic instability, telomere attrition, epigenetic alterations, cellular senescence, mitochondrial dysfunction, loss of proteostasis, and altered intercellular communication. Although phenotypes and mechanisms vary widely, it appears that all stem cell populations decline in function with age. With a greater understanding of stem cell aging and its reversal, it may one day be possible to rejuvenate tissues and increase human health- and lifespan.

1.1.3 Aging and the stem cell niche

The term “niche” was first introduced in 1978 by Schofield as he described the functionality of hematopoietic cells in a local environment [104]. This local environment, consisting of neighboring cells and ECM, regulates SC behavior, and is essential for their function [105, 106] The niche thus provides soluble, adhesive, and physical signals to stem cells, which are critical for maintaining stem cell functions. Due to the complex composition of niches, they function by integrating a surplus of signals, both local and systemic, to ensure appropriate and coordinated responses of SC to the changing needs of tissues [107, 108]. Thus, aging of the SC environment can, in part, also critically modulate stem cell function. Mammalian spermatogonial stem cells (SSCs), for example, can function for much longer than an average lifetime when transplanted to a young environment [109, 110]. Also, niche deterioration has received much attention as a mechanism of germline stem cell (GSC) aging [111-113]. Senescent niche cells might affect neighboring stem cells by secreting tumor-

promoting mitogens and pro-inflammatory cytokines that, through paracrine signaling, negatively affect SC function [114]. Consistent with this, studies utilizing heterochronic transplantation and parabiosis experiments show that primarily cell-extrinsic mechanisms drive aging in satellite cells [115-117], NSCs [118, 119], and GSCs [109]. Aged niche cells can also fail to send proper signals to stem cells, thereby affecting cell fate choices. For example, increased Fgf2 in the aged satellite cell niche of mouse muscle impairs self-renewal [116]. Inflammation markers also increase in the aging niche, e.g., in HFSCs, and impair stem cell function [120]. Although HSC aging is thought to be mainly cell-intrinsic, recent studies have shown that the aged HSC microenvironment contributes, at least partially, to the skewing of aged HSCs towards a myeloid lineage. This happens through the secretion of increased levels of pro-inflammatory ligands [121, 122]. Other niche factors are also beginning to emerge in the HSC research, confirming the contribution of the aged niche towards altered SC fate [92, 123]. A recent study confirmed the role of the niche in epithelial stem cell aging [124]. A decrease in stemness-maintaining Wnt signaling caused a functional decline of ISC due to the production of Notum, an extracellular Wnt inhibitor, in aged niche cells, the Paneth cells. Another recent study observed the stiffening of the central nervous system microenvironment with age. This mechanical change is sufficient to cause age-related loss of function of oligodendrocyte progenitor cells [125]. Thus, understanding how aging affects the composition and function of stem cell niches and whether niche-targeted therapies could be used to enhance tissue homeostasis and regeneration potential during aging may be an exciting avenue of future research. Since precise transcriptional networks and epigenetic barriers control stem cell function and state, understanding stem cell aging also requires understanding the underlying epigenetic and transcriptional changes.

1.2 Chromatin architecture and epigenetic regulation of gene expression

The cell is often referred to as the basic functional unit of life. Complex multicellular organisms consist of hundreds to billions of cells with diverse functions and phenotypes. Astonishingly, all the instructions to build such various cell types in an organism are stored as heritable information in the genome – a linear polymer of deoxyribonucleotides, the DNA.

1.2.1 Chromatin

DNA resides in the nucleus of the cell and is organized together with histone proteins in a higher-order structure called chromatin. The DNA helix is wrapped in a highly compacted order of 1.7 turns (146 base pairs) around an octamer of histone proteins, also called nucleosome, to fit it, despite a total physical length of 2m (in humans), into a nucleus of an average diameter of 6 μm [126]. The core histones consist of H2A, H2B, H3, and H4, and can be exchanged by variant histones, including H3.3, macroH2A, and H2A.Z. The composition and post-translational modification of nucleosomes reflect distinct functional states [127]. They regulate chromatin accessibility through a variety of mechanisms, such as altering transcription factor (TF) binding through steric hindrance and modulating nucleosome affinity for active chromatin remodelers [128]. The chromatin itself folds into building blocks, known as topologically associating domains (TADs), which often span hundreds of kilobases (500-800 kb) [129]. TADs are the boundary elements or linear units of chromatin that fold into 3D structures. They serve as functional platforms for physical looping interactions between genes and proximal as well as distal regulatory elements, e.g., enhancer-promoter interactions. TADs are enriched with several genomic features such as CTCF (a transcriptional repressor), especially at TADs boundaries.

Heterochromatin is a tightly packed form of DNA, which comes in multiple varieties between the two extremes of constitutive heterochromatin and facultative heterochromatin [130]. Both are responsible for critical genome functions; constitutive heterochromatin is typically situated at pericentromeric and telomeric domains of chromosomes. Constitutive Heterochromatin is also enriched for the histone methylation marks H3K9me2 and H3K9me3. It exhibits a dense organization throughout interphase, enrichment for repetitive DNA sequences, relatively low

transcription levels, and precise replication timing [131]. Facultative heterochromatin is associated with transcriptional regulation of developmental genes and employs different histone marks and readers, e.g., through the Polycomb-family of proteins. While densely arranged within facultative and constitutive heterochromatin, histones are depleted at regulatory loci, including within enhancers, insulators, and transcribed gene bodies [132]. Internucleosomal DNA is often bound by TFs, RNA polymerases, or architectural proteins with linker histones, which facilitate higher-order chromatin organization and regulate access to DNA [133-135]. This landscape of chromatin accessibility broadly reflects regulatory capacity — rather than a static biophysical state — and is a critical determinant of chromatin organization and function. The accessible genome comprises ~2–3% of the total DNA sequence yet captures more than 90% of regions bound by TFs [136]. TFs have a broad range of functional roles, providing dynamic regulation of transcription on short timescales and establishing and maintaining persistent epigenetic canalization of cell types that share a common genome.

1.2.2 The Histone code

Apart from packaging the genome, histone proteins are subject to various chemical modifications that dynamically adjust the readout of the genetic information. Diverse environmental stimuli require a living cell to vigorously adapt to which genetic information is read out and set into operation. Each histone harbors a flexible N-terminal tail protruded from the histone core [137]. The histone tail is important for interactions both inside and outside of nucleosome, and is subjected to a variety of post-translational modifications, including methylation (me), acetylation (ac), ubiquitination (ub), phosphorylation (ph), and SUMOylation (su) [138] (Fig. 2). These modifications have essential roles in the regulation of chromatin structure, and therefore affect gene expression, silencing, and many other DNA processes such as replication, recombination, and DNA repair machinery. The complexity of possible combinations of post-translational modifications of histones and the impact on genomic functions led to the proposal of the histone code hypothesis, emphasizing the important role of epigenetic marks to the genetic code [139, 140]. H3K4 and H3K36 methylation, and H3 and H4 acetylation characterize active genes. These modifications function to

neutralize histone charges and recruit chromatin remodeling proteins that lead to the unraveling of the chromatin structure, allowing access to the basal transcriptional machinery [141]. In contrast, gene silencing results in the recruitment of chromatin modifiers (HDACs, HMTs) and repressive complexes, such as Polycomb proteins [142]. This leads to chromatin condensation (heterochromatin). H3K27 and H3K9 methylation characterize condensed chromatin. Together, the cofactors and regulatory proteins affecting these epigenetic modifications define the chromatin landscape that dictates the expression profile of the cell. A further layer of gene activation and silencing, as well as genome compaction, can be achieved through DNA methylation [142]. Active genes display DNA hypomethylation at gene promoter regions, while gene silencing results in the recruitment of DNA methylation machinery (DNMTs, MBPs), and DNA hypermethylation. Having this multilayered transcriptional control mechanism serves as a system of checks and balances that allows fine-tuning and adaptability of the gene expression profile of the cell.

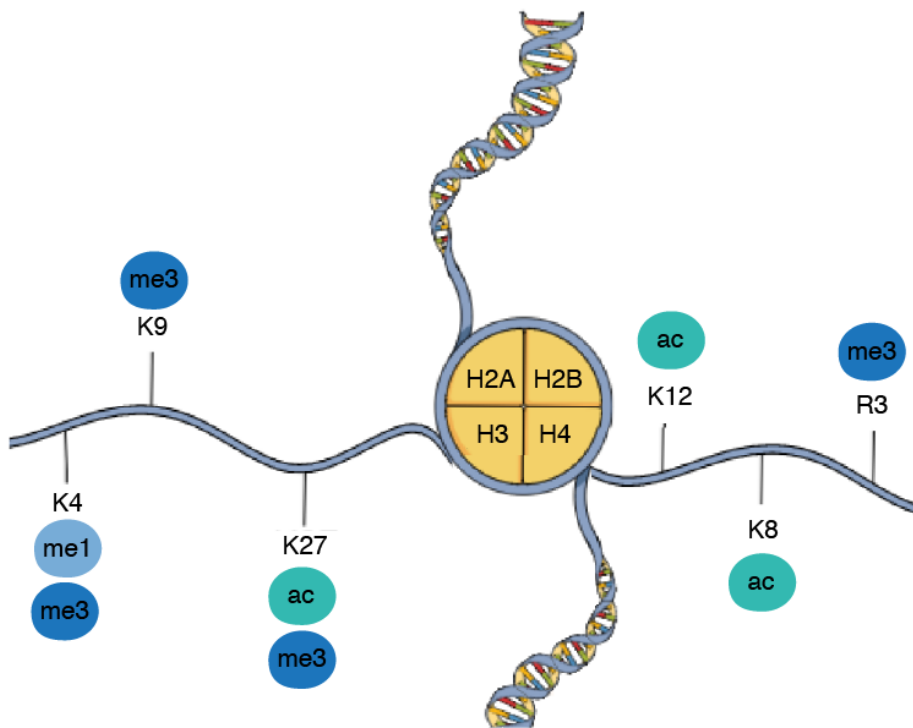


Fig. 2. Nucleosome and the histone code

DNA wound around the histone octamer, forming a nucleosome. Posttranslational modifications of histone tails regulate gene expression. H3K4 methylation, and H3 and H4 acetylation characterize active genes. H3K27 and H3K9 methylation characterize condensed

chromatin. Other lysins can be modified as well. Further modifications are possible, such as ubiquitination, phosphorylation, and SUMOylation. Adapted from [143].

1.2.3 Promoters, enhancers and regulation of transcription by RNA polymerase II

RNA polymerase II (RNAPII) is an enzyme that transcribes all protein-coding and many non-coding genes, while RNAPI and III transcribe genes encoded for transfer RNA, ribosomal RNA, and various small RNAs. RNAPII consists of twelve subunits, of which RPB1 is the largest. RPB1 has a unique carboxyl-terminal domain (CTD), which acts as a binding scaffold for many nuclear factors involved in steps of the transcription process [144, 145]. All the amino acids within the CTD are highly modified by various post translational modifications. CTD phosphorylation recruits factors that regulate chromatin states and RNA processing, integrating transcription with genome architecture and stability [146]. During transcriptional initiation, the CTD becomes phosphorylated at Ser5 (S5p). S5p plays a direct and essential role in recruiting and facilitating the capping enzyme, synthesizing the 5'-cap structure on the nascent RNA. It also contributes to the recruitment of other factors involved in the transition process from initiation to elongation state of RNAPII, early transcription termination, as well as histone modification [146]. Shortly after promoter escape, the level of S5p decreases. Throughout the productive elongation state of RNAPII S2p levels increase. This mark helps in the recruitment of splicing and polyadenylation factors, as well as H3K36 histone methyltransferases, promoting compatible chromatin remodeling for a stable transcription process [146, 147]. Transcription typically initiates at a defined position, the transcription start site (TSS), at the 5' end of a gene, which we refer to as gene start. The TSS is embedded within a core promoter, which is a short sequence encompassing ~50 base-pairs (bp) upstream and ~50 bp downstream of the TSS. Promoter sequences define the direction of transcription and indicate which DNA strand will be transcribed. The core promoter serves as a binding platform for the transcription machinery, which comprises Pol II and its associated general transcription factors [148]. Coordination of chromatin modification, mainly through the control of post-translational modification of histones, also has a vital role in transcription initiation [149, 150]. The recruitment of all of these co-activators and co-repressors of

transcription initiation is controlled by transcription factor binding to cis-acting DNA sequences that can lie within the core promoter or in more remote locations (enhancers and repressors) [151]. Besides binding transcription factors, enhancers recruit transcription cofactors and can increase transcription from a core promoter independent of their relative distance and orientation [152, 153].

1.2.4 Bivalency maintains genes “ready to be transcribed”

Mammalian SCs, in particular embryonic SCs, display a unique epigenetic and transcriptional state termed bivalent or poised state. As with the Histone code, gene promoters and enhancers are decorated in each cell type by precise combinations of histone marks according to their current transcriptional status. H3K4me3 is typically associated with activation, while H3K27me3 is associated with repression. Simultaneous occupancy of these histone methylation marks characterizes promoter bivalency [154] (Fig. 3). While the associated genes are repressed, bivalent promoters are pre-loaded with poised RNAPII [155, 156]. The function of these bivalent domains is to maintain the genomic loci in a state that is both rapidly responsive to developmental cues and, at the same time, refractory to subthreshold noise [154, 157]. Similarly to bivalent promoters, poised enhancers are characterized by the presence of both H3K4me1, typically associated with active enhancers, and H3K27me3, and likely play a key role during differentiation. Bivalency is a chromatin property initially thought to be tightly linked to the pluripotent state of stem cells in mammals. However, recent findings suggest that they represent a universal mechanism for tissue-specific gene regulation [158]. Bivalent domains strongly correlate with abundance of CpG islands [159]. Regions of DNA where a cytosine nucleotide is followed by a guanine nucleotide are called CpG sites. CpG islands are genomic regions with a high frequency of these CpG sites. CpG islands thus appear to play a significant role in the establishment of bivalent domains. Unmethylated CpG islands are critical factors in controlling H3K4me3 levels through the recruitment of Trithorax-group proteins and TET proteins. On the other hand, CpG islands likewise play an essential role in establishing and maintaining H3K27me3 at bivalent domains, through polycomb group proteins. One possible concept implies that productive transcription, through the proper assembly of TFs, coactivators, and the splicing machinery, prevents stable PRC2

recruitment or binding around the TSS. On the other hand, either the absence of transcription or transcription at levels below a certain threshold is sufficient to allow PRC2 recruitment to promoter CpG islands [154, 160]. Higher levels of transcription appear to displace PRC2 and thus H3K27me3, whereas low levels permit default recruitment of PRC2 to CpG islands. Removal of H3K27me3 is expected to render bivalent promoters more amenable for transcription, in part due to the reduced compaction. In contrast, when PRCs establish a stronger foothold around promoters, H3K27me3 acts as a stronger barrier for activation, forging repression. Interestingly, promoters that lose both H3K4me3 and H3K27me3 have a high probability of becoming DNA-hypermethylated [161].

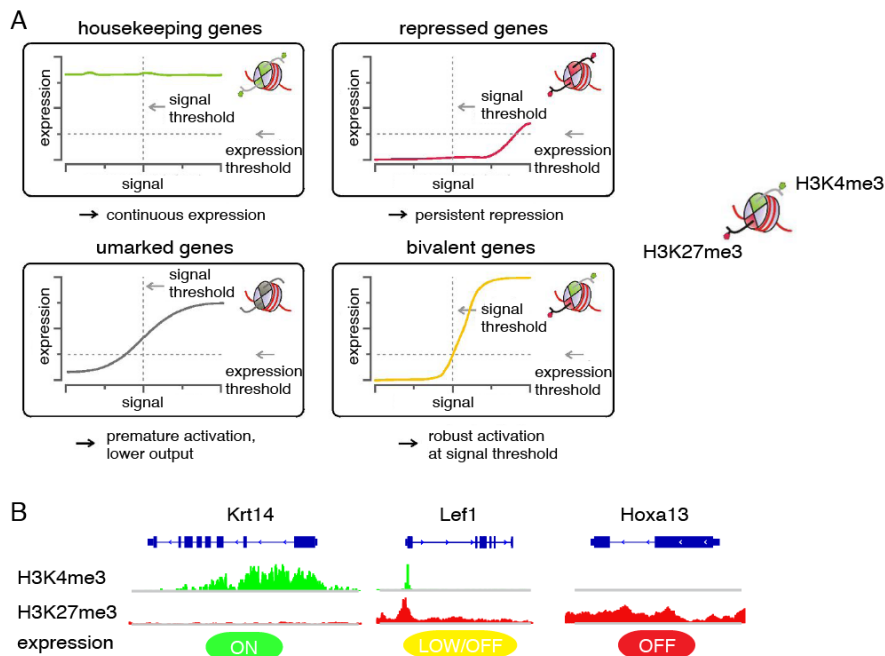


Fig. 3. Bivalency characterizes a dynamic equilibrium between activation and repression

A. In the bivalent state, activating stimuli and repressive complexes counterbalance each other. For differentiation, genes need to be activated once a signal reaches a certain threshold, ensuring that significant expression of these genes does not occur prior to that threshold. Only H3K4me3-marked genes, such as housekeeping genes, are constitutively active. In contrast, fully repressed genes require high levels of signal for activation. Genes carrying neither active nor repressive marks may be induced, but the absence of repressive signals renders them vulnerable to noise and may lead to subthreshold activation. Bivalent genes are fully active

once the correct threshold is reached because the transcription machinery is already pre-loaded. However, higher levels of signal are required to displace the counterbalancing repressive factors. Adapted from [154] **B.** Examples of constitutively active (*Krt14*), bivalent (*Lef1*) and repressed (*Hoxa13*) genes in HFSCs. The ChIP-seq traces are based on [162].

1.2.5 Aging and epigenetics

Accumulating evidence links aging to epigenetic alterations that involve alterations in DNA methylation patterns, posttranslational modification of histones, and chromatin remodeling. However, similar to the above-discussed factors of aging, the extent or even the direction of heterochromatin changes (lost or acquired) induced by aging differ between cells, organs, and species, thus highlighting the complexity of the epigenetic mechanisms underlying aging [163]. In several cases, loss of heterochromatin marks, including DNA methylation, H3K9me3, H4K20me3, and histones, have been reported with age. Therefore, it has been proposed that aging is at least partially associated with the disruption of heterochromatin [164-167]. However, H3K9me3 increases in the head of aging *Drosophila melanogaster*, and H4K20me3 is enriched in the aged liver and kidney of *Rattus norvegicus* [168]. Aging-associated epigenetic drifts of H3K27me3, H3K4me3, and H3K36me3, a transcriptional elongation marker, are even more unpredictable and cell context-dependent [168]. Particularly in mammalian systems, there is a global and local change in DNA methylation. For example, global DNA hypomethylation during aging has been reported in mice, rats, and humans [169, 170]. Promoter hypermethylation of polycomb-target genes was described in several aging tissues, like blood, mesenchymal stem cells, ovary, brain, kidney, and skeletal muscle [171-175]. Redistribution of DNA methylation and hypermethylation of promoters of genes involved in cell cycle and senescence has also been reported [165, 176].

Interestingly, analysis of a large panel of DNA methylation samples identified an age predictor that correlates the methylation levels of a few hundred CpG sites with chronological age and applies to a large panel of tissues [177]. Many of these 353 CpGs investigated are located close to poised promoters of bivalent genes, suggesting that aging may correlate with reduced plasticity in the expression of some bivalent genes, instead of changing active gene transcription [177]. In line with this observation,

bivalent gene promoters acquire DNA methylation in aged tissues and are also methylated and stably silenced in cancer [171, 172, 178-180]. In aged mouse muscle stem cells, increased heterogeneity of the DNA methylation status at various promoter regions was associated with increased transcriptional noise of the genes under their control [181]. This is in line with several single-cell sequencing studies in mice and humans, revealing increased cell-to-cell variation and increased gene expression noise in aging heart, muscle, pancreas, and dermal cells when compared to their younger counterpart [182-186].

It is possible that these epigenetic changes increase overall heterogeneity between cells in a tissue and that such an increase may drive aging [187]. The development of new single-cell approaches may help to integrate how different epigenetic modifications become altered with aging. Understanding these changes in more detail, as well as their drivers, may also lead to a strategy of rejuvenation.

1.3 Mechanotransduction and its role in epigenetic - and stem cell - regulation

Mechanotransduction describes a cellular process that converts mechanical stimuli into biochemical signals to generate responses that enable cells to adapt to their physical surroundings [188]. Physical forces or mechanical interactions are one of the most fundamental driving forces in determining size and geometry in any biological systems [189-191]. All cells, from the simplest form to the most complex organism, are mechanosensitive [192, 193]. They are exposed to different types of mechanical stimuli *in vivo*: cyclic stress (heart), shear stress (fluid flow over the cell surface), stretch or tensile strain (skin), distension (bladder), compression (bone, cartilage) (Fig. 4). Each of these stimuli plays a specific role in the regulation of proliferation, differentiation, migration, or morphology of the individual cells [194, 195]. Any disruption or altering cellular response to mechanical stimuli can lead to severe human diseases such as deafness, muscular dystrophies, developmental disorders, cancer, and most importantly to this work, premature aging [188]. Therefore, it is crucial to understand the molecular principles of sensing mechanical stimuli and the subsequent cellular response. Cells can sense the extracellular matrix's rigidity or geometry through integrins in focal adhesion complexes [196], stretch-activated receptor assemblies

sense the microenvironment and adapt their permeability to various extracellular ions [197]. Cadherin assemblies sense mechanical signals at cell-cell junctions and mechanically couple neighboring cells [198]. Additionally, numerous other well-characterized receptors, such as G protein-coupled receptors and Notch receptors, have been shown to respond to mechanical signals in the microenvironment [199]. The polymerization state of actin regulates the cytoplasmic-to-nuclear localization of various mechanosensitive transcription factors, such as the YAP/TAZ and MAL-SRF transcription factors pathway [200, 201]. Mechanotransduction through both the MAL-SRF and YAP/TAZ pathways requires active Rho-GTPase signaling and actomyosin-mediated contractility, which results in the translocation of these transcription factors from the cytoplasm to the nucleus where they initiate their respective transcriptional activities. The cytoskeleton networks also bridge the cell membrane and the nucleus through the linker of nucleoskeleton and cytoskeleton (LINC) complex, thereby allowing direct transmission of mechanical signals to the nucleus [202, 203].

Interestingly, the nucleus' mechanical properties adapt to mechanical stimuli, thereby regulating gene expression. The mechanical properties of the nucleus are determined by the interplay of cytoskeleton–nucleus links, by the integrity and composition of the nuclear lamina and by the degree of DNA packaging into chromatin [204, 205]. For example, on stiff substrates, the apical actin stress fibers compress the nucleus into a flat ellipsoid. In contrast, on soft substrates, the more relaxed depolymerized actin structures result in the loss of mechanical tension and a spherical nucleus [206, 207]. Cells grown on stiff substrates also have higher lamin A/C levels than their counterparts grown on soft substrates, and nuclear stiffness scales with levels of nuclear lamin A/C [208, 209]. In progeria, a genetic disorder of premature aging, mutations in lamin A/C correlate with abnormal nuclear morphology [210].

Sensing mechanical signals from the microenvironment has important functional implications, especially for stem cells, to adapt to various tissue microenvironments [211, 212]. For example, mesenchymal stem cells sense the underlying stiffness of the extracellular matrix as part of their differentiation into various cell types [213]. Hematopoietic stem cells, in the bone marrow, sense shear forces generated by the blood flow, thereby enabling them to differentiate into the various blood lineages [214]. Epithelial cells can undergo an epithelial-mesenchymal transition in response to local

mechanical signals, which is crucial in establishing early-developmental expression programs [215].

In human epidermal progenitor cells, a long-term, mechanical force-driven increase in H3K27me3 is involved in restricting lineage commitment [216]. Extrinsic mechanical strain induces the formation of a perinuclear F-actin ring, which results in a depletion of free nuclear G-actin. As nuclear actin is an important transcriptional cofactor, this decrease in nuclear actin leads to a downregulation of global transcription. Although this transcriptional repression is global, it specifically enables accumulation of H3K27me3 on promoters of lineage-specific differentiation genes, thereby decreasing differentiation [216].

Mechanotransduction also plays a role in DNA damage protection [217]. Recently, it has been shown in human epidermal progenitor cells that high mechanical stretch deforms the nucleus, which cells initially counteract via a calcium-dependent nuclear softening driven by the loss of H3K9me3-marked heterochromatin [218]. The resulting changes in chromatin rheology and architecture protect the genetic material from mechanical forces. When high-amplitude stretch persists, it induces supracellular alignment of tissue to redistribute the mechanical force before it reaches the nucleus. This tissue-scale mechanoadaptation, mediated by cell-cell contacts, allows cells to restore the initial chromatin state [218].

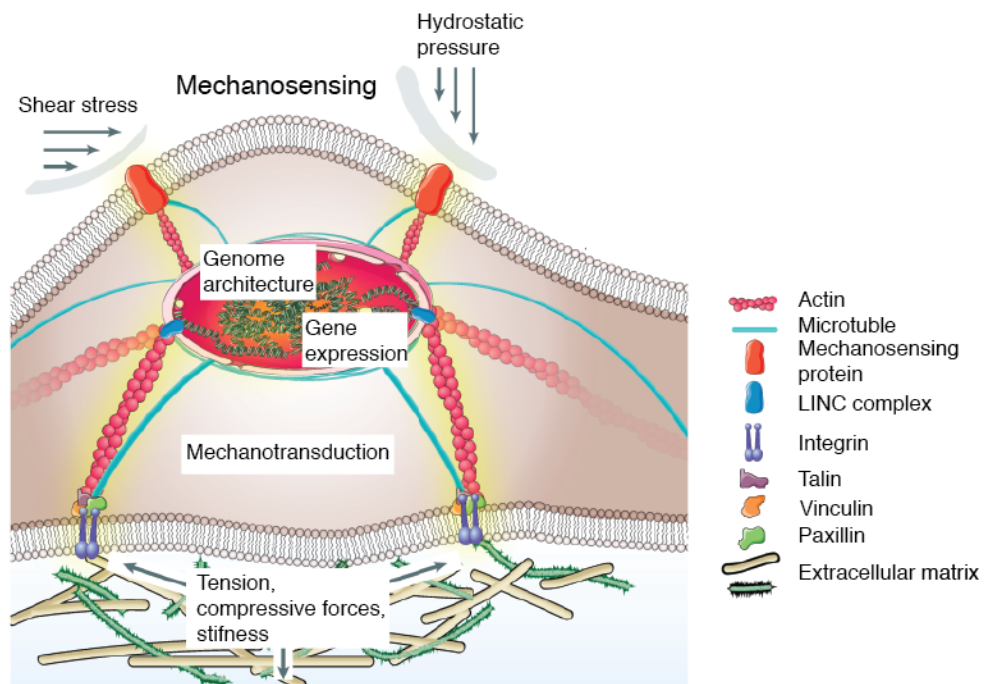


Fig. 4. Sensing and transduction of mechanical signals

Cells are exposed to many types of forces, including shear stress, hydrostatic pressure, compressive forces, tension and stiffness. Membrane surface receptors, such as integrin, focal adhesion complex, or ion channels, can sense these forces signals and transmit them through the actin cytoskeleton to the nucleus, which in turn generates cellular responses. Also, the nucleus itself can sense forces. Adapted from [219].

1.4 Mammalian skin

In this thesis, hair follicle stem cells (HFSCs) were used as a paradigm to study the effect of aging on stem cells. HFSCs reside in the so-called bulge niche within hair follicles of the mammalian skin. The skin consists of a multilayered, stratified epithelium, the epidermis, that covers the surface of the entire body. It serves as a barrier to protect the body from internal water loss and external environmental insults, like toxins, pathogens, or temperature changes. Due to this front-line defense function, it must self-renew, to rapidly replace lost or damaged cells, every 7-10 days [220]. Epidermal stem cells reside in the basal layer of this stratified epithelium, where they initiate a transcriptional program of terminal differentiation while moving upwards to give rise to the spinous layer, the granular layer, and finally the cornified layer. In

addition to the epidermis, the skin harbors multiple specialized appendices such as the hair follicle that is maintained by its stem cell population, the HFSCs [221, 222]. Hair follicles self-renew through cyclical bouts of growth (anagen), degeneration (catagen), and rest (telogen). At the start of the hair cycle, complex signaling crosstalk with neighboring niche-resident cells activate quiescent HFSCs, which reside in the so-called bulge niche, to proliferate and migrate to supply the cells needed for hair follicle down-growth [223, 224]. Besides their role in HF cycling, HFSCs can participate in wound repair and may serve as origin for several squamous cell carcinomas. The skin consists further of the underlying mesenchymal compartment - the dermis, and an adipose subcutis underneath. A basement membrane separates the epidermis and dermis.

1.4.1 Hair Follicle morphogenesis and cycling

Hair follicles play a crucial role in skin homeostasis and are also vital in thermoregulation, social communication, and sensory processes. The morphogenesis of HFs is a tightly controlled process that relies on the precise signaling crosstalk between the epidermis and the underlying mesoderm. In mice, HF morphogenesis is initiated at embryonic day (E) 14, when a dermal condensate of specialized fibroblasts forms in the dermis adjacent to the yet undifferentiated epidermis. Inductive epidermal signals act on the dermal condensate, which subsequently signals back to the epidermis leading to placode formation. A complex signaling network of activating and inhibitory signals secreted and received by the placodes and the dermal condensate allows further HF morphogenesis. Also, it promotes neighboring cells to adopt IFE fate resulting in coordinated HF spacing [225]. By E16, the placode further develops into a hair germ (HG), and the dermal condensate differentiates into the dermal papilla (DP). During organogenesis, the HG grows downwards and forms a peg that subsequently engulfs the dermal papilla at around E18. HF keratinocytes that are in direct contact with the DP become hair matrix cells. Hair matrix cells proliferate and move upwards to differentiate into six cylindrical layers of inner root sheath (IRS) and the hair shaft. The outer layer of the HF, the outer root sheath (ORS), forms a continuum with the IFE and is surrounded by the BM [226-228]. During postnatal life, hair follicles are periodically regenerated through a continuous cycle that comprises three distinct

phases: anagen (growth phase), catagen (regression phase), and telogen (resting phase) [228, 229] (Fig. 5). At the beginning of the anagen phase, stem cells present in the bulge region of the hair follicle proliferate and generate ORS cells. Before activation of hair follicle stem cells, secondary hair germ cells rapidly proliferate and produce the transit-amplifying cells (TACs) in the germinal matrix. Subsequently, the TACs differentiate into the IRS cells and hair shafts [230, 231]. During catagen, cells in the ORS and the germinal matrix undergo apoptosis, and the lower two-thirds of hair follicles regress. In telogen, hair follicle stem cells are relatively quiescent, and the bulge of the hair follicles is in contact with the dermal papilla. During the early adult life, between postnatal day 18 (P18) and 70, body hair growth is mostly synchronized [228, 232]. Generally, based on studies of C57BL/6 mice, between P18 and P23, hair follicles go through a short period of telogen phase before initiating a new anagen phase, which produces a new hair follicle between P23 and P35. By P37, the anagen hair follicle starts to regress and enters a transient catagen phase, during which the lower portion of the hair follicle is degraded. At the same time, the DP moves upward with the remaining epithelial cells. These cells eventually form an hair germ beneath the bulge stem cell compartment. By ~P44, with the completion of hair follicle regression and hair germ formation, the hair follicle enters a prolonged telogen phase. This telogen phase is considerably longer than between P18 and P23 and typically lasts four weeks before the hair follicle enters the next anagen phase by ~P70 [233].

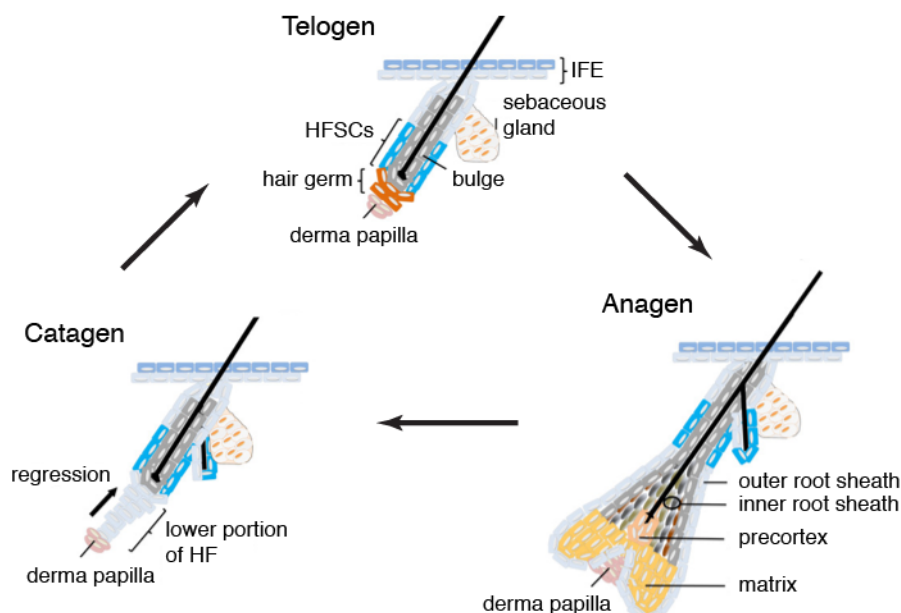


Fig. 5. HF cycling

During the resting phase (Telogen), HFSCs residing in the outer layer of bulge remain in quiescence. At the onset of the growth phase (Anagen), stem cell progenies located in sHG proliferate and initiate HF regeneration in response to the activating signals. HFSCs begin to proliferate and give rise to outer root sheath, cells migrating downward from the bulge and feeding into the bulb of matrix at the base of the newly formed HF. At the same time, hair germ develops into matrix, and then terminally differentiate to form hair shaft and inner root sheath. When the HF enters a destructive phase (Catagen), the lower part of the HF undergoes apoptosis and the epithelial strand regresses upward. Once the dermal papilla is drawn upward toward the bulge, the HF re-enters telogen. Adapted from [234].

1.4.2 Hair Follicle Stem Cells

HFs rely on stem cells located in distinct anatomical regions to supply differentiated progeny. They include slow-cycle epithelial stem cells of the bulge [235], fast-cycling epithelial progenitors in the secondary hair germ [236], dermal stem cells of the lower dermal sheath [237, 238], and melanocyte stem cells [239]. The SC behavior is tightly linked to signals from various sources, including intradermal adipocytes [240], dermal fibroblasts [241], blood vessels [242], lymphatic vessels [243] and peripheral nerves [244]. Characterizing these dynamic signaling networks within the niche is critical for understanding how stem cells self-renew, differentiate, maintain tissue homeostasis, and how their dysfunction contributes to disorders. At the end of HF morphogenesis, the quiescent HFSC niche, the bulge, is formed below the SG [235]. It contains SCs that are marked by their expression of keratins (K15, K5, K14), the cell surface markers CD34 and Leucine-rich repeat-containing G protein-coupled receptor 5 (Lgr5) and integrins ($\alpha 6\beta 4$ and $\alpha 3\beta 1$). To initiate the hair cycle and to start cell proliferation, HFSCs need to become activated. SC activation relies, among others, on the regulation of the two critical signaling pathways: Wnt and Bone Morphogenetic Proteins (BMPs) signaling [232].

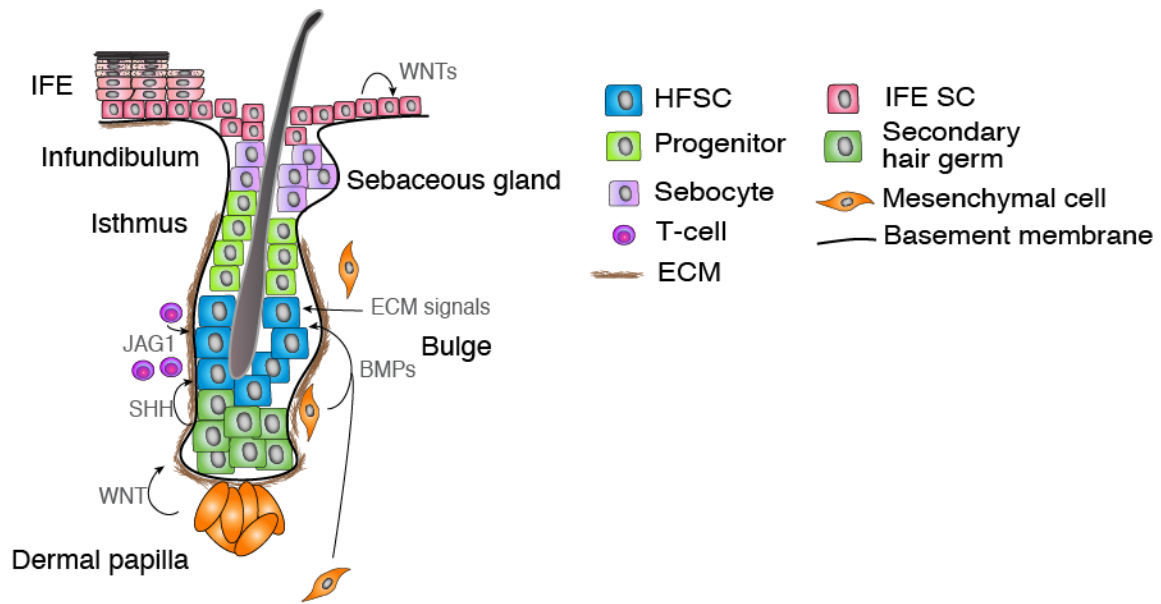


Fig. 6. HFSCs and their niche

The interfollicular epidermis of the skin is continuously renewed by epidermal stem cells. Epidermal stemness is maintained by autocrine WNT signals and by contact with the basement membrane. Once these cells initiate differentiation, they move upwards and give rise to various differentiated layers. The hair follicle is compartmentalized into multiple micro-niches that are maintained by distinct stem cell populations. CD34+ HFSCs reside in the bulge niche, where they are activated through signaling with their immediate progeny (hair germ cells) and mesenchymal dermal papilla cells to initiate differentiation and hair follicle growth. Further instructive signals are provided by the surrounding niche basement membrane, proximal dermal fibroblasts and T cells. Adapted from [108].

1.4.3 Signaling during HF cycle

Since activating and inhibitory signals can both be present in the HFSC niche, the probability of HFSC activation is the readout of the summation of both activating and inhibitory signals [245, 246]. The two main counteracting signals are BMP and Wnt/ β -catenin signaling pathways [247, 248]. High BMP signaling keeps HFSCs in an inactivated state, while Wnt/ β -catenin signaling promotes HFSC activation and maintains HF growth [245-250]. Moreover, the TGF- β 2, Foxp1, and oncostatin M and SHH signaling pathways also regulate the hair cycle [245, 251-253]. Factors that can tilt the balance of Wnt/ β -catenin and BMP signaling can modulate HFSC activity, thereby suppressing or promoting anagen entry [254].

When Wnt signaling is induced in the hair follicle, both in the bulge compartment and hair germ progenitors, hair growth is activated [255-257]. The activated Wnt signaling in the epithelial cells is likely downstream of the signaling events from the DP [256]. Wnt ligands bind to the frizzled receptor leading to the inactivation of a downstream destruction complex, thus enabling β -catenin to accumulate in the cytosol and to enter the nucleus to activate transcription of Wnt target genes [258]. Deletion of β -catenin or Wntless genes in the skin, required for transcriptional activation of the Wnt pathway and secretion of Wnt ligands, respectively, comprises the telogen-to-anagen transition [249, 250, 256]. The epidermal deletion of β -catenin or its downstream mediator Lef-1 leads to hair loss [259, 260]. In the absence of β -catenin, HFSCs fail to differentiate into follicular keratinocytes and adopt epidermal fate [259]. In the nuclei of Wnt responding cells, TCF3/4 switch from association with TLE4, which negatively regulates gene expression, to association with stabilized, nuclear β -catenin to activate a subset of Wnt-targeted genes. TLE4 overexpression, delayed the transition to Wnt activation and hair growth [261]. The potent role of Wnts in regenerating hair was highlighted by their ability to induce wound-induced hair neogenesis in mice [262]. Wnts are, in this case, induced by Fgf9, which is produced by T cells, when these cells enter the wound dermis [263].

BMP signaling plays an essential role in regulating HFSC quiescence. BMPs belong to the Tgf- β superfamily, and upon binding to their receptor, they signal through R-Smads, Smad1, -5, and -8 [264]. Bmpr1a is a crucial receptor for the epithelial cells to interpret BMP ligands. When Bmpr1a was specifically deleted from adult HFSCs, HFSCs lost quiescence and became hyperproliferative but did not lose their SC identity

[265]. However, differentiation of the expanded HFSCs and progenitors appears to be compromised, and the *Bmpr1a* cKO mice fail to regenerate hair shafts. Thus, BMP signaling seems to have a dual role in maintaining HFSC quiescence and promoting terminal differentiation of HFSCs, likely through its action in distinct hair follicle cell populations. Multiple sources of BMP ligands have been identified in the skin. In the adipocytes located in the subcutaneous epidermis, BMP2 was found to be periodically expressed. The oscillation of BMP2 expression in adipocytes is correlated with the anagen-to-telogen transition, hair growth, and HFSC quiescence [248]. In late anagen to the middle of telogen, BMP2 is highly expressed in adipocytes, and HFSCs are rested in a refractory phase, generally resistant to activation signals. During the late telogen to early anagen transition, BMP2 expression in adipocytes is reduced considerably and correlates with the permissive phase for HFSC activation. In addition to BMP2 produced by adipocytes, BMP6 is found to be secreted by the inner bulge layer [230]. BMP6 expression in these cells plays a role in restricting HFSCs from activation. Also, the DP produces BMP6 [266]. It remains an open question of how BMP producing cells coordinate to govern HFSC quiescence and whether there is a hierarchical organization of BMP producing cells in their ability to regulate HFSCs.

In contrast to the Wnt and BMP signaling pathways, FGF signaling pathways have shown diverse regulatory outcomes. The DP produces FGF7 and FGF10, and their presence stimulates hair growth initiated in the HG [236]. In contrast, FGF18 is produced mainly by the inner bulge layer and the bulge HFSCs [267]. Genetic deletion of *Fgf18* significantly shortens the duration of the quiescent telogen phase, leading to activation of hair growth and HFSC division. It has been suggested that *Fgfr2* IIIb is responsible for transducing the FGF7/10 signaling, whereas *Fgfr3c* is responsible for mediating the effect of FGF18 [267, 268]. Due to the diversity and complexity of FGF signaling, further research needs to dissect the downstream mediator of FGF7/10-*Fgfr2b* and FGF18-*Fgfr3c* axis to completely understand how different FGFs produce different HF-SC responses [269].

In addition to signaling pathways regulating the interaction between SCs and their niche, there is increasing evidence documenting interactions between SCs and their progenies. In this regard, the *Shh* signaling pathway plays a critical role in promoting HFSC cell division shortly after the activation of hair growth. *Shh* is prominently produced by a subset of transit-amplifying cells located in the hair bulb. These cells

form when the newly growing hair progresses through the anagen phases. TACs produced Shh stimulates HFSCs cell division in a cell non-autonomous manner [270]. This regulation for the HFSC division could be an adaptive mechanism to control the number of HF-SCs.

Epigenetic regulators such as Ezh1/2 and Dnmt1 have also been shown to play a role in maintaining HFSCs. Mouse models with deletion of the PRC2 component Ezh1/2 and subsequent depletion of the histone H3K27me3 mark can still specify HFSCs but show proliferation and differentiation defects, which lead to the rapid loss of the entire hair follicle lineage [271]. In contrast to this rapid decline, the genetic deletion of Dnmt1 leads to progressive loss of hair regeneration over a year [272].

1.4.4 The extracellular matrix

The ECM is a complex non-cellular network present within tissues. The ECM is mainly composed of fibrous proteins (e.g., collagen, fibronectin, laminin, and elastin) and proteoglycans (e.g., perlecan), which determine the biochemical and mechanical properties of the tissue. The ECM also serves as a reservoir for specialized proteins (e.g., growth factors). It was previously thought to be an inert structure that provided a platform for cell adhesion. It is now known that the ECM also provides both biochemical and biomechanical cues that regulate cell behaviors like adhesion, migration, proliferation, and differentiation [273, 274].

Therefore, the ECM and ECM-associated proteins are critical components of stem cell niches determinants of cellular fate during development, homeostasis, and disease [108, 273, 275, 276]. In bidirectional crosstalk between the cell and its environment, tissue-resident cells are responsible for and responsive to the ECM [277-279]. Cells modify their secreted ECM products in response to various stimuli, including mechanical cues, oxygen, and nutrient concentration [279]. In turn, the ECM sends mechanical and biochemical signals to cells through cell surface receptors, subsequent activation of intracellular signaling cascades, and changes in gene expression [280]. Interestingly, numerous studies have shown that an acellular ECM is sufficient to maintain stem cells and promote self-renewal *in vitro*. [281-284]. Collagens are one of the main components of ECMs and play an essential role in structuring and shaping the tissue and determine its mechanical properties. The

collagen superfamily comprises 28 members that are all characterized by their triple-helical structure. Three collagen α -chains can form either hetero- or homotrimers resulting in a structural triple helix. Collagens are classified into fibril-forming, network-forming, microfibrillar, fibril-associated collagens with interrupted triple helix (FACIT), and transmembrane collagens [285-287].

Collagen synthesis is a complex stepwise process, with many processing steps in the endoplasmatic reticulum, Golgi, and after secretion in the extracellular space. Lysyl oxidases then crosslink collagen molecules leading to fibril formation. The subsequent interaction with other collagens and macromolecules of the ECM defines the specific structure and biological activity of the tissue [288].

Glycoproteins are proteins that contain covalently bound oligosaccharide chains. They are highly abundant in the ECM and are comprised of a variety of different subgroups with specific properties. For instance, LNs, elastic fibers, fibronectin (FN), tenascins, thrombospondins, and matrilins can be found ubiquitously or in a tissue-restricted manner [289]. LNs are essential components of BM. Elastic fibers regulate the bioavailability of specific growth factors.

The elastic fiber network consists of fibrillins, fibulins, microfibril-associated glycoproteins, and growth factor binding proteins [290].

FN is a ubiquitously expressed glycoprotein that is secreted as a dimeric protein, and contains multiple binding domains for protein interactions. It interacts with the cell surface by binding to integrins or syndecans, and with other ECM proteins such as thrombospondin-1, tenascin-C, fibrillin-1 as well as extracellular enzymes [291]. The expression and local assembly of FN-containing ECM are crucial for morphogenesis and differentiation [292].

Proteoglycans consist of a core protein and glycosaminoglycan (GAG) chains. According to their GAG chains, they can be grouped into proteoglycans containing dermatan sulfate, heparan sulfate, chondroitin sulfate, and keratin sulfate chains. Proteoglycans can be membrane-bound, where they can act as co-receptors of growth factor receptors or as adhesion receptors. Secreted into the ECM space, they bind to a variety of other ECM molecules and regulate morphogenic gradients of growth factors and chemokines [293].

All these components determine together topography, viscosity, and mechanical properties of the ECM. In particular, elastic fibers, fibrillar collagens, and GAGs provide

ECM's mechanical properties, while fibrous proteins provide tensile strength (collagens, elastin) [294, 295]. Based on its composition, the ECM can have the characteristics of a soft material, easily deformable at low forces, or of a hard material, which requires greater forces to generate deformation [219]. Also, the ECM's topographical features, including pore size, fiber diameter, and feature elevation, are sensed by cells [296]. Interestingly, it seems that the ECM architecture provides a mechanical memory correlating with stem cell differentiation toward selected lineages [213, 294, 297].

1.4.5 ECM structures in the dermis

The dermis is a connective tissue layer between the epidermis and the subcutaneous fat layer. In addition to ECM, it contains ECM-producing fibroblasts, immune cells (lymphocytes, neutrophils, monocytes, and mast cells), blood, and lymphatic vessels. The dermis subdivides into two parts: the papillary dermis (*stratum papillare*) next to the epidermis and the BM, and the reticular dermis (*stratum reticulare*) underneath. The papillary dermis is composed of loose, small diameter collagen fibers and immature elastic fibers. In contrast, the reticular dermis holds large-diameter collagen fibers and mature elastic fibers, decorated with proteoglycans and fibril-associated macromolecules. Fibril-forming collagens, including collagen type I, III, and V, are the most abundant collagens in the dermis. They interact with FACIT collagens type XII and XIV and assemble into large, parallel fibril bundles. The BM contains non-fibril-forming collagens (collagen type IV), collagens intercalated into fibril bundles (type VI), or collagens anchoring epidermis and dermis (type VII). Proteoglycans in the skin include heparan sulfate proteoglycans, chondroitin-6-sulfate proteoglycans, which are associated with the BM, whereas chondroitin sulfate (versican) or dermatan sulfate proteoglycans (lumican, decorin, biglycan) are found in the dermis. Decorin and biglycan contribute to collagen fibrillogenesis by connecting type I collagen and FACIT collagens. At the same time, lumican controls collagen fibril diameter and fibril spacing [298-300].

1.4.6 The skin basement membrane

In the skin, a BM physically separates the epidermis and dermis. It serves as an anchoring platform for keratinocytes, stabilizes the tissue, and controls the release and diffusion of growth factors. Hemidesmosomes mediate stable anchorage of the epidermis to the BM. Similar to most BMs, the skin BM consists of LNs, type IV collagen, glycoproteins, nidogen, and perlecan [301, 302]. Type VII collagen, produced by fibroblasts, anchors the BM to the underlying dermis [303]. Both keratinocytes, as well as fibroblasts, express and deposit LNs into the epidermal BM [304]. The most relevant LNs in the BM of the skin are LN-332 and LN-511. LN-511 is highly expressed during the growth phase of the HF, and it has a growth-promoting effect, whereas LN-332 suppresses HF growth and is subsequently involved in HF regression [305, 306]. Both LN-332 and LN-511 bind to $\alpha 3\beta 1$ integrins, although LN-511 binds with a higher affinity to $\alpha 3\beta 1$ integrin compared to LN-332 [307]. LN-332 also binds to the hemidesmosome-forming integrin $\alpha 6\beta 4$. Besides $\alpha 6\beta 4$ integrin, skin hemidesmosomes contain type XVII collagen and tetraspanin CD151, and they are connected to the intermediate filament network inside the cell. Disturbances in hemidesmosome formation lead to skin blistering due to BM instability [308].

1.4.7 Aging in the skin

Human skin aging is a complex process that has been studied extensively. It combines endogenous factors leading to intrinsic aging and exogenous factors, like sun radiations, air pollution, and nutrition. Intrinsic skin aging, also called chronological aging, results from gene mutations, cellular metabolism, and changes in the hormonal microenvironment. Clinically, intrinsically aged skin appears thin, finely wrinkled, smooth, dry, unblemished, sallow, and pale, with elasticity loss. UV-induced extrinsic aging, also called photoaging, is clinically characterized by deep wrinkles, laxity, roughness, sallowness, increased fragility, blister formation, pigmentary changes, telangiectasias, impaired wound healing, and benign and malignant growths [309, 310]. At the molecular level, an intrinsically aged skin experiences epidermal hypoplasia, although the number of layers remains unchanged [311, 312]. Basal cells exhibit an increased heterogeneity in size with an overall elevated volume [313]. The stratum corneum experiences a slow replacement of lipids, negatively affecting the

barrier function [314]. The number of melanocytes decreases, and inactive melanocytes accumulate in HFs of aged skin, causing hair greying [315, 316]. The dermal-epidermal junction flattens out. Loss of fibroblast cellularity co-occurs with gradual loss of dermis thickness and general atrophy of the ECM. Collagen and elastic fiber levels are reduced and disintegrated, either due to decreased synthesis, increased degradation, or both [317]. A thickened epidermis characterizes Photoaged skin due to a chronic wound healing response. Faulty degradation of corneocyte desmosomes leads to a thickened stratum corneum [318]. Further, the expression of type VII collagen in the dermo-epidermal junction is reduced. Fibrillin appears significantly dystrophic, truncated, and depleted in the upper dermis while the mid and deep dermis accumulates abnormal elastic tissue [319]. Collagen content, especially collagen type I, decreases in photoaged skin [320]. Various matrix metalloproteinases and other proteases are responsible for the degradation of connective tissue components, such as collagen. UVA and UVB irradiation induce these proteases *in vivo* and *in vitro*, resulting in reduced collagen content [321]. Aging is associated with decreased migration and proliferation, delaying epithelialization. Excessive inflammation leads to increased levels of proteases (MMPs, elastase) and matrix degradation. Production of and responses to specific cytokines involved in matrix production is reduced in aged fibroblasts, increasing excessive degradation at wounded sites [322].

Aged mouse skin displays similarities to aged human skin, without the extrinsic component in laboratory mice. Macroscopically old mice show hair loss and hair greying. At the molecular level, the skin shows decreased dermal cellularity and thickness, and increased subcutaneous adipose layer (hypodermis). Optical coherence tomography studies have shown that the epidermis becomes thinner in aged mice, and collagen content decreases with age, similar to humans [323]. A study in hairless mice noted that total collagen synthesis expressed as a percentage of total protein synthesis did not change with age. However, hydroxylation of collagen, incorporated in freshly synthesized collagen, decreased with age. The proportion of type III collagen and fibronectin biosynthesis increased in hairless mice [324]. Mouse models of premature aging have shown a slower wound closure rate, reduced amounts of collagen deposition, and collagen mRNA expression, resulting in an impaired wound healing response [325, 326].

In mammals, aged skin is accompanied by a marked reduction in hair cycling and appearance of bald patches, indicating that HFSCs are either lost, differentiate, or change to an epidermal fate during aging. Skin aging is associated with reduced potency of HFSCs, already at stages where HFSCs are still present at numbers comparable to young mice [327-329]. Later during aging, severe hair loss has been reported, which is associated with hair follicle destruction and reduced HFSC numbers [330]. Age-related declines in SC activity and tissue fitness have been described for both epidermis [120, 331] and HFs [332-336]. Recent research shows that aged HFSCs maintain their identity and do not shift to an epidermal fate [337], in contrast to aged fibroblasts, which become more heterogenic and gain adipogenic traits [185]. Interestingly, both cell types exhibit altered extracellular matrix gene expression, and aged HFSCs show a decline in hair regeneration following wounding. This is in line with many other cases that implicate the role of an aging hair follicle microenvironment [120, 335, 338-340], and with the knowledge about aging stem cell niches in other tissues (s. 1.1.3). However, the mechanism of how niche changes affect aging stem cells is still unknown. Thus, we are trying to answer this question in this thesis.

2 Aim of the thesis

Aging is the process of tissue and organ function decline with age. Loss in stem cell number or activity over time is one possible explanation for this decline. However, little is known about mechanisms leading to stem cell exhaustion in aged tissues. This study aimed to understand cause and drivers of stem cell exhaustion in the hair follicle. In particular, I want to understand:

1. What are the age-related changes in hair follicle stem cells that lead to stem cell exhaustion?
2. What is the role of the microenvironment in hair follicle stem cell aging?
3. Do changes in chromatin architecture contribute to altered stem cell fate in aging?

3 Materials and Methods

3.1 Chemicals and reagents

Unless denoted explicitly, common chemicals and reagents used in this study were purchased from the following suppliers: Merck (Darmstadt, Germany), Carl Roth (Karlsruhe, Germany), Sigma Aldrich (Munich, Germany).

3.2 Mice

Wild type C56BL6/J mice were used for aging experiments. Male mice between 24-30 weeks were used as young controls (~6 months), and male mice between 100-110 weeks (~24 months) were used as the aged group. Tenascin X- and Collagen XIV-deficient mice have been reported previously [341, 342]. All animals in the same experimental groups were bred in the same animal facility and housed in the same room, wild-type mice in the specific-pathogen-free mouse facility of the Center of Molecular Medicine (CMMC) and Max Planck Institute for Biology of Ageing (MPI-Age), Cologne, TNX mice in the animal facility of the Department of Biochemistry, University of Cologne, Germany. All mice were provided with ad libitum standard rodent diet and water. DNA was isolated from tail clips for genotyping. No statistical method was used to predetermine sample size, and the experiments were not randomized. All animal experiments were performed by guidelines and animal licenses of the State Office North Rhine-Westphalia, Germany.

3.3 Isolation of primary epidermal cells

Epidermal cells were isolated from telogen-stage (P21-P23 or 8-9 weeks old), 6 or 24 months old C56BL/6J mice. Mice were sacrificed by cervical dislocation and shaved. After a quick wash with water, mice were incubated subsequently in 70% ethanol, distilled water, and in PBS, each for 1 min. After removal of tail and limbs, the skin was peeled off, and the subcutaneous fat was removed by scraping with a round surgical blade (No 22). For further sterilization, the skin was incubated in a 2x antibiotic/antimycotic solution (Sigma A5955) for 5 min at RT. The skin was cut into smaller pieces and transferred epidermal side up to 0.8% trypsin (Gibco 27250-018) in PBS for 50 min at 37 °C. Skin pieces were subsequently transferred to a 10 cm petri

dish containing MEM (Spinner's modification, Sigma) + FCS to stop the trypsinization. The epidermis was then separated from the dermis using forceps and finally minced into small pieces. The epidermis suspension was disrupted by passing through a 50 ml pipette 8-10 times and filtered first through 70 μm , then 40 μm cell strainers, and centrifuged at 900 rpm for 5 min. The supernatant was removed, and the cells were resuspended in the applicable media and used for downstream applications.

3.4 HFSC organoids and hydrogels

3.4.1 3C HFSC organoids

Epidermal cells were cultured in 3C organoid conditions to study HFSCs in vitro, as has been described earlier [343]. It is based on a 3D extracellular matrix environment and defined soluble factors and allows expansion and long-term maintenance of HFSCs. In this system, cultured epidermal cells form an equilibrium of HFSCs and non-HFSCs. For 3D culture, 8×10^4 freshly isolated epidermal cells were suspended in 40 μl ice-cold 1:1 mixture of KGM and growth factor-reduced Matrigel (Corning) that was dispensed as a droplet in 24-well or 6 cm cell culture dishes. The suspension was allowed to solidify for 30 min and then overlaid with 500 μl of 3C medium and incubated at 37°C, 5% CO₂. The medium was exchanged the next day after initial seeding and after that every second day. Cells were extracted from Matrigel by mechanical homogenization and incubation in 0.5% Trypsin, 0.5 mM EDTA, for 10 min at 37°C.

3.4.2 Collagen hydrogels

PEG-crosslinked Collagen hydrogels were used to generate organoids with defined stiffnesses and to study the effect of stiff microenvironments on HFSCs. These hydrogels were prepared as described previously [344].

Collagen I (Millipore 08-115) was mixed with a reconstitution buffer and cells in 3C medium in a ratio of 4:1:7 to yield a final Collagen I concentration of 1.6 mg/ml. To tune stiffness, PEG-diNHS (Sigma-Aldrich E3257, Mw 456.36) was dissolved in dimethyl sulfoxide (DMSO) at a concentration of 50 mg/ml. The solution was then added to the collagen/Cell/reconstituting solution mixture at a final PEG-diNHS to collagen-mass ratio of 0.17. The hydrogel/cell mixtures (80,000 cells in one hydrogel droplet on a 24-well plate) were allowed to polymerize at 37°C for 1 h and then cultured in 3C medium

at 37°C, 5% CO₂. Elastic moduli of the hydrogels were validated by atomic force microscopy, as described below. Cells were extracted from hydrogels by mechanical homogenization and incubation in 2 mg/ml collagenase A (Merck 10103586001) for 10 min, then 0.5% Trypsin (Gibco), 0.5 mM EDTA, for 10 min at 37°C.

Keratinocyte Growth Medium (KGM):

MEM Spinner's modification (Sigma)

Insulin (Sigma)	5 μ g/mL
EGF (Sigma)	10 ng/mL
Transferrin (Sigma)	10 μ g/mL
Phosphoethanolamine (Sigma)	10 μ M
Ethanolamine (Sigma)	10 μ M
Hydrocortisone (Calbiochem)	0.36 μ g/mL
Glutamine (Gibco)	2mM
Penicillin, Streptomycin (Gibco)	100 U/mL
Chelated fetal calf serum (Gibco)	10%
Y27632 (Miltenyi Biotec)	5 μ M
VEGF (Miltenyi Biotec)	20 ng/mL
FGF-2 (Miltenyi Biotec)	20 ng/mL

Reconstitution buffer

Sodium hydrogen carbonate	0.26 M
HEPES	0.2 M
Sodium hydroxide	0.05 N
Hanks' Balanced salt solution (Sigma H1641)	1x

3.5 siRNA knockdown and colony forming assay

HFSCs were cultured in 3C organoids, as described above, for 12 days and then transferred to a 6-well plate. 7 μ l of lipofectamine RNAiMAX reagent was diluted in 150 μ l of OptiMEM (Gibco 11058-021). 3 μ l of siRNA (10 μ M) was diluted in 150 μ l of OptiMEM. Diluted lipofectamine RNAiMAX was added into diluted siRNA (1:1) and incubated for 5 min at RT. 300 μ l of siRNA-lipix mix was then added to HFSCs (1 well of 6-well plate). All siRNAs were from Thermo Fisher (Silencer select 4390771, Hmga2

siRNA ID: s67600, Lef1 siRNA ID: s69161, Cdc34 siRNA ID: s103506, Wnt7a siRNA ID: s76098). After 24 h of transfection, cells were used for colony forming assay. J2 feeder cells (ATCC) were treated with 0.5 mg/ml Mitomycin C in DMEM with 10% FBS and Penicillin/Streptomycin for 2 h at 37 °C. HFSCs plated at low clonal density (103 cells/6 well) on Mitomycin C treated J2 feeders and cultured for 3-4 weeks in FAD medium (DMEM+Ham's F12 with 5 µg/ml Insulin, 10 ng/ml EGF, 1.8x10⁻⁴ M Adenin, 0.5 µg/ml Hydrocortisone, 10% Chelated FCS, 10⁻¹⁰ M Cholera toxin). Colonies were fixed with 4% PFA and subsequently stained with 0.1% crystal violet and quantified.

3.6 Chemical treatments

Where indicated, cells were treated with Cyclophamide hydrate (10 µM, Sigma) or α -Amarnitin (50 µg/ml for 6h, Sigma). The vehicle DMSO or H₂O was used as a control for all treatments.

3.7 Depilation and Edu injections

Depilation of hair with wax is the gold standard to induce hair follicle anagen entry and HFSC activation *in vivo*. Mice were anesthetized with isoflurane, the wax was applied on the dorsal skin, and the hairs were plucked off by using hair removal strips. 22 h after depilation mice were injected i.p. with Edu (50mg/kg body weight) and 24 h after depilation tissues biopsies were collected for histological analyses and FACS sorting followed by qPCR as described below.

3.8 Flow cytometry

Flow cytometry and fluorescence-activated cell sorting (FACS) are techniques that simultaneously measure and analyze cell size, granularity, and fluorescence intensity of single cells. Laser light is illuminated on the cells in the sample stream, thereby getting scattered and measured by optical detectors. Each event or cell in the flow produces specific information or parameter based on its light scattering and fluorescent properties, providing data on cell morphology and chemical characteristics [345]. FACS systems have an added feature which allows them to physically separate cells of interest from a heterogeneous sample, based on their optical properties.

We used flow cytometry to analyze the percentage of HFSCs and sort HFSCs for downstream applications. Cells were isolated as described above. Cells were then pelleted by centrifugation for 5 min at 900 rpm at 4°C, resuspended in FACS buffer and stained for cell surface markers CD34-eFluor 660 and ITGA6-eFluor 450 for 30 min on ice. Cells were washed with FACS buffer, and 7-aminoactinomycin D (7-AAD) was added to each sample for the detection of live/dead cells 15 min before the analysis. Before the first measurement, flow cytometer settings and compensation settings were calibrated, and antibody dilutions were titrated. Cells were analyzed using FACSCanto II (BD Biosciences) or sorted using FACSAria Illu Svea (BD Biosciences) and FACSAria Fusion (BD Biosciences). Each machine was equipped with FACSDiva software (BD). Sorted cells were collected into 1.5 ml conical tubes with cell culture medium at 4°C, centrifuged, and either snap-frozen in liquid nitrogen or resuspended in medium and cultured. Flow cytometry analysis of processed samples was carried out using FlowJo software. Cells were gated according to their size and granularity (FSC-A/SSC-A), cell doublets were excluded (FSC-W/SSC-H), and live cells were discriminated by 7-AAD (FSC-A/PerC-CP-Cy7). From the live cell population, cells were gated for their expression of α 6-integrin (eFluor 450) and CD34 (eFluor 660).

FACS Antibodies

CD34-eFluor 660 (Thermo Fisher Scientific 50-0341-82)	1:100
ITGA6-eFluor 450 (Thermo Fisher Scientific 48-0495-82)	1:300
7AAD (Thermo)	1:100

FACS buffer

EDTA	2 mM,
FBS (Gibco)	2%
PBS	1x

3.9 Immunofluorescence and confocal microscopy

Tissue preservation is one of the most critical aspects of histochemical techniques that maintains morphology but also allows antibody penetration and antigen preservation. Paraformaldehyde or glutaraldehyde fix the tissue by reacting with alkaline amino acid residues, thereby crosslinking neighboring proteins. Methanol, ethanol, or acetone fix the tissue by denaturing wherein the solubility of proteins gets reduced due to the disruption of tertiary protein structures.

Embedding fixed tissue into paraffin wax maintains tissue architecture and enables cutting of thin sections. Unfixed tissues can be cryopreserved and inserted into a cryo-resisting matrix that allows sectioning at temperatures below -10 °C.

Laser confocal scanning microscopy (LCSM) is an optical imaging technique that uses a spatial pinhole to block out-of-focus light during imaging, which increases optical resolution and contrast and removes blur from outside of the focal plane of the image [346].

3.9.1 Paraffin sections

Mice were sacrificed at indicated time points, and tissue samples were taken. The samples were wrapped in filter paper to avoid tissue deformation during tissue processing. The isolated samples in filter paper were placed into embedding cassettes and transferred into freshly prepared, ice-cold paraformaldehyde (4 % PFA in phosphate-buffered saline (PBS)) and incubated 1-2 h on ice for fixation. Subsequently, the fixed samples were transferred to 70 % ethanol and incubated at 4 °C overnight. For dehydration and paraffin processing, samples were placed into an automated tissue-processing machine (detailed program below). Embedding into paraffin was done using the embedding machine. Paraffin blocks were stored at room temperature (RT) until cutting. Before cutting, paraffin blocks were cooled to -20 °C, and 6-8 µm sections were cut using the microtome. Sections were floated on water at 45 °C for at least 5 min to ensure tissue straightening. Slides were dried overnight at 37 °C and stored at RT.

Paraffin sections were deparaffinized, two times for 5 min Xylol, followed by rehydration using a graded alcohol series (100 % isopropanol, 95 %, 75 %, 50 % ethanol, and distilled water; 5 min each). Antigen retrieval releases protein crosslinks

that were formed during formalin fixation, and hidden antigen sites are uncovered. It was carried out using a target retrieval solution pH6 (Dako S1699) or pH9 (Dako S2367) in a pressure cooker, where samples are cooked in high pressure for 20 min followed by 1 h of cooling. Slides were then stained as described below.

Tissue processor program

70 % ethanol 1,5 h

80 % ethanol 1,5 h

96 % ethanol 1,5 h

100 % ethanol 1 h

100 % ethanol 1 h

Xylol 1,5 h

Xylol 1,5 h

Paraffin 2 h

Paraffin 2 h

Paraffin 2 h

3.9.2 Cryo-sections

For cryo-sections, unfixed tissue samples were placed into cryomolds containing OCT Tissue Tek and allowed to freeze on dry ice. Frozen blocks were stored at -80 °C, and 6-8 µm thick sections were cut at -20 °C using the cryostat. Sections were stored at -80 °C or immediately processed for stainings. For staining, cryosections were then air-dried for 20 min and fixed with the indicated fixative (see table for primary antibodies). Fixation was carried out as follows:

For acetone and methanol fixation, dried slides were covered with ice-cold acetone/methanol and incubated at -20 °C for 10 min. Acetone/methanol was then removed, and slides were rehydrated with PBS.

For PFA fixation sections were covered with freshly prepared, ice cold 4 % PFA in PBS and incubated for 10 min at RT. The fixative was then removed, and slides were washed with PBS. The tissue was subsequently permeabilized by treatment with 0,2 % Triton-X-100 in PBS for 10 min at RT.

For both paraffin and cryofixed sections, samples were blocked in 5% normal goat serum, 3% BSA in PBS for 1 h at RT, and incubated with primary antibodies diluted in DAKO antibody diluent (Agilent, S3022) overnight in a moist chamber at 4°C. Subsequently, slides were washed 3 times for 5 min with PBS and bound primary antibody was detected by incubated with Alexa-Fluor 488-, 568- or 647 -conjugated antibodies (Invitrogen) for 1 h at RT in the dark. Nuclei were counterstained with 4', 6-diamidino-2-phenylindole (DAPI, Invitrogen). After washing slides 3x with PBS and a quick wash with H₂O, they were mounted in Elvanol and dried at RT in the dark.

Elvanol

Mowiol (Roth 0713) 2.4 g

Glycerol 7.5 ml

Milli-Q water 11.7 ml

=> stirred for 2 h at RT

Tris-HCl, pH 8.5 4.8 ml

=> stirred at 53 °C until dissolved

Dabco (Roth 0718) 0.02 g

=> stored at -20 °C

Primary antibodies

CD34	Thermo Fisher (14-0341-82)	1:100
Sox9	Santa Cruz (sc-20095)	1:100
Keratin-15	Thermo Fisher (MS-1068)	1:300
pMLC2	Cell Signaling (#3674)	1:100
RNAPII pS2	Abcam (ab5095)	1:900
Ki67	Abcam (ab15580)	1:1000
Lef1	Cell Signaling (#2230)	1:100
E-Cadherin	BD Biosciences (610181)	1:300
Laminin-332	gift from R.E. Burgeson [347]	1:20,000
Laminin α 5	gift from L. Sorokin [348]	1:20,000

Secondary antibodies

Goat anti-guinea pig IgG	A488	Invitrogen 982288
Goat anti-mouse IgG	A488	Invitrogen A11001
Goat anti-mouse IgG	A568	Invitrogen A11004
Goat anti-mouse IgM	A488	Invitrogen A21042
Goat anti-rabbit IgG	A488	Invitrogen A11008
Goat anti-rabbit IgG	A568	Invitrogen A11011

3.9.3 Hydrogels

Collagen hydrogels were fixed with 4% PFA for 60 min, followed by two washes with 100 mM Glycine, PBS for 10 min. The gels were permeabilized and blocked with 0.3% Triton X-100, 3% BSA, 5% NGS, in PBS at RT overnight, and then incubated with the primary antibody in 0.3% Triton X-100, 1% BSA, in PBS at RT overnight. After three washes with 0.3% Triton X-100, PBS for 10 min, the hydrogels were incubated with the secondary Ab in 0.3% Triton X-100, 1% BSA, in PBS at RT overnight. Samples were washed 3x with 0.3% Triton X-100, in PBS for 10 min, and quickly with H₂O, then mounted in Elvanol and dried at RT in the dark.

3.9.4 Edu staining

5-ethynyl-2'-deoxyuridine (EdU) is a thymidine homolog that is incorporated into DNA during DNA synthesis and can be detected by click chemistry reaction: EdU reacts copper (I)-catalyzed with azide, and the product is a stable triazole ring linked to a fluorophore.

EdU staining was carried out on paraffin sections. Paraffin sections were deparaffinized and rehydrated. Samples were incubated in staining solution for 30 min at RT. After three washes for 5 min in PBS, antigen retrieval and antibody staining were performed as described above.

EdU staining solution

Tris, pH 8,5	100 mM
CuSO ₄	1 mM
488-Azide (Invitrogen A10266)	10 μM

Ascorbic acid

100 mM

3.9.5 H&E staining

Hematoxylin and Eosin (H&E) staining method is a standard histological method that allows the detection of several distinct tissue structures. The principle is based on the application of hemalum, an oxidation product of hematoxylin. Hemalum colors nuclei in blue while Eosin serves as a counterstain and colors eosinophilic structures, mainly structures that are basic, in different shades of red.

Paraffin sections were deparaffinized as described above and stained for 50 s with hematoxylin, then blued in tap water. Sections were counterstained for 10 sec with Eosin and subsequently washed in water. Sections were then dehydrated (50 %, 75 %, 95 % ethanol, isopropanol 2 min each) and washed 2 x 2 min in Xylol. Stained tissues were mounted on No. 1 rectangular coverslips with Cytoseal XYL mounting medium (Thermo). Images of H&E stained tissue samples were obtained using Nikon Eclipse Ci (Nikon) 20x air objective.

Hematoxylin: Shandon Gill3 Hematoxylin

Eosin: Shandon Eosin Y, Aqueous

3.9.6 Confocal microscopy

All fluorescence images were collected by laser scanning confocal microscopy (SP8X; Leica) with Leica Application Suite software (LAS X version 2.0.0.14332), using a 40x, 63x or 100x immersion objectives. Images were acquired at room temperature using sequential scanning of frames of 1 μ m thick confocal planes (pinhole 1), after which the planes were projected as a maximum intensity confocal stack for visualization and sum intensity confocal stack for quantification. Images were collected with the same settings for all samples within an experiment.

3.9.7 Image analyses

Images were analyzed using Fiji [349]. Fields were randomly selected based exclusively on the presence of nuclei, as assessed by DAPI staining. For quantification of nuclear intensities, areas of interest were generated using automated thresholding of the DAPI staining, after which mean fluorescence intensities of nuclear stainings were quantified within the regions of interest from sum projection images obtained as described above.

3.10 Atomic force microscopy

Atomic force microscope (AFM) nanoindentation is a useful tool to determine elastic properties of biological samples and materials. Cantilevers serve as soft nanoindenters allowing local testing of small and inhomogeneous samples like cells, tissues, or materials. The data obtained by indentation measurements (force spectroscopy mode) are plots of force against piezo displacement. The cantilever is moved towards the sample by a distance z (height (measured)) and bending into the opposite direction (x) while the sample is indented by δ . Finally, δ is calculated by subtracting the cantilever deflection from the height (measured). For soft materials and biological samples, the Poisson's ratio is generally set to 0.5 (incompressible materials like rubber). These parameters with the properties and geometry of the indenter are used in the Hertzian model to calculate the Young's modulus of a sample.

3.10.1 Atomic force indentation spectroscopy of hydrogels

We used atomic force indentation spectroscopy with a Bioscope II head (Veeco) mounted onto an Olympus IX73 microscope to determine and validate the elastic modulus of the hydrogels. For these micromechanical measurements, colloidal probes, AFM cantilevers with round tips (CP-PNPL-SiO-B-5, sQube), with a sphere diameter of $3.5 \mu\text{m}$ and nominal spring constants of 0.08 Nm^{-1} were used. For all indentation experiments, forces of up to 3 nN were applied, and the velocities of the cantilever approach and retraction were kept constant at $2 \mu\text{m/s}$, ensuring the detection of elastic properties alone. All measurements were performed at RT. Analyses were performed with AtomicJ v.1.7.2 [350]: Young's modulus of the samples was calculated using the Hertzian model corrected by the tip geometry, and a Poisson's ratio of 0.5

was assumed. Before the fitting, the offset was removed from the baseline of all force curves, the contact point was identified, and cantilever bending was subtracted.

3.10.2 Atomic force indentation spectroscopy of hair follicle basement membranes

AFM measurements of hair follicle basement membranes were performed by Yekaterina A. Miroshnikova (University of Helsinki, Finland) using a JPK NanoWizard 2 (Bruker Nano) atomic force microscope mounted on an Olympus IX73 inverted fluorescent microscope (Olympus) and operated via JPK SPM Control Software v.5. Freshly cut 16 μm cryosections were equilibrated in PBS supplemented with protease inhibitors, and measurements were performed within 20 min of thawing the samples. Triangular non-conductive Silicon Nitride cantilevers (MLCT, Bruker Daltonics) with a nominal spring constant of 0.01 Nm^{-1} were used for the nanoindentation experiments of the apical surface of cells and the nucleus. For all indentation experiments, forces of up to 3 nN were applied, and the velocities of the cantilever approach and retraction were kept constant at 2 $\mu\text{m s}^{-1}$, ensuring an indentation depth of 500 nm. Analyses were performed with JPK Data Processing Software (Bruker Nano). Before fitting the Hertz model corrected by the tip geometry to obtain Young's Modulus (Poisson's ratio of 0.5), the offset was removed from the baseline, contact point was identified, and cantilever bending was subtracted from all force curves.

3.11 RNA isolation

The RNeasy Plus Mini Kit or Micro Kit (Qiagen), depending on the amount of material, was used for RNA isolation following the manufacturer's instructions. In brief, cells or tissue extracts were lysed in RNA lysis buffer and homogenized on ice by passing them through a 20 G needle five times. Genomic DNA was removed by passing the RNA lysate through a gDNA eliminator column (Qiagen). Ethanol was added to precipitate the RNA that is subsequently trapped in a spin column. After washing, the RNA is finally eluted in distilled water. RNA was either used directly for downstream applications or stored at $-80\text{ }^{\circ}\text{C}$.

3.12 RNA sequencing and analysis

3.12.1 RNA-seq library construction

HFSCs were purified from the freshly isolated epidermis using flow cytometry and RNA isolated as described above. After the quantification and quality control using Agilent 2200 TapeStation, total RNA amounts were adjusted, and libraries were prepared using the Ovation RNA-Seq System V2 (NuGen) followed by subsequent library preparation using the Nextera XT library preparation kit (Illumina). Paired-end RNA sequencing was carried out on Illumina HiSeq3000 machines by using the 2x150-bp protocol and three biological replicates per condition.

3.12.2 Bioinformatic analysis

After quality control with FastQC v.0.11.2 [351], adapter sequences were removed with Flexbar [352]. After preprocessing, reads were mapped to the mouse reference genome build GRCm38.p5 using STAR version 2.5.2b [353]. Gene expression was subsequently estimated using featureCounts version v1.6.2 [354]. FeatureCounts results were aggregated over all samples, and differential gene expression was calculated using the R package DEseq2 version 1.22.2 [355]. Genes with an adjusted p-value ≤ 0.05 were considered significant. Gene set enrichment analysis was performed on a pre-ranked gene list (ranked according to log₂ fold change) and compared to the Broad Institute Molecular Signatures Database collection of chemical and genetic perturbations (C2 CGP, a total of 3395 gene sets) using the web-based tool available from the Broad Institute [356]. Enrichments with an FDR value < 0.25 were considered significant. Further gene ontology term analyses were performed using Homer v4.10 [357] as well as Metascape [358]. DeepTools version 3.3.1 [359] was used to calculate the correlation between samples, normalize reads to 1x depth of coverage, and generate heatmaps. Sequencing tracks were visualized with Integrative Genomics Viewer version 2.4.14 [360].

3.13 ATAC sequencing and analysis

ATAC-seq is a technique used to assess genome-wide chromatin accessibility and requires only a low number of cells. Next-generation sequencing (NGS) adapters are coupled to the hyperactive transposase Tn5, which allows simultaneous fragmentation of chromatin and integration of those adapters into open chromatin regions. Sequenced libraries can then be analyzed for areas of the genome with open or accessible chromatin.

3.13.1 ATAC-library construction

ATAC-seq libraries were prepared as previously described [361]. Briefly, nuclei of 50K freshly FACS-sorted single HFSCs were prepared by lysing cells with cold lysis buffer for 15 min on ice. Nuclei were then collected by spinning at 6000 g for 10 min at 4°C, resuspended in Tagment DNA Buffer and Tagment DNA Enzyme (TruSight One Kit), and incubated for 30 min at 37°C. Samples were purified with MinElute PCR purification kit (QIAGEN) and PCR-amplified with 10-12 cycles. Concentration and quality of Libraries were confirmed with D1000 Tape Station (Agilent) before sequencing. Libraries were paired-end sequenced with the 2x75bp protocol on Illumina HiSeq4000 according to manufacturer's instruction.

ATAC-Lysis buffer

Tris-HCl, pH 7.4	10 mM
NaCl	10 mM
MgCl ₂	3 mM
IGEPAL CA-630	0,1%

3.13.2 Bioinformatic analysis

Nextera adapters were trimmed using Flexbar version 2.5. [352] and reads aligned against the GRCm38.81 mouse genome using BWA MEM version 0.7.12 [362] using standard parameters. Differential peaks were called and analyzed using THOR version 0.1 [363]. DeepTools version 3.3.1 [359] was used to calculate the correlation between samples, normalize reads to 1x depth of coverage, and generate heatmaps. Sequencing tracks were visualized with Integrative Genomics Viewer version 2.4.14 [360]. Annotation of peaks and genome ontology was done with Homer v4.10 [357]. Gene ontology term analyses were performed using Homer as well as Metascape [358]. Genomic annotations were visualized using ChIPseeker version 1.2.6 [364]. ChIP datasets on H3K4me3 and H3K27me3 in HFSCs were downloaded from GSE31239 to compare differential ATAC seq peaks with chromatin features. These data sets were mapped as described above. Heatmaps of the H3K27me3 and H3K4me3 signal over the differential peak regions were then generated with Deeptools and split into 5 clusters using the k-means algorithm. Clusters were annotated and analyzed with Homer and Metascape.

3.14 qPCR

Quantitative real-time polymerase chain reaction (q-PCR) is a PCR-based method that detects and visualizes the amplified DNA product using fluorescent dyes in real-time. This method is used to measure gene expression at the RNA level quantitatively.

After RNA isolation, quantification, and quality control (as described above), RNA was subjected to reverse transcription using SuperScript VILO Master Mix (Thermo) following the manufacturer's protocol. PCR was performed with CFX384 Touch Real-Time PCR Detection System (Bio-Rad) using the PowerUp SYBR Green Mastermix (Thermo).

Gene expression changes were quantified using normalization to Actb, followed by the comparative Ct (cycle threshold) method with primer efficiency correction:

Efficiency (E) was calculated from the slopes of a cDNA dilution (1:5, 1:10, 1:20) calibration curve according to the equation: $E = 10^{(-1/\text{slope})}$

The calculation of the ratio was made according to the equation:

$$\text{Ratio} = ((E_{\text{target}})^{\Delta C_{\text{t target}}(\text{control-sample})}) / ((E_{\text{reference}})^{\Delta C_{\text{t reference}}(\text{control-sample})})$$

ΔC_{t} = crossing point difference of cyclic threshold

All primers were designed to span exons. The following primer sequences were used:

Gene	Forward Sequence	Reverse Sequence
Actb	TCAAGATCATTGCTCCTCCTG	TACTTCTGCTTGCTGATCCAC
Bmp4	CAGGGCTTCCACCGTATAAA	CAGGGCTCACATCGAAAGTT
Ccnd2	GCAGACCTTCATCGCTCTGT	CAGGCTTTGAGACAATCCACAT
Ccne1	AAGGGAGAGAGACTCGACGG	TGGGTCTTGCAAAAACACGG
Cdc34	ACCCAAACATCTATGAGACAGGG	ACTCTGTGGGTTCGTCAACTG
Cdk11	CTTCACGAGCTGGATCGGTA	TGGTCCAGTGAGAAGCCGTG
Hmga2	CCCTCTAAAGCAGCCCAGAA	GTTGTGGCCATTTCTAGGTC
Lef1	GTCCGAAATCATCCCAGCCA	TGCTTTCCTTCATCAGGGTGT
Rspo3	GACAGTTGCCCAGAAGGGTT	TGGCCTCACAGTGTACAATACT
Wnt2b	TAGACACGTCCTGGTGGTACA	TAGCATAGACGAACGCTGCC
Wnt7a	TTTCAGTTCCGAAATGGCCG	ATCGCATAGGTGAAGGCAGC

cDNA synthesis reaction (SuperScript VILO Master Mix (Thermo))

RT Mastermix 4 μ l

RNA 0.1 μ g

adjusted to 20 μ l with RNase-free water

cDNA synthesis program

25 °C 10 min

37 °C 2 h

85 °C 5 min

hold at 4 °C, cDNA was stored at -20 °C

qPCR reaction

(Measurements were always performed in quadruplicates)

2X SYBR Green PowerUp (Thermo)	5 μ l
primers (10 μ M)	0.5 μ l
cDNA (diluted 1:5)	0.5 μ l
Nuclease-free water	4 μ l

3.15 Nascent RNA analysis

Nascent RNA was captured with the Click-iT® Nascent RNA Capture Kit (ThermoFisher C10365) to study changes in the transcriptome and newly synthesized mRNA. This kit facilitates the partitioning of the freshly synthesized transcripts from the already existing RNA. The captured transcripts can then be used as a template for cDNA synthesis and subsequent analysis using qPCR. The first step is the incubation of cells with an analog of uridine, 5-ethynyl uridine (EU, an alkyne-modified nucleoside), which is efficiently and naturally incorporated into the nascent RNA. After the incubation, total RNA is isolated and used in a copper-catalyzed click reaction with azide-modified biotin, which allows capturing nascent RNA transcripts on streptavidin magnetic beads.

3 h before sample collection 2 mM EU (Jena Bioscience CLK-N002) was added to the medium. Total RNA was then isolated using the RNeasy Plus Mini Kit (Qiagen), as described above. The Click-iT® Nascent RNA Capture Kit was subsequently used to isolate nascent RNA, following the manufacturer's instructions: 1 μ g of EU-labeled RNA was biotinylated with 0.5 mM biotin azide in Click-iT reaction buffer for 30 min. The samples were subjected to ethanol precipitation and resuspended in distilled water. RNA binding reaction mix including the biotinylated RNAs was heated at 68°C for 5 min and then mixed with Dynabeads MyOne Streptavidin T1 magnetic beads, followed by incubation at room temperature for 30 min while gently vortexing. The beads were immobilized using the DynaMag-2 magnet and washed with Click-iT wash buffer 1 and 2. The washed beads were resuspended in 1x SuperScript VILO Master Mix (Thermo) and used for cDNA synthesis. qPCR was performed as described above. All primers were designed to span Intron-Exon junctions. Following primers were used:

Gene	Forward Sequence	Reverse Sequence
Actb	CAGTGAGGTAAGCCACGAG	TTTGCAGCTCCTTCGTTGCC
Hmga2	AATCCTCCTCTGCGGACTCT	CAGGCGACTCCTGGTTACAG
Krt14	GGGACAATACAGGGGCTCTTC	GGCAGAGGAGACAGCCTATTT
Lef1	CCCGGCAATCCATTTTTAGCC	TACCACCTCGAGAGGGAACA
Rspo3	TGTTTTCTGCTGGTCTGGG	ACCAAGGAGGATATAATTGAATGGG
Tubb5	TCTGACGGGTGGAGAATGC	GAGGGAAATCGTGACATCC
Wnt2b	ACCCGAGTTGTGTCATACCC	AGGGTACCCAGAGTGGCATA
Wnt7a	TGGTCCAGCACGTCTTAGTG	AAAGCCGTAGCTGGCTAACA

3.16 Chromatin immunoprecipitation

Chromatin Immunoprecipitation (ChIP) coupled with quantitative PCR can be used to detect protein-DNA interaction at known genomic sites. We used ChIP-qPCR to study epigenetic changes:

Cells were crosslinked with 0.25% methanol free formaldehyde (ThermoFisher 28906) in Fixation Buffer. Fixation was terminated by adding 0.125 M glycine in PBS for 5 min at RT. Cells were subsequently washed twice with PBS, after which cells were pelleted by centrifugation at 5000 rpm for 10 min at 4°C. Cell pellets were lysed in lysis buffer after which nuclei were passed through 10 strokes of Dounce homogenization to aid nuclear release. Lysates were sonicated using a Covaris M220 ultrasonicator (4-9 °C temperature range; 15% duty factor 75% peak power) for 10 min to fragment DNA. After sonication, samples were subjected to centrifugation at 21000xg for 5 min at 4 °C, and the supernatant was collected as the chromatin fraction. DNA concentration was measured using the Qubit DS High-sensitivity kit (Invitrogen), and sample concentrations were adjusted to be equal. 10% of chromatin was collected as input, and 2 μ l was analyzed using Agilent 2200 TapeStation to ensure optimal shearing (200-800 bp fragments), and the rest was subjected to immunoprecipitation. For this, 380 μ l of ChIP dilution buffer and 3 μ g of antibody (H3K27me3 Cell Signaling #9733, or IgG control Cell Signaling #5415) were added and samples were incubated in an end-over mixer for 16 h at 4 °C. 30 μ l protein G Dynabeads were subsequently added

to each sample, which were then further rotated in an end-over mixer for 4 h at 4 °C. Beads were collected using a magnet and washed once with ChIP dilution buffer, followed by washes in wash buffer 1, wash buffer 2, and finally with 20 mM Tris pH 8,0, 1 mM EDTA. Samples were subsequently eluted in 50 mM Tris pH 8.0, 0,1 mM EDTA, 1% SDS at 65 °C for 30 min. 8 μ l 1M NaCl and 5 μ l of 20mg/mL Proteinase K were added to the samples to reverse crosslinks, which were then incubated first 3h at 42 °C, and then 65 °C for 16 h. Subsequently, 10mg/ml RNAse A was added for 2 h 37 °C. DNA was purified by phenol:chloroform extraction, followed by ethanol precipitation, after which DNA content was quantified using Qubit.

ChIP DNA was analyzed by qPCR as described above and ChIP DNA was normalized to input DNA to get the enrichment as percentage of input. % input was calculated according to the equation:

$$\% \text{ input} = 2^{-\Delta\text{Ct}} \times 100$$

$$\Delta\text{Ct} = \text{Ct ChIP DNA} - (\text{Ct input} - \text{DF})$$

$$\text{DF (dilution factor)} = \log_2 (10\%)$$

Samples were analyzed by qPCR using the following primers:

Gene	Forward Sequence	Reverse Sequence
Actb	CCGTAAAGACCTCTATGCCAACAC	GCTAGGAGCCAGAGCAGTAATCTC
B2M	AGGAGACTGGTGACGACCTC	GGCGCGCGCTCTTATATAGT
Bmp4	GTCTCTTTACAGCGCCGACA	ATGGAACGCTGTTCGTGAGG
Bmp7	GACCCGAGGTCACTTGCTG	GAGTAAAGGACAGGGGCGTC
Gapdh	TGAAATGTGCACGCACCAAG	GGAACCATCACCCGGTCAC
Hmga2	TACTGGGACGCTCGGCA	TTCTTTCCCCGCCTAACATTTTC
Lef1	GCGATCCCCAGAAGGAGAAG	CTGGCTGGGATGATTTTCGGA
Rps26	ACTTTCAGGTCCCTACCGTC	AAGATGGTGAGTGTTCGCCG
Rspo3	GAAAACCAGAGCAGCGGGA	GGCTGTGTTTCGGACAATTTGA
Tubb5	CTGAAAGGATGGACCGGAGC	TAGAACCTTCCTGCGGTCGT
Wnt2b	AGAGCAATGCACTCGTTCCA	GTGTAGACACGTCCTGGTGG
Wnt7a	TGCCGGATCTACTGTGCTTG	GCACGCAATTCCACAGACTC

Fixation Buffer

Hepes-KOH, pH 7.5	50 mM
NaCl	100 mM
EDTA, pH 8.0	1 mM
EGTA, pH 8.0	0.5 mM
Tris-HCl pH 8	25 mM

Lysis buffer

Tris-HCl pH 8	25 mM
EDTA	2 mM
SDS	0.5%
Protease inhibitor	

ChIP dilution buffer

Tris-HCl pH 8.1	20 mM
EDTA	2 mM
NaCl	150 mM
TritonX-100	1%

Wash buffer 1

Hepes pH 7.9	50 mM
NaCl	500 mM
EDTA	1mM
Triton X-100	1%
Na-deoxycholate	0.1%
SDS	0.1%

Wash buffer 2

Tris pH 8.0	20 mM
EDTA	1 mM
LiCl	250 mM
NP-40	0.5%
Na-deoxycholate	0.5%

3.17 Mass spectrometry

Mass spectrometry is a sensitive technique used to detect, identify and quantitate molecules based on their mass-to-charge ratio. This can give qualitative and quantitative information on the elemental, isotopic, and molecular composition of samples. In Proteomics, mass spectrometry is used to identify and quantify a protein from the mass of its peptide fragments.

3.17.1 Protein and peptide sample preparation

Back skin of mice (200 mg wet weight) were snap frozen in liquid nitrogen and crushed using a mortar and pestle. Samples were resuspended in GdmCl reduction and alkylation buffer (6M GdmCl, 20mM TCEP, 80mM CAA, 100mM Tris pH 8.5), boiled for 10 min to denature proteins and subsequently mixed (six times for 30 s, cooled on ice in-between) using a FastPrep-24 instrument (MP Biomedicals). Lysates were then sonicated using a Bioruptor sonicator (Diagenode) (15 cycles of 30 s) and diluted with 25mM Tris, pH 8.5. 200 μ g of protein was subsequently digested overnight with Lys-C (Promega Corp., VA1170) and Trypsin-Gold (Promega Corp., V5280) in a 1:50 ratio at 37 °C. On the following day, samples were sonicated again and further digested for 3 h with Lys-C and trypsin (1:100 ratio). Following digestion samples were acidified to block trypsin activity and peptides were cleaned with custom-packed C18-SD STAGE tips [365].

3.17.2 TMT labeling, mass spectrometry and analysis

The following steps were performed by Xinping Li and Ilian Atanassov from the MPI-AGE Mass Spectrometry facility, Cologne:

Four micrograms of desalted peptides were labeled with tandem mass tags (TMT10plex, Thermo Fisher cat. No 90110) using a 1:20 ratio of peptides to TMT reagent. TMT labeling was carried out according to manufacturer's instruction with the following changes: dried peptides were reconstituted in 9 μ L 0.1M TEAB to which 7 μ L TMT reagent in acetonitrile (ACN) was added to a final ACN concentration of 43.75%, after 60 min of incubation at room temperature the reaction was quenched with 2 μ L 5% hydroxylamine. Labeled peptides were pooled, dried, resuspended in 0.1% formic

acid (FA), split into two samples, and desalted using home-made C18 STAGE tips [365]. One of the two samples was fractionated on a 150mm, 300 μ m, 2 μ m C18, AcclaimPepMap (Product No. 164537, Thermo Fisher) column using a Ultimate3000 (Thermo Fisher). The column was maintained at 30°C. Buffer A was 5% acetonitrile 0.01M ammonium bicarbonate, buffer B was 80% acetonitrile 0.01M ammonium bicarbonate. Separation was performed using a segmented gradient from 1% to 50% buffer B, for 90min and 50% to 95% for 20 min with a flow of 4 μ L/min. Fractions were collected every 150 sec and combined into nine fractions by pooling every ninth fraction. Pooled fractions were dried in Concentrator plus (Eppendorf), resuspended in 2 μ L 0.1% FA for mass spectrometric analysis. Peptides were separated on a 50cm, 75 μ m Acclaim PepMap column (Product No. 164942 ThermoFisher) using a 120min linear, 6% to 31% buffer B; buffer A was 0.1% FA, buffer B was 0.1% FA, 80% ACN. The column was maintained at 50°C. Eluting peptides were analyzed on an Orbitrap Lumos Tribrid mass spectrometer (Thermo Fisher). Synchronous precursor selection based MS3 was used for TMT reporter ion signal measurements. Proteomics data was analysed using MaxQuant version 1.5.2.8 [366]. Differential expression analysis was performed using limma [367] in R.

3.18 Skin decellularization

Decellularization is the process to isolate the extracellular matrix (ECM) of a tissue from its inhabiting cells, leaving an intact ECM scaffold of the original tissue. Skin scaffolds were generated to study the effect of changes within the ECM on cells:

Back skin of mice was shaved and remaining hair was removed by depilation cream. 2 cm x 2 cm pieces were dissected and incubated in 0.02% Trypsin 0.5 mM EDTA for 2 h at 37°C to remove cells. Biopsies were then washed three times in DMEM, 10% fetal calf serum (FCS) to neutralize trypsin and subsequently incubated in 3% Triton-X for 3h and then in 4% Sodium deoxycholate for 3h on a shaker. After three washes in DMEM, 10% FCS biopsies were transferred to 24 well Cell Culture Inserts (Merck PIHP01250). 1x10⁶ HFSCs were added into the inserts, spun down briefly with centrifugation and cultured for 2d in 3C medium. Biopsies were subsequently switched to high Calcium (1 mM) 3C medium and cultured for another 2d prior to fixation in 4% PFA and immunofluorescence.

3.19 Statistics and reproducibility

Statistical analyses were performed using GraphPad Prism software (GraphPad, version 8). Statistical significance was determined by the specific tests indicated in the corresponding figure legends. In all cases where a test for normally distributed data was used, normal distribution was confirmed with the Kolmogorov–Smirnov test ($\alpha = 0.05$). All experiments presented in the manuscript were repeated at least in 3 independent experiments/biological replicates.

3.20 Data availability

All analysis scripts and data that support the conclusions are available on request. Sequencing data has been deposited at GEO (GSE148619). The proteomics data have been deposited to the ProteomeXchange Consortium via the PRIDE partner repository [368] with the dataset identifier PXD018352.

4 Results

All multicellular organisms undergo a decline in tissue and organ function as they age. Loss over time in SC number, activity, or both have been proposed to be responsible for this decline [5]. Consistent with the SC aging hypothesis, SC aging phenotypes have been described for multiple tissues, including the hematopoietic system, intestine, muscle, brain, skin, and germline [369]. However, how aging impacts adult SCs function, and thus tissue maintenance is not clear.

4.1 Ageing induces HFSC exhaustion

In the skin, aging is associated with reduced potency of HFSCs, already at stages where HFSCs are still present at numbers comparable to young mice [327-329]. Later during aging, severe hair loss has been reported, which is associated with hair follicle destruction and reduced HFSC numbers [330]. We were interested in identifying primary causes of loss of HFSC potency, and thus sought to study the stage in which the decline of HFSC numbers was initiated as a sign of HFSC exhaustion and the onset of aging. A previous PhD student from our lab, Sushmita Ghatak, found a robust and reproducible reduction of HFSCs in 24 months old mice in independent young/aged mouse cohorts from 3 mouse facilities, irrespective of HF density or HF activation state [370]. Consistent with these previous results, we found that the hair coat of 6 months and 24 months old mice appeared normal (Fig. 7 A) as well as the hair follicle morphology, assessed by immunofluorescence staining for the HFSC marker CD34 (Fig. 7 B, C). FACS analysis using the markers integrin $\alpha 6$ and CD34 confirmed a reduction of stem cells (Fig. 7 D).

These results prompted us to investigate the cause of stem cell reduction further. For this, we utilized next-generation sequencing techniques, to further characterize differences between young and aged HFSCs. With RNA-sequencing, we analyzed the transcriptome, and with ATAC-sequencing, we assessed age-dependent alterations in genome-wide chromatin accessibility. Finally, we overlaid these data sets with published ChIP-sequencing data [162] to identify the epigenetic context in which these differences occur (Fig. 8).

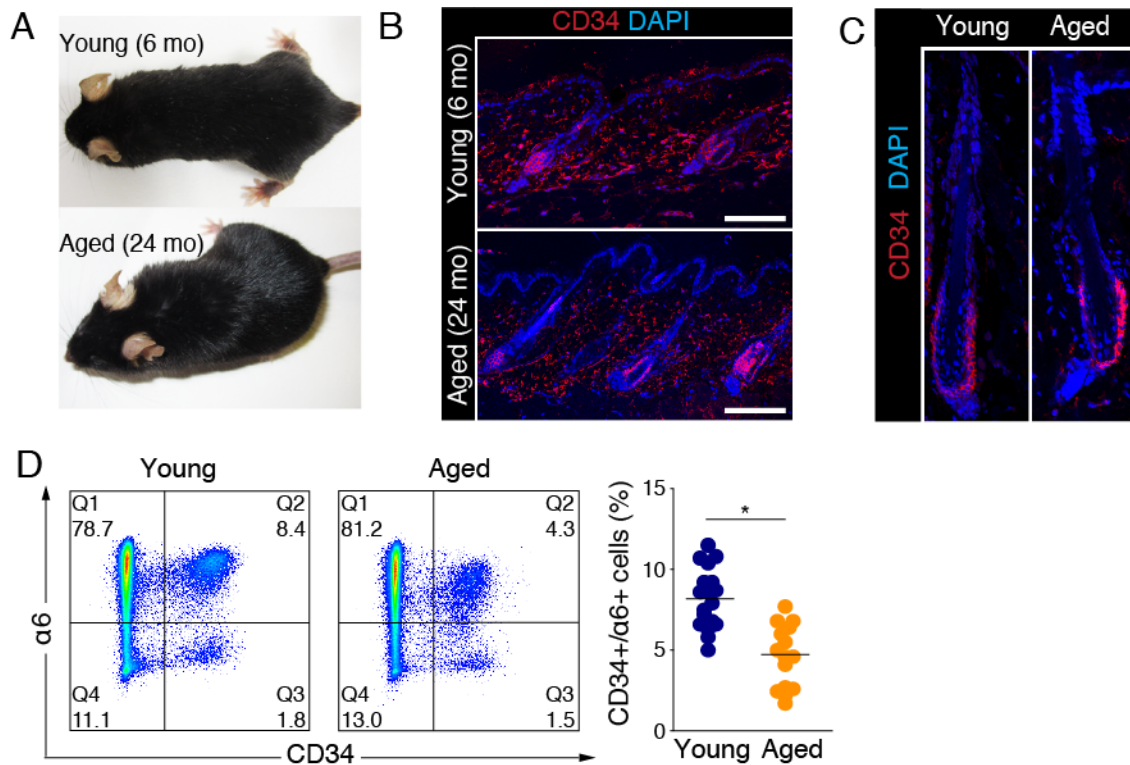


Fig. 7. Aging is associated with loss of HFSCs

A. Representative images of young (6 month) and aged (24 month) mice show no visible differences in haircoats. **B.** Representative CD34 (magenta) and nuclear (dapi; cyan) immunofluorescence images of hair follicle density from young (6 months) and old (24 months) mice shows no difference. Scale bar 100 μ m. **C.** Immunofluorescence images of HF from young adult and aged mice. Note comparable hair follicle morphology and presence of CD34-positive HFSCs within the bulge niche. Scale bar 30 μ m. **D.** Representative FACS plots and quantification of CD34 and α 6 integrin-stained young and aged epidermal cells. Quantification of cells (%) in each quadrant (Q) is shown. Note reduced numbers of CD34+/ α 6 integrin+ cells in aged skin (n=16 mice/group; *p=0.0327, student's t-test).

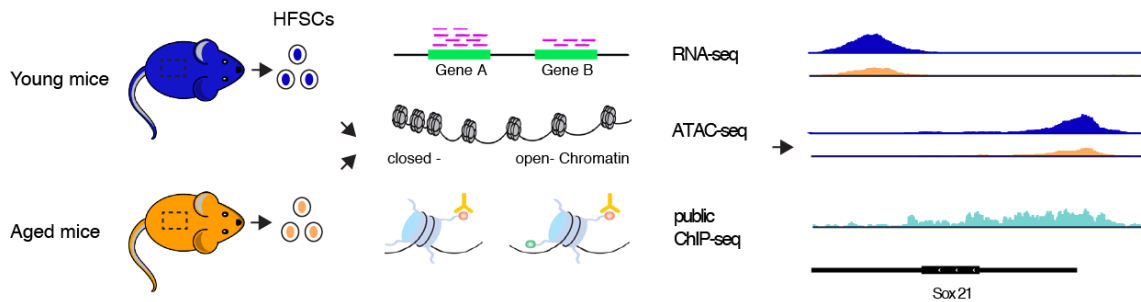


Fig. 8. Next generation sequencing analysis of young and aged HFSCs

Schematic representation of approaches and workflow. We used next-generation sequencing techniques to characterize young and aged HFSCs. RNA-sequencing was used to analyze the transcriptome, and ATAC-sequencing to assess age-dependent alterations in genome-wide chromatin accessibility. We then overlaid these data sets with published ChIP-sequencing data. Adapted from [371].

4.2 Minor differences in the transcriptomes of young and aged HFSCs

We used high-throughput RNA sequencing to transcriptionally profile young (yHFSCs) and aged HFSCs (aHFSCs) and explore the molecular mechanisms underlying age-dependent HFSC reduction. However, we found only 112 genes up-regulated and 227 genes down-regulated in aHFSCs (n=3 mice/group; $p_{adj} < 0.05$; Fig. 3 A). Pathway analysis of the genes up-regulated in aHFSCs revealed genes that play a role in the differentiation of various cell types, like osteoblasts (Rorb, Ahr, Mef2c) and neural crest cells (Gata6, Espn, Slc1a3, Mef2c), response to wounding (Anxa6, Smoc2, Gata6, Itgb3), Actin cytoskeleton organization (Fhod3, Espn, Baiap2, Washc2c) and extracellular structure organization (Smoc2, Tnxb, Aebp1, Itgb3) (Fig. 9 B). Further analysis of transcription factor motifs at the promoter regions of these genes showed an enrichment of the NF1 – family motif (Fig. 9 C). Interestingly, recent research suggests that the NF1 family safeguards the HFSC epigenome [372]. GO-term analysis of down-regulated genes in aHFSCs discovered genes that play a role, amongst others, in ribonucleoprotein complex biogenesis (Rps7, Rps8, Rpl5, Rpl7), oxidative phosphorylation (Mdh1, Pnp, Hprt1, Paics), signaling by hedgehog (Hhip, Prkar2b, Ptch1, Epha4) and cell cycle (Bod1, Map9, Bup3, Znf207) (Fig. 9 D). Analysis of TF motif binding sites displayed enrichment for Elk4, Elf1, Sp5, Egr1, and Gabpa (Fig. 9 E). Interestingly Sp5 is a direct target of beta-catenin and was shown to repress

epidermal differentiation gene expression during hair follicle development [373] and to diminish the expression of genes previously activated by the WNT pathway [374]. *Egr1* is a downstream target of ERK signaling and involved, among other things, in cell growth and proliferation [375, 376]. It has also been shown to respond downstream of mechanical cues [377]. As a next step, we overlaid the differentially expressed genes with genes, previously identified as HFSC signature [162]. We found that 29 of those signature genes overlapped with down-regulated genes, while 12 genes are up-regulated in aHFSCs (Fig. 9 F). These results imply that the identity of old HFSCs becomes less well defined, translation and cell cycling are reduced while processes such as extracellular structure organization and cytoskeleton organization are increased.

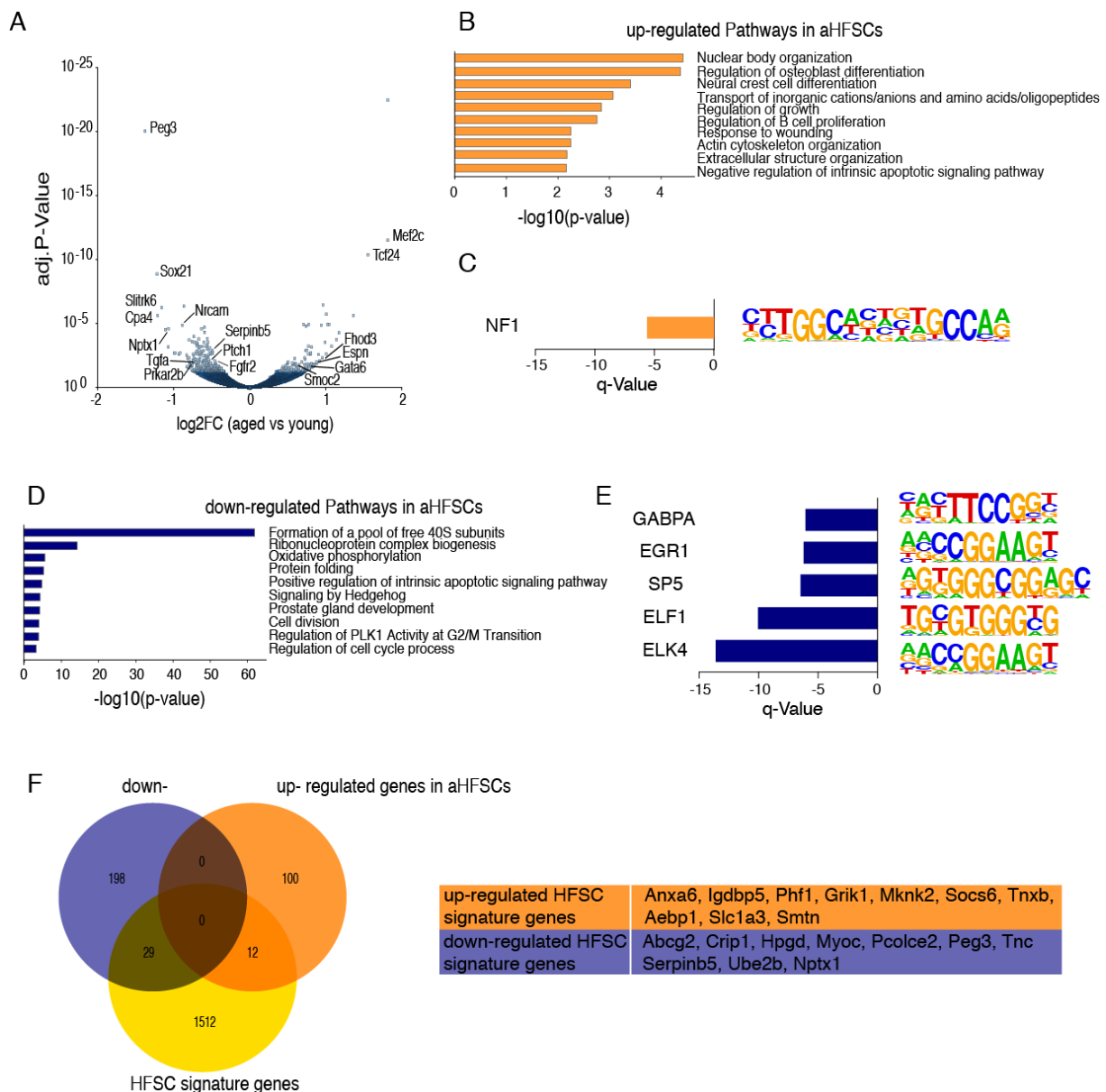


Fig. 9. Minor changes in the aging transcriptome of HFSCs

A. Volcano plot of significantly altered transcripts in young and aged HFSCs. Genes involved in differentiation such as *Mef2c* and *Gata6* are upregulated in aHFSCs, whereas cell cycle and SHH associated genes are downregulated ($n=3$ mice/group; $p_{adj}<0.05$). **B.** Gene ontology term analyses of up-regulated genes with age implicate differentiation processes, response to wounding, actin cytoskeleton organization and extracellular structure organization. **C.** Motif scanning of up-regulated promoters indicate a possible role of the NF-1 transcription factor family. **D.** Gene ontology term analyses of down-regulated transcripts in aHFSCs implicate ribonucleoprotein complex biogenesis, oxidative phosphorylation, signaling by hedgehog and cell cycle. **E.** Analysis of TF motif binding sites showed enrichment for *Elk4*, *Elf1*, *Sp5*, *Egr1*, and *Gabpa*. **F.** Overlap of differential expressed genes with HFSC signature genes [162] revealed 29 HFSC signature genes are down-regulated, while 12 are up-regulated in aHFSCs.

4.3 ATAC-seq reveals reduced chromatin accessibility in aHFSCs

Since the rather small changes in the transcriptome of aHFSCs seemed not to fully explain the stem cell exhaustion, we proceeded to analyze the state of chromatin more globally. We used genome-wide transposase-accessible chromatin sequencing (ATAC-seq) [361] to determine the genome-wide chromatin accessibility landscape in FACS-purified young and aged HFSCs. ATAC-seq incorporates a genetically engineered hyperactive Tn5 transposase that simultaneously cuts open chromatin and ligates high-throughput sequencing adapters to these regions, which can then be sequenced. We assessed differential accessibility between these two groups and discovered that young HFSCs showed significantly more accessible genomic regions than aged (6745 in young/ 1104 in aged; Fig. 10 A). Although the overall distribution of reads was comparable in young and aged HFSCs, the differentially accessible regions were enriched for promoters and CpG islands in young (1154 peaks at promoters in young, 90 peaks at promoters in old), and enriched for retroviral elements in old (Fig. 10 B, C). This finding suggests that accessibility was specifically lost at promoters of coding genes in aged HFSCs and gained in non-coding areas. Transposable elements and intergenic regions are typically silenced by H3K9me3 [378]. Consistently, we observed a reduction in overall constitutive heterochromatin marked by H3K9me3 in the aged HFSCs through immunofluorescence staining (Fig. 10 D), following previous studies indicating loss of heterochromatinization upon aging

[379]. Interestingly, we found in our staining facultative heterochromatin, marked by H3K27me3, increased in aged HFSCs (Fig. 10 D). This observation might explain the reduced accessibility at promoters.

Gene ontology (GO)-term analyses implicated in particular genes involved in tissue development and cell differentiation to be less accessible in aged HFSCs. In contrast, genes involved in actin cytoskeleton organization and regulation of cell adhesion are more accessible (Fig. 10 E).

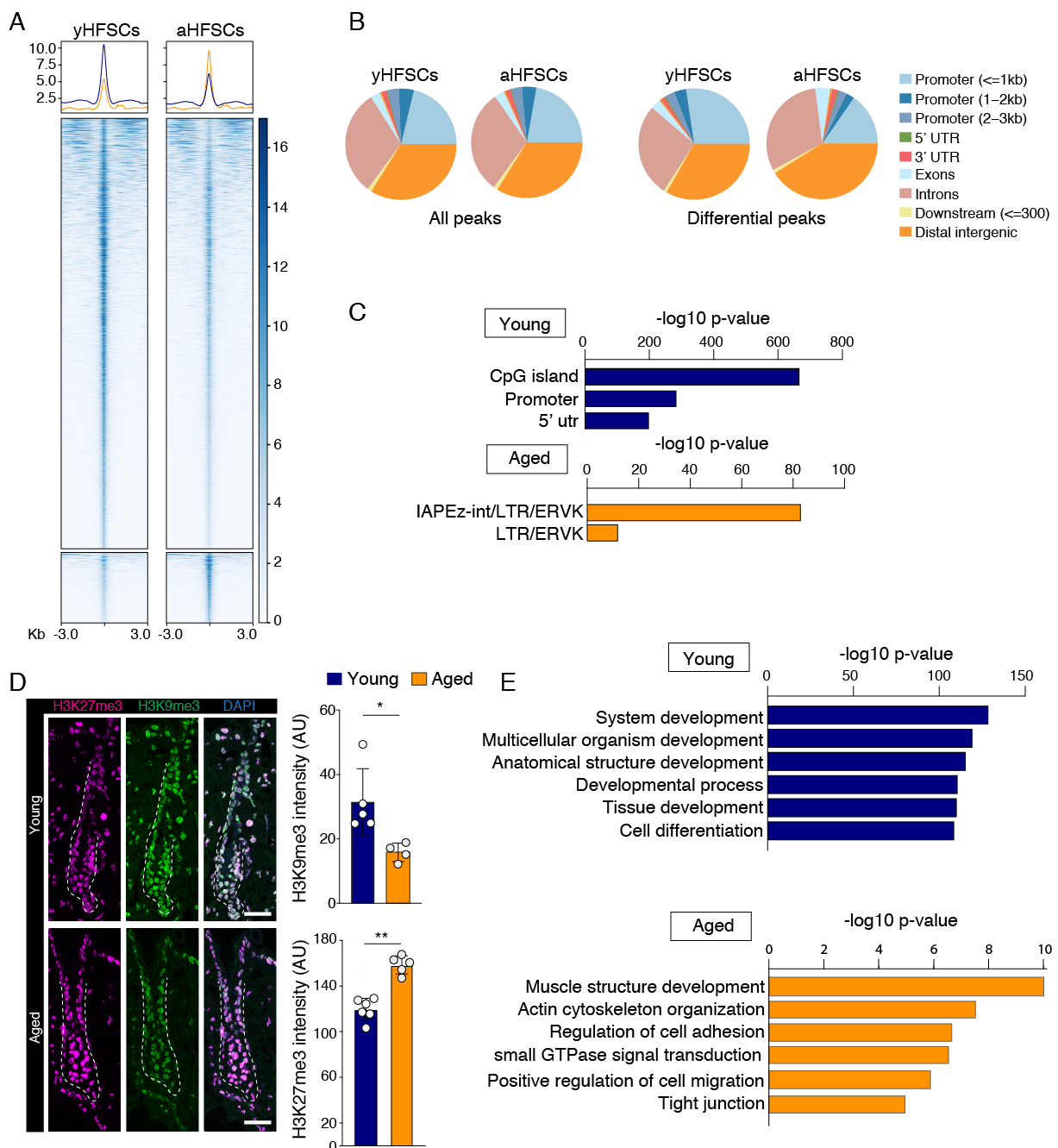


Fig. 10. Reduced chromatin accessibility in aHFSCs

A. Heatmap and intensity profiles of differentially accessible ATAC-seq peaks. Note widespread reduction in chromatin accessibility in aged HFSCs ($n=4$ mice/group). **B.** Distribution of all (left panels) and differential (right panel) ATAC seq peaks reveals comparable distribution of ATAC seq peaks in general but increased representation of promoters in regions more accessible in young HFSCs and increased representation of intergenic regions in aged HFSCs. **C.** Genome ontology analysis of differentially accessible ATAC seq peaks shows enrichment for CpG islands and promoter regions in regions more accessible in young HFSCs, whereas more accessible peaks in aged HFSCs are enriched in transposable elements. **D.** Representative immunofluorescence images and quantification shows reduced H3K9me3 and increased H3K27me3 in aged bulge HFSCs ($n= 5$ young/4 aged mice (H3K9me3) 6 young/5 aged mice (H3K27me3); $*p=0.0159$, $**p=0.0043$, Mann-Whitney). Dotted line outlines hair follicle and dermal papilla, scale bars 30 μm . **E.** Gene ontology term analyses implicate development and cell differentiation processes to be less accessible, while genes involved in actin cytoskeleton organization and regulation of cell adhesion are more accessible in aged HFSCs.

4.4 Majority of differential intergenic peaks are most likely primed enhancers

Peaks within promoters constitute only a small proportion of all ATAC-seq peaks, while the majority are found in distal enhancers [361]. We noticed the same pattern in our data and to better understand altered the epigenetic landscape of the enhancer regions we overlaid the differential accessible, intergenic areas with chromatin immunoprecipitation sequencing data for H3K4me1, H3K27me3 and H3K27ac from purified HFSCs [380], as well as RNAseq data that we generated for the purified young and aged HFSCs (Fig. 11 A). Interestingly, most regions were marked by H3K4me1. H3K4me1 marks active and primed enhancers, which can be distinguished based on the presence and absence of H3K27ac, respectively [381]. However, very few regions are marked by H3K27ac, indicating that the majority of the differential intergenic areas are primed enhancers. Enhancers can be very distant in a linear genome but spatially proximal (in 3D) to their target genes. This leads to the difficulty of predicting direct target genes of enhancers. As in many other studies, we linked distal peaks to the closest gene [382-384]. GO-term analyses using this annotation revealed in particular

enhancers involved in cell-cell adhesion, tissue development, cell differentiation, and proliferation to be less accessible in aged HFSCs (Fig. 11 B). In contrast, enhancers involved in cell adhesion, MAPK cascade, and cell migration were more accessible (Fig. 11 C). A motif analysis of the intergenic peaks more accessible in aHFSCs discovered a possible role of the NF1 TF-family, Lhx2, Ctf, and Dlx3 (Fig. 11 E). Interestingly, the NF1 family was also an enriched motif for the up-regulated genes, based on our RNA-seq data. Ctf can function as a transcriptional activator, a repressor, and is one of the core architectural proteins that help establish chromatin organization [385]. Lhx2 is a crucial TF for HFSC maintenance [386]. Dlx3 is an essential regulator of hair follicle differentiation and cycling. Dlx3 transcription is mediated through Wnt, and it is involved in the regulation of transcription by BMP signaling [387]. The motif analysis for intergenic peaks less accessible in aHFSCs revealed enrichment for the AP1 TF (Fig. 11 D). AP-1 is a heterodimer composed of proteins belonging to the c-Fos, c-Jun, ATF, and JDP families. It is involved in a wide range of cellular processes, including cell growth, differentiation, and apoptosis. In the skin, it has been shown to regulate differentiation genes and the expression of keratins in the HF [388]. Similar to the RNA-seq data, these results indicate a more diffuse stem cell identity in old HFSCs. However, comparing differential intergenic peaks with differential expressed genes from our RNA-seq showed only a small overlap: 5 genes overlapped between up-regulated genes and more accessible distal peaks in aHFSCs (e.g. Mef2c, Lmo7, and Ly6e) and 37 genes overlapped between down-regulated genes and less accessible distal peaks in aHFSCs (e.g. Sox21, Tnc, Dlc1, Hhip, and Ptch1) (Fig. 11 F). The lack of overlap could be due to the difficulty of predicting direct target genes of enhancers, and more sophisticated prediction models might change this in the near future. It may also be that additional factors, such as HFSC activation signals, are required to activate these enhancers to change the expression of their target gene, consistent with the notion that these enhancers are primed, but not active.

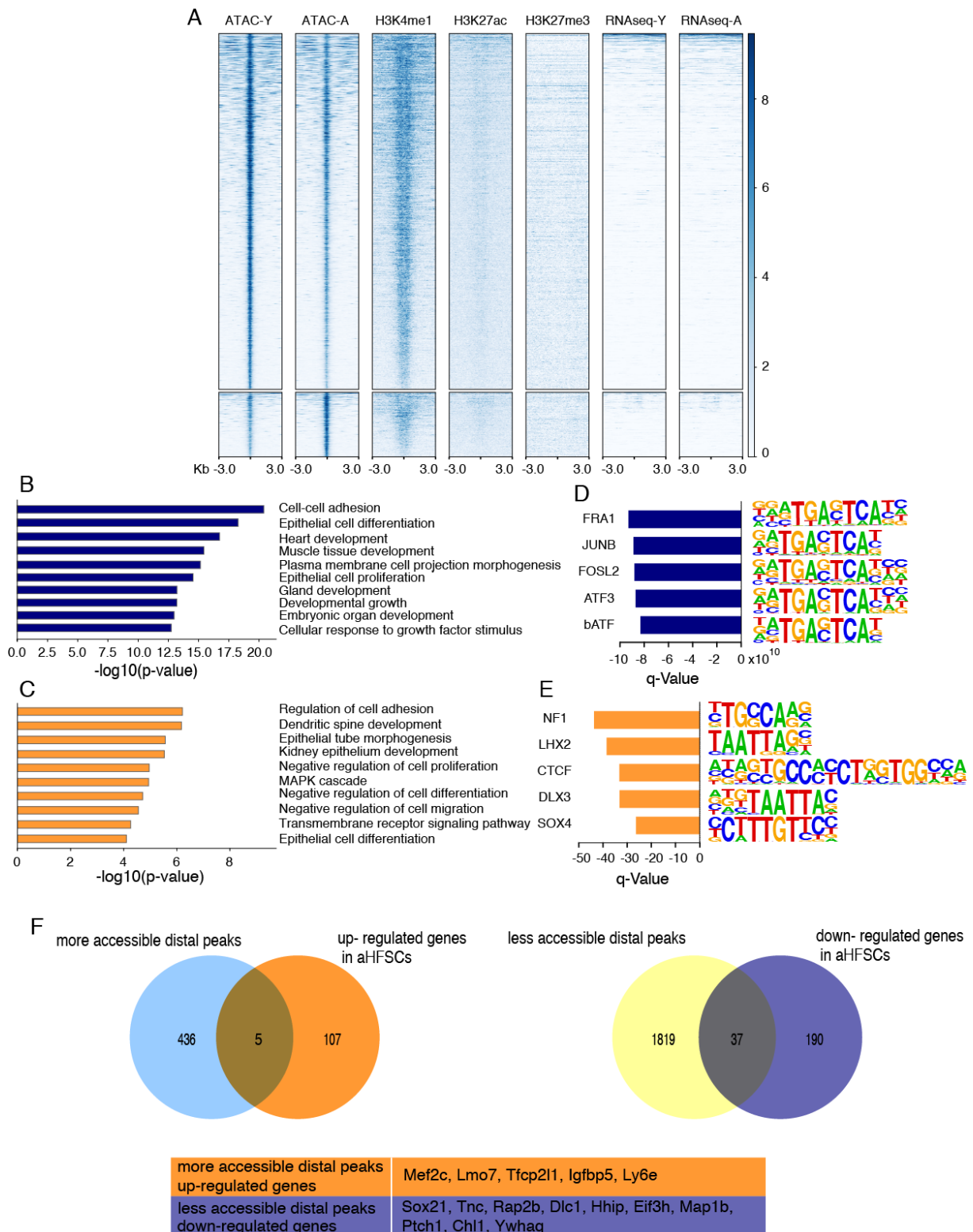


Fig. 11. Majority of differential distal peaks are primed, but not active, enhancers
A. Heatmap of differentially accessible intergenic combined public data sets for H3K4me1, H3K27ac, H3K27me3 as well as the transcripts of these regions quantified by RNAseq from young and aged HFSCs. Note most regions where high on H3K4me1, but low on H3K27ac and no detectable transcripts are found, indicating a primed state. **B.** Gene ontology term

analysis implicate processes such as cell-cell adhesion, tissue development, cell differentiation, and proliferation to be less accessible in distal enhancers. C. Distal enhancers involved in actin cytoskeleton organization and regulation of cell adhesion are more accessible in aged HFSCs. D. Motif analysis of intergenic peaks less accessible in aHFSCs revealed enrichment for the AP1 TF. E. Motif analysis of intergenic peaks more accessible in aHFSCs discovered the NF1 TF-family, Lhx2, Ctcf, and Dlx3. E. Comparing differential intergenic peaks with differential expressed genes from our RNA-seq showed only a small overlay.

4.5 CpG enriched Promoters are less accessible in aHFSCs

Given the rather small overlap between differentially expressed genes and the distal, differentially accessible chromatin regions, we next sought to understand the epigenetic landscape of the promoter regions with changed chromatin accessibility in aHFSCs in more detail. We overlaid the differentially accessible promoter regions with published ChIPseq data for H3K4me3, H3K27ac, and H3K27me3 from purified HFSCs [380], as well as our own RNAseq data (Fig. 12 A). H3K4me3 is associated with transcriptional start sites of actively transcribed genes [389], H3K27me3 is associated with repressive chromatin, and H3K27ac is associated with active promoters and enhancers [390]. Interestingly, the more accessible regions showed no signal for H3K4me3 and H3K27ac, but some enrichment for H3K27me3 and almost no RNA-seq signal. These results indicate that the more accessible promoters are inactive. The less accessible promoter regions could be separated into three different groups: broad H3K4me3 with broad H3K27ac, broad RNA-signal, and no H3K27me3; sharp H3K4me3 with little H3K27ac, little RNA-seq signal and increasing H3K27me3; low H3K4me3 with no H3K27ac, almost no RNA-seq signal and strong H3K27me3. Together with the findings at the distal intergenic peaks, these results imply that the majority of changes in the accessibility occurs at non- or low- active promoters and enhancers. GO-term analyses revealed particularly promoters of genes involved in tissue development, epithelial cell differentiation, and cell fate commitment to be less accessible in aged HFSCs. In contrast, promoters of genes involved in calcium signaling become more accessible (Fig. 12 B). Interestingly, while less accessible promoters were enriched for CpG islands, more accessible promoters were not (Fig. 12 C). Similar to the motifs found at the less accessible distal peaks, the less accessible promoters showed enrichment for the Ap1 TF-family (Fig. 12 D). Further

found motifs were Klf5 and p63, key regulators of stemness. It has been reported that Klf5 expression is downregulated in quiescent stem cells of hair follicles [391], while overexpression of Klf5 in adult mice leads to hyperkeratosis, follicle occlusion, and epidermal erosions [392]. The transcription factor p63 is required for the development of the stratified skin epithelium and hair follicles and suppresses hair follicle differentiation in mice [393]. The motive of P53 was enriched, together with the motif for CTCF, and again NF-1, at the more accessible promoters. When we compared the overlap between differential accessible promoters with differential expressed genes, the resulting overlay was again minor: Only two genes of the more accessible promoters and up-regulated genes matched (Mef2c, Piwil2), while 18 genes matched between less accessible promoters and down-regulated genes in aHFSCs (e.g., Sox21, Peg3, Fgfr2, Prkar2b) (Fig. 12 E). As stated above, the majority of changes in the accessibility occurs at non- or low- active promoters and enhancers, which might also explain the small overlap between ATAC-seq and RNA-seq results. Notably, the transcripts and ATACseq peaks that match, are also those with the most significant fold change in both assays.

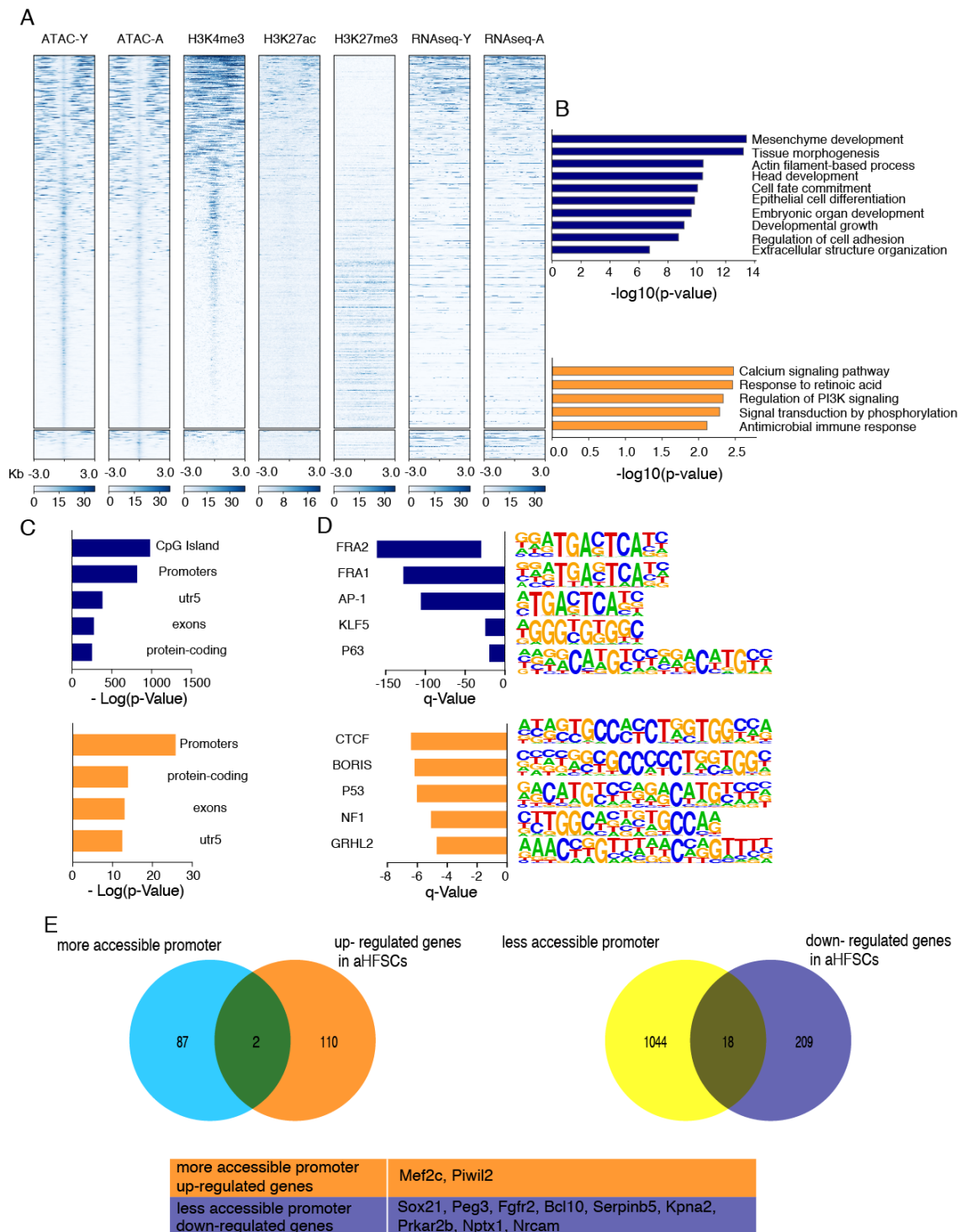


Fig. 12. Aging leads to decreased accessibility at CpG enriched promoters

A. Heatmap of differentially accessible promoter regions combined with public data sets for H3K4me3, H3K27ac, H3K27me3 as well as the transcripts of these regions quantified by RNAseq from young and aged HFSCs. **B.** Gene ontology term analyses implicate promoters of genes involved in tissue development, epithelial cell differentiation, and cell fate commitment become less accessible with age while, promoters of genes involved in the calcium signaling pathway become more accessible. **C.** Genome ontology analyses of

differentially accessible promoters showed enrichment for CpG islands in less accessible regions but not in more accessible regions. D. Motif analysis of less accessible promoters showed enrichment for the Ap1 TF-family, Klf5 and p63, while the motives such as P53, CTCF and again NF-1 are enriched at the more accessible promoters. E. Comparing differential accessible promoters with differential expressed genes from our RNA-seq resulted again in only a small overlay.

4.6 Age-induced decreased chromatin accessibility specifically at bivalent promoters

Since the heatmap of the differential accessible promoter regions (Fig. 12 A) implied that the promoter regions with reduced chromatin accessibility in aged HFSCs could be clustered into different categories, we performed K-means clustering of the data (Fig. 13 A). Intriguingly, this analysis revealed that one dominant class of genes with reduced accessibility in aged HFSCs contained both H3K4me3 and H3K27me3 marks at their promoters as a feature of a bivalent domain (Fig. 13 A, cluster C4). These genes were not transcribed in either young or aged HFSCs, excluding transcriptional heterogeneity as a cause for both active and silencing marks (Fig. 13 A). SCs must safeguard their undifferentiated state while ensuring stringent governance of differentiation trajectories. Mammalian SCs, in particular embryonic SCs, display a unique epigenetic and transcriptional state termed bivalent or poised state characterized by the simultaneous promoter occupancy of histone methylation marks indicative of active and silenced states, H3K4me3 and H3K27me3, respectively [154]. The function of these bivalent domains is to maintain the genomic loci in a state that is both rapidly responsive to developmental cues and, at the same time, refractory to subthreshold noise [154, 157].

GO-term enrichment analyses revealed that this cluster of differentially accessible, poised genes were enriched for developmental and cell type-specification genes (Fig. 13 B), as expected based on studies of poised genes in other SCs [157]. A vast majority of the genes had CpG-island containing promoters (116 out of 131). They included essential HFSC differentiation genes such as Lef1, multiple Bmps, Wnt, and Tcf genes, as well as genes involved in SC self-renewal [105] (Fig. 13 C), which are under the control of polycomb and H3K27me3 in HFSCs [380]. Examination of the

epigenetic features of these genes confirmed reduced accessibility in aged HFSCs, presence of both H3K4me3 and H3K27me3, as well as the absence of transcription (Fig. 13 D). Collectively these data indicate aging-induced decreased chromatin accessibility specifically at key HFSC differentiation and self-renewal gene promoters, which are in a poised state.

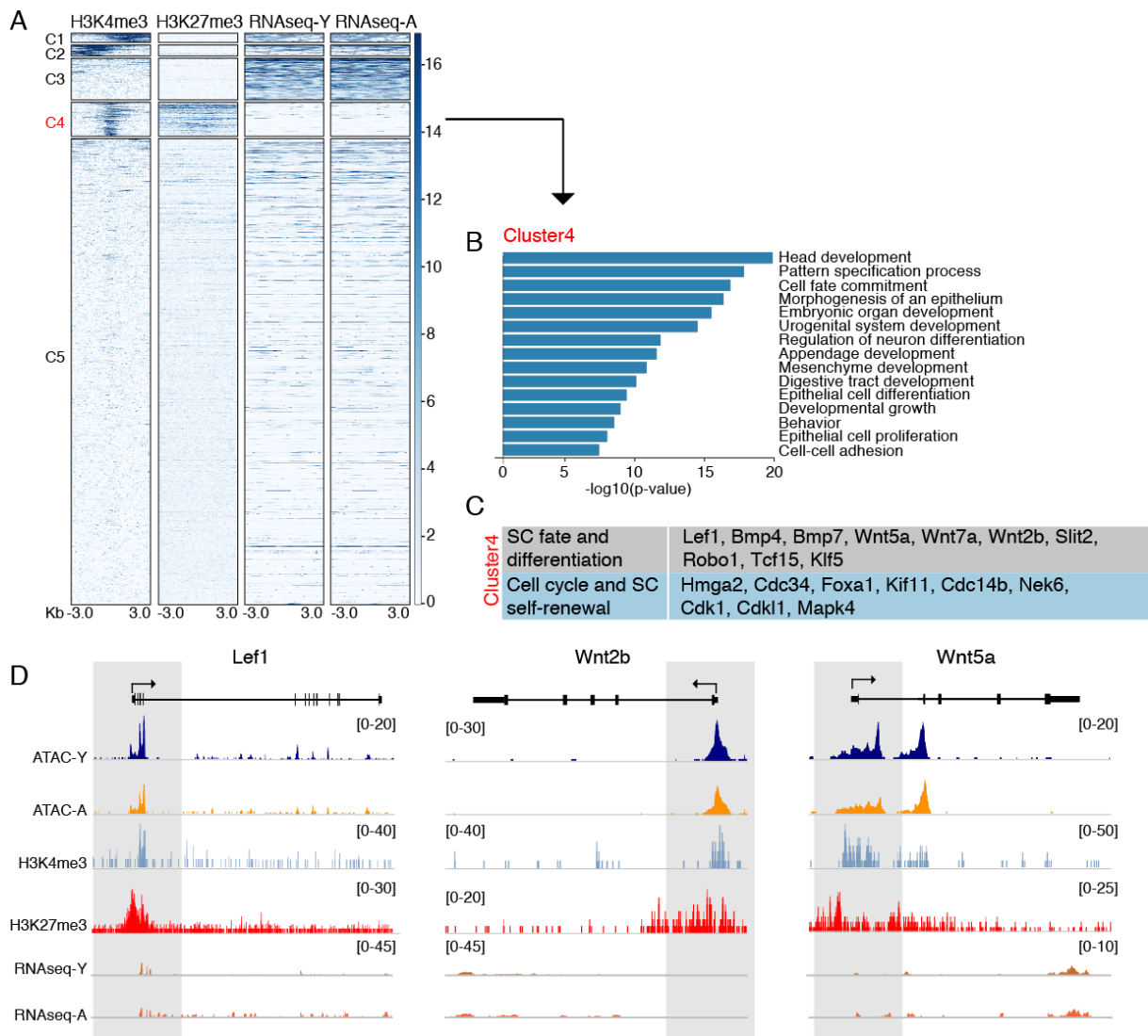


Fig.13. Bivalent genes are less accessible in aHFSCs

A. K-means clustering of peaks with decreased accessibility in aged HFSCs based on the status of H3K4me3 and H3K27me3 at these genomic regions in HFSCs as well as the transcripts of these genes quantified by RNAseq from young and aged HFSCs. Note cluster C4 where both high H3K4me3 at promoters and high H3K27me3 at gene bodies, but no detectable transcripts are found, indicating a bivalent state. B. Gene ontology term analyses of genes found in cluster 4 implicate developmental processes, cell fate and differentiation. C.

Representative genes from cluster 4 with functions in stem cell fate, differentiation and self-renewal include key genes required for HFSC activation and differentiation. D. Representative genome browser views of genes from cluster 4 show reduced promoter accessibility in aged HFSCs in ATAC seq, presence of both H3K4me3 and H3K27me3 at promoters and no significant transcription by RNAseq. Peak intensity range is indicated in brackets.

4.7 Aging leads to compromised activation of poised genes and loss of SC potential

To understand the functional significance of reduced accessibility at poised promoters, we considered that loss of bivalent promoters at self-renewal and differentiation genes would compromise HFSC self-renewal as well as render aged HFSCs refractory to activation signals. To test this, we induced hair follicle anagen entry and thus HFSC activation *in vivo* by depilation [394] (Fig. 14 A) and observed that young HFSCs were efficiently activated and entered the cell cycle upon depilation, whereas aged HFSCs failed to respond (Fig. 14 B). Importantly, and consistent with cell-cycle entry, poised genes were activated by depilation in young HFSCs/progenitors but remained mostly silenced in aged cells (Fig. 14 C). Interestingly, previous work from our lab showed that a majority (~70%) of young HFSCs had incorporated BrdU, that was administered in the drinking water continuously for eight weeks, whereas this was reduced to less than half in aged HFSCs, pointing to reduction in the cycling of aHFSCs [370]. This compromised HFSC potency was also confirmed using a colony-forming assay in which aged HFSCs formed substantially fewer colonies than young HFSCs [370]. Interestingly, when we knocked-down genes from the bivalent cluster, *Wnt7a*, *Cdc34*, *Lef1*, *Hmga2*, and used a colony-forming assay to investigate HFSC potency, we found fewer colonies as well (Fig. 14D). This result confirms an important role of these genes in the maintenance of HFSCs.

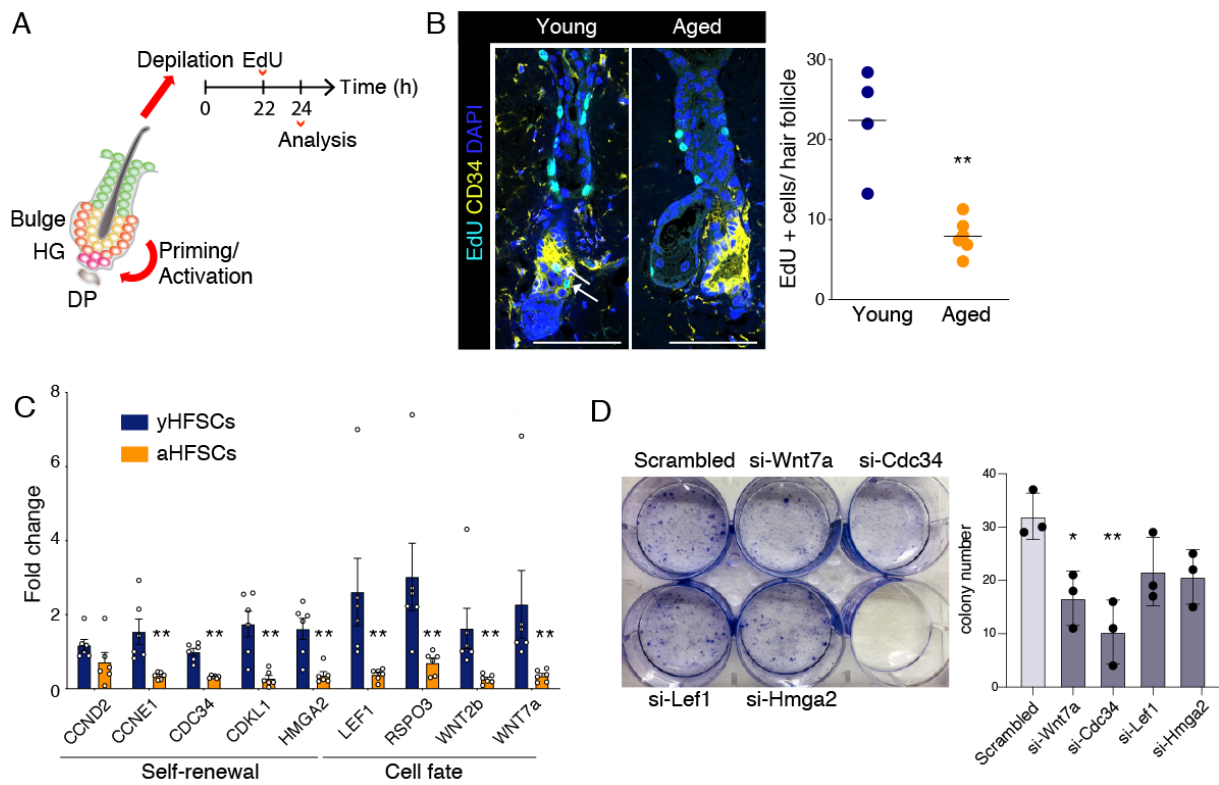


Fig. 14. Compromised activation of poised genes and SCs in aged mice

A. Schematic illustration of depilation experiment to induce HFSC activation. **B.** Representative immunofluorescence image and quantification of EdU-positive cells (white arrows) within the hair follicles shows efficient cell cycle entry of young HFSCs in contrast to aged ($n=4$ mice (young)/6 mice (aged); $**p=0.0095$, Mann-Whitney). Scale bars $75 \mu\text{m}$. **C.** Quantitative RT-PCR of selected genes with poised promoter state and reduced accessibility in aged HFSCs upon depilation. Note reduced expression in aged HFSCs/progenitors (mean \pm SEM; $n=6$ mice/group; $*p=0.0502$, $**p=0.022$, Mann-Whitney). **D.** Representative images and quantification of total colony number from siRNA transfected HFSCs plated in clonal density on feeders. Note significantly reduced colony-forming ability in si-Wnt7a and si-Cdc34 transfected HFSCs, si-Lef1 and si-Hmga2 transfected cells show a similar trend ($n=3$ mice/group; $*p=0.0205$, $**p=0.0023$, Student's t -test).

4.8 Synthetic niche restores stem cell potential of aHFSCs

Surprisingly, previous research from our lab revealed that aged HFSCs, transplanted into young nude mice, were as potent in regenerating hair as their young counterparts [370]. This finding suggested a role for the niche in the decline of SC potency in old mice. To challenge this hypothesis, we cultured young and aged HFSCs using an *ex vivo* HFSC organoid culture system, where critical niche components such as EGF, FGF-2, and various laminins and heparan sulfate proteoglycans (Matrigel) are provided and which allows for long-term maintenance of HFSCs [343]. Also, in this system, aged HFSCs were capable of expanding and maintaining their state comparable to young HFSCs (Fig. 15 A). Old stem cells also grew similar to young HFSCs in response to blocking differentiation through inhibition of Shh using cyclopamine, indicating comparable self-renewal and maintenance capacity (Fig. 15 A). Poised gene transcription was activated equivalently both in young and aged HFSCs (Fig. 15 B). Collectively, these experiments showed that aged HFSCs show compromised self-renewal, activation potency, and attenuated activation of poised genes. Importantly, these compromised functional SC properties are restored upon providing a young niche or a youthful synthetic niche.

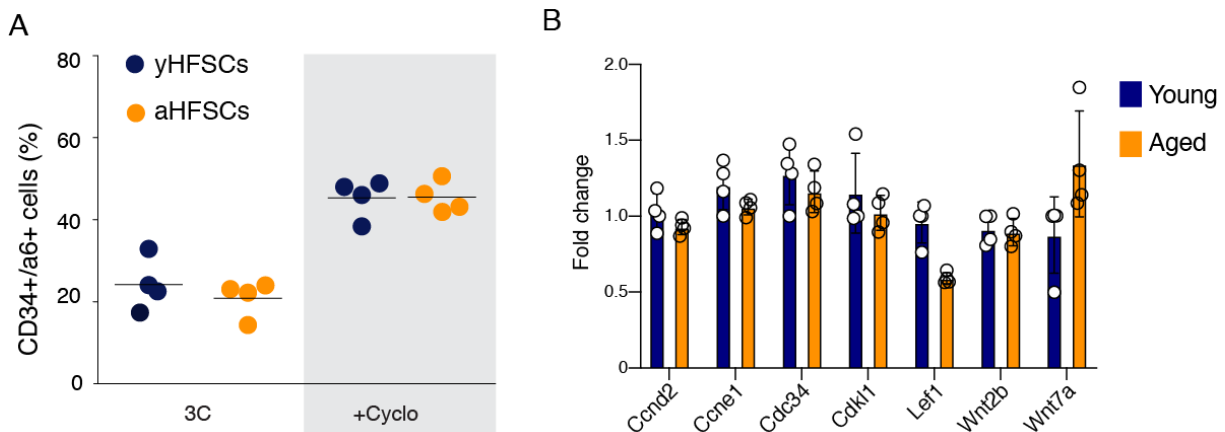


Fig. 15. Aged SC potential is restored when cultured in synthetic niche

A. Quantification of CD34+/\u03b16 integrin+ cells from HFSC organoid cultures generated from young and aged epidermis with and without cyclopamine treatment. Note comparable levels of CD34+/\u03b16 integrin+ in cultures from young and aged cells (n=4 donor mice/group). All bar graphs show mean \pm SD. **B.** Quantitative RT-PCR of selected genes with poised promoter state

and reduced accessibility in vivo from young and aged HFSCs in 3C organoid cultures. No significant differences in expression are observed (mean \pm SEM; n=4 mice/group).

4.9 Mass spectrometry analysis of aged skin reveals changes in ECM composition

To understand which changes in the old niche could contribute to HFSC aging, we next determined the whole skin proteome of young and aged mice (Fig. 16 A). We used a mass spectrometry protocol optimized for ECM proteins, which resulted in 3458 quantified proteins in young/old skin with 440 proteins significantly altered between the two conditions ($p_{adj} < 0.05$). Strikingly, the most up-regulated protein group terms in aged mice were linked to the extracellular matrix (ECM; Collagens VI, VII, XI), basement membrane (BM; Laminins, Collagen IV), BM crosslinking (Loxl1), ECM expression (Ctcf), as well as cell adhesion and contractility (integrins, Rock1) (Fig. 16 B, C). Appropriately, the protein group Collagen biosynthesis and modifying enzymes (Sparc, P4ha2, Plod1, Tnc) was among the most down-regulated ones (Fig. 16 D). Together, these changes suggest that aging alters the mechanical properties of the niche. Further downregulated protein groups were: Regulation of translation (Eif5a, Rps3, Gcn1) and M Phase (Tubg2, Mta3, Rcc1). We performed immunostaining of selected targets to confirm the mass spectrometry data and found both Laminin 332 and 511 increased in aged BMs (Fig. 16 E, F). Also, previous research in our lab had revealed thickening of the BM throughout the epidermis and HF by electron microscopy and stiffening of the BM by atomic force microscopy in aged skin [370], thus further supporting the findings of the proteome analysis, indicative of increased BM protein expression and crosslinking.

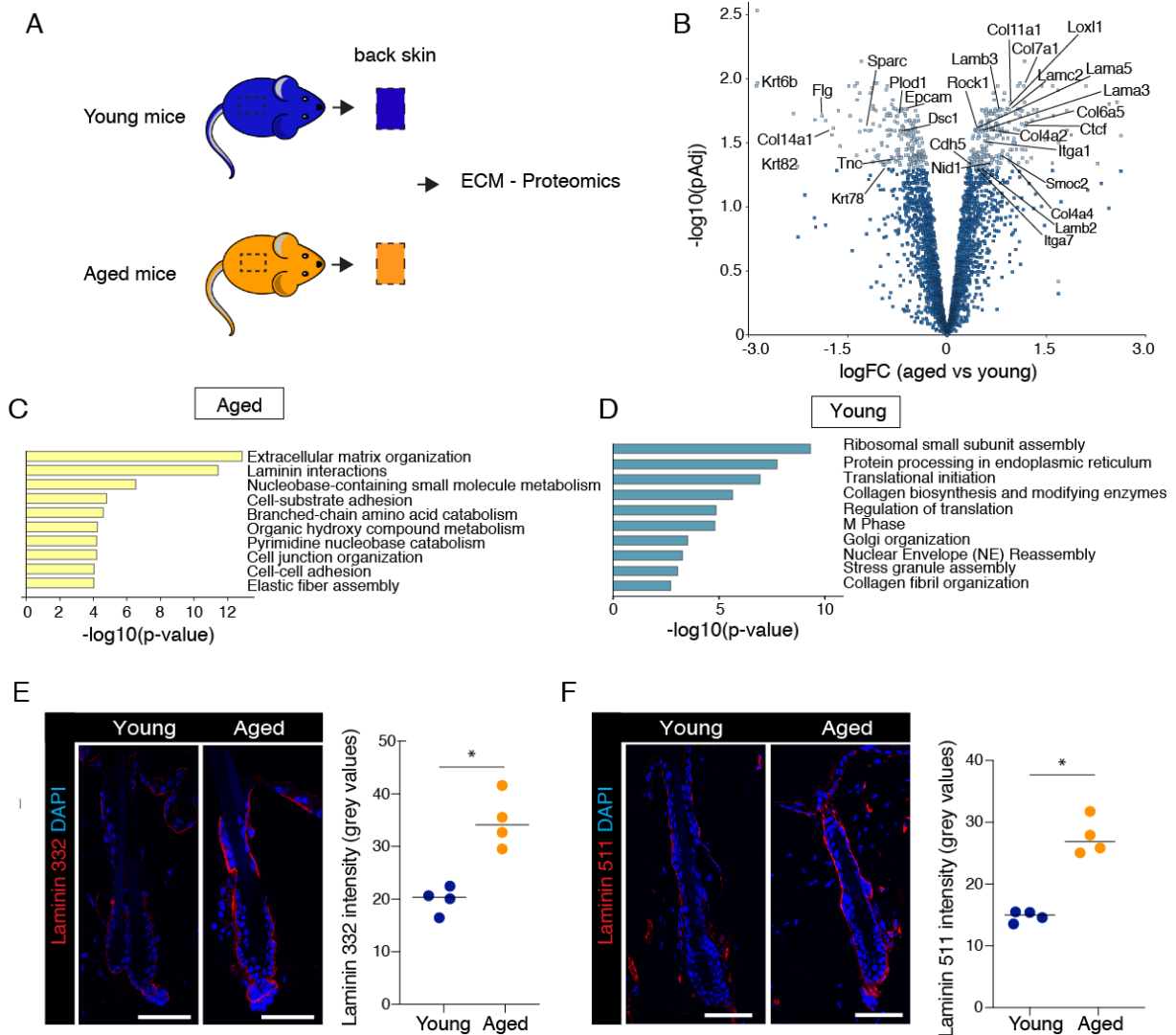


Fig. 16. Widespread biochemical alterations in the extracellular matrix

A. Whole skin proteome of young and aged mice was determined using a mass spectrometry protocol optimized for ECM proteins. **B.** Volcano plot of significantly altered proteins in young and aged skin. Basement membrane components such as laminins and collagen IV and its crosslinker *Loxl1* are upregulated in old skin whereas extracellular matrix modulators such as *Tenascin C* and *Collagen XIV* are downregulated ($n=4$ mice/group; $p_{adj}<0.05$). **C., D.** GO-term analysis of differentially expressed protein implicates ECM and BM components as most enriched protein classes. Collagen biosynthesis and modifying enzymes were among the most down-regulated classes. **E.** Representative immunofluorescence images and quantification of Laminin 332 staining show increased levels in aged BMs ($n=4$ mice/group, $*p=0.0286$, Mann-Whitney; Scale bars $50\ \mu\text{m}$). **F.** Representative immunofluorescence images and quantification of Laminin 511 staining show increased levels in aged BMs ($n=4$ mice/group, $*p=0.0286$, Mann-Whitney; Scale bars $50\ \mu\text{m}$).

4.10 HFSC niche is stiffer in aged mice

Based on the proteomic data of increased BM synthesis and crosslinking, we hypothesized that the BM could be stiffer, also locally within the HFSC niche. Using high-resolution atomic force microscopy-based force indentation spectroscopy on skin sections, we measured the elastic moduli of the aged BM around the HF bulge (Fig. 17 A, B). Indeed, our experiments showed increased elastic moduli of the BM of old mice around the HF bulge (Fig. 17 B), confirming age-induced stiffening of the HFSC niche.

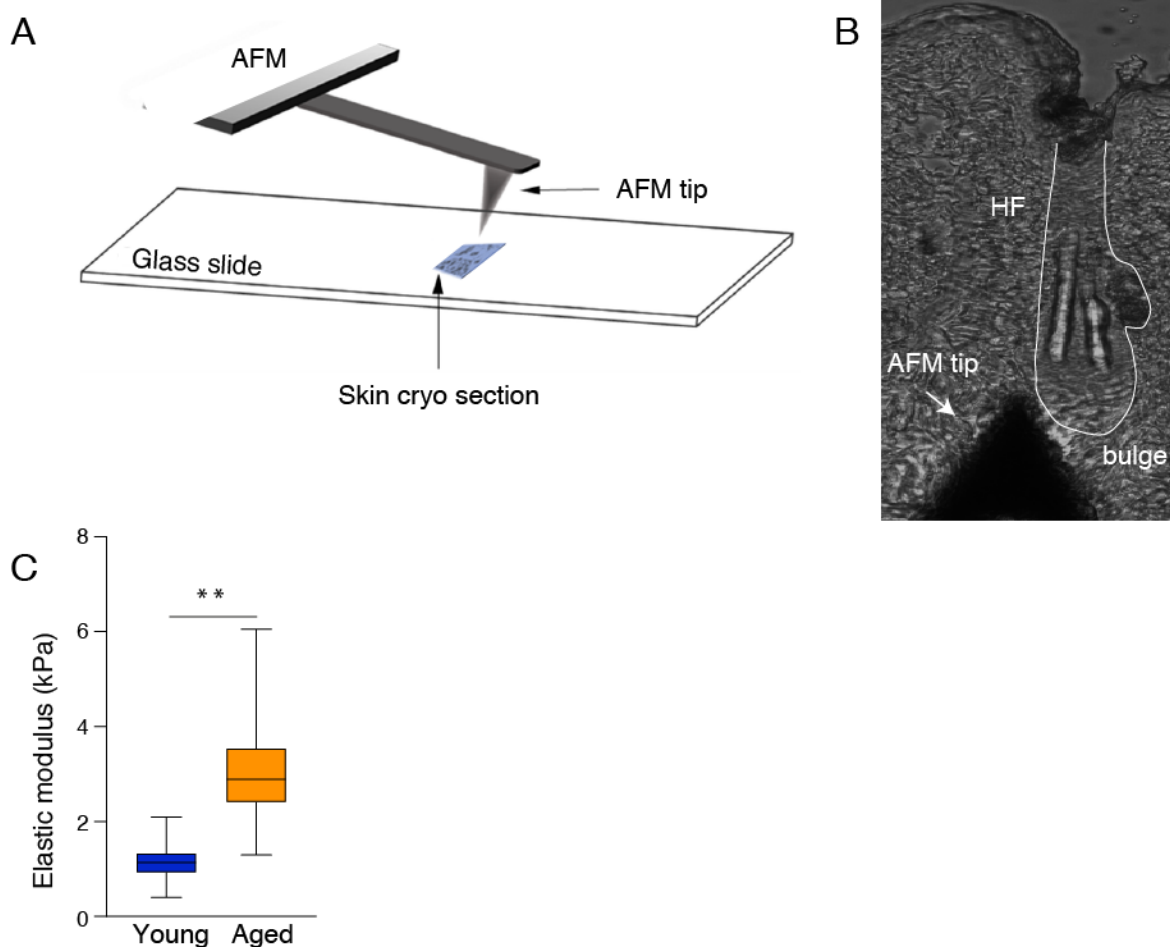


Fig. 17. Aging increases elastic modulus of HFSC BM

A. High-resolution atomic force microscopy-based force indentation spectroscopy on skin sections, modified from [395] **B.** Light microscopy image of AFM measurement. White line outlines the HF. BM was measured around the HF bulge. **C.** Box and whiskers plot of atomic force microscopy force indentation measurements of BM stiffness. Note increased BM stiffness

in aged mice ($n=1000$ force curves pooled across 5 mice/group; $**p=0.0079$, Kolmogorov-Smirnov).

4.11 Altered BM composition, mechanics, or both influences HFSC potency

Next, we asked if an aged BM could contribute to compromising SC potency. To test this, we prepared cell-free mouse scaffolds of young and old skin and cultured young, organoid-derived HFSCs on the young and old cell-free BMs for four days (Fig. 18 A). Immunofluorescence imaging for Col IV and LN 332 of the decellularized epidermis showed that the BM of the cell-free scaffolds remained intact (Fig. 18 B). Strikingly, when we cultured young HFSCs on the BM scaffolds, young BMs promoted both effective HFSC proliferation and activation/differentiation, as assessed by Ki67 and Lef1 staining. In contrast, old BMs failed to do so (Fig. 18 C). Therefore, altered BM composition, mechanics, or both influence HFSC behavior.

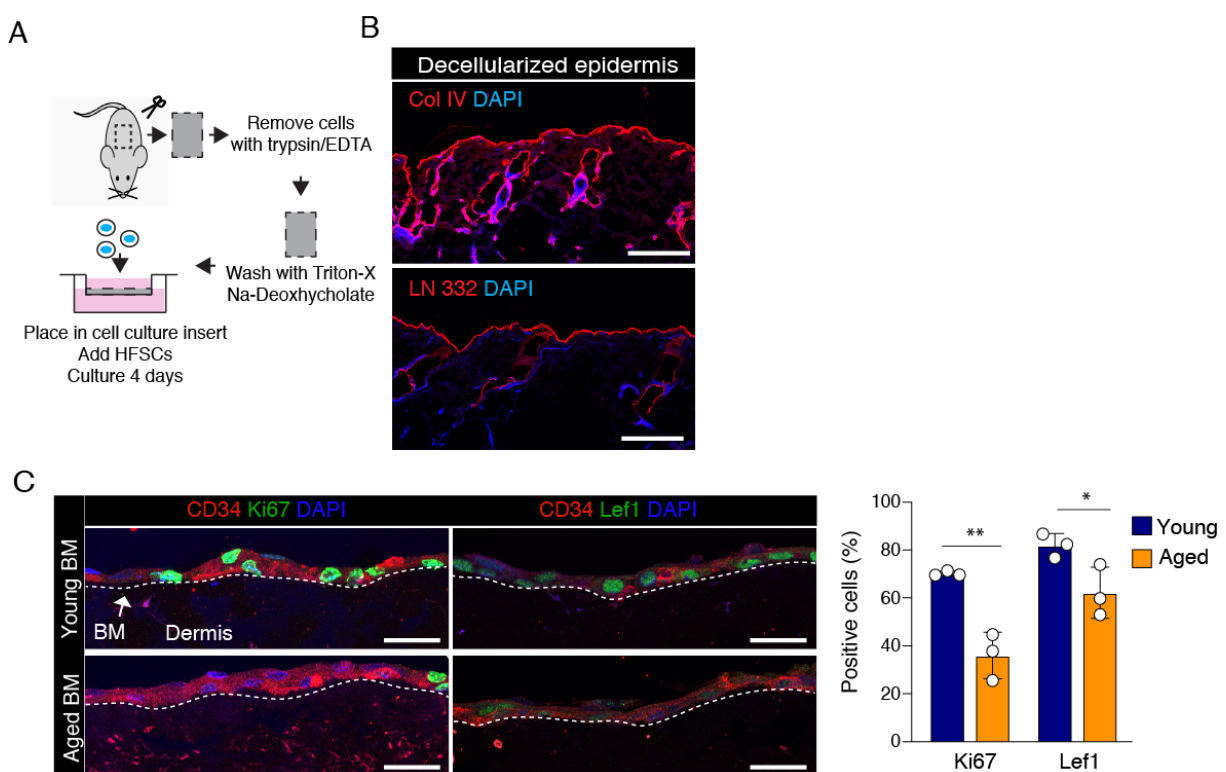


Fig. 18. Aged BM scaffolds influence HFSC potential

A. Schematic illustration of decellularized basement membrane scaffold preparation from young and aged mice. **B.** Representative immunofluorescence images of decellularized

basement membrane scaffolds showing absence of epidermal cell nuclei but intact basement membranes as marked by Collagen IV and Laminin 332 staining. Scale bars 100 μm . **C.** Representative *Ki67* and *Lef1* immunofluorescence images and quantification of young organoid-derived HFSCs plated on decellularized BM scaffolds derived from young and aged mice. Note reduced presence of *Ki67*- and *Lef1*-positive cells in BM scaffolds from aged mice ($n=3$ mice/group; $**p=0.0037$, $*p=0.044$, Student's *t*-test). Scale bars 25 μm .

4.12 Activation of the poised SC self-renewal and differentiation genes is attenuated in stiff hydrogels

Wondering if matrix stiffness would be sufficient to change HFSC potency and the activation of poised self-renewal and differentiation genes, we thus modified the HFSC organoid culture system. We tuned the stiffness of the hydrogels by crosslinking collagen with a PEG-based crosslinker (Fig. 19 A, B). AFM measurements confirmed that we were able to mimic the stiffness of young and aged BMs, 1-3 kPa, and 5-6 kPa, respectively (Fig. 19 C). Intriguingly, adjusting the hydrogel stiffness was sufficient to attenuate the activation of the poised SC self-renewal and differentiation genes (Fig. 19 D).

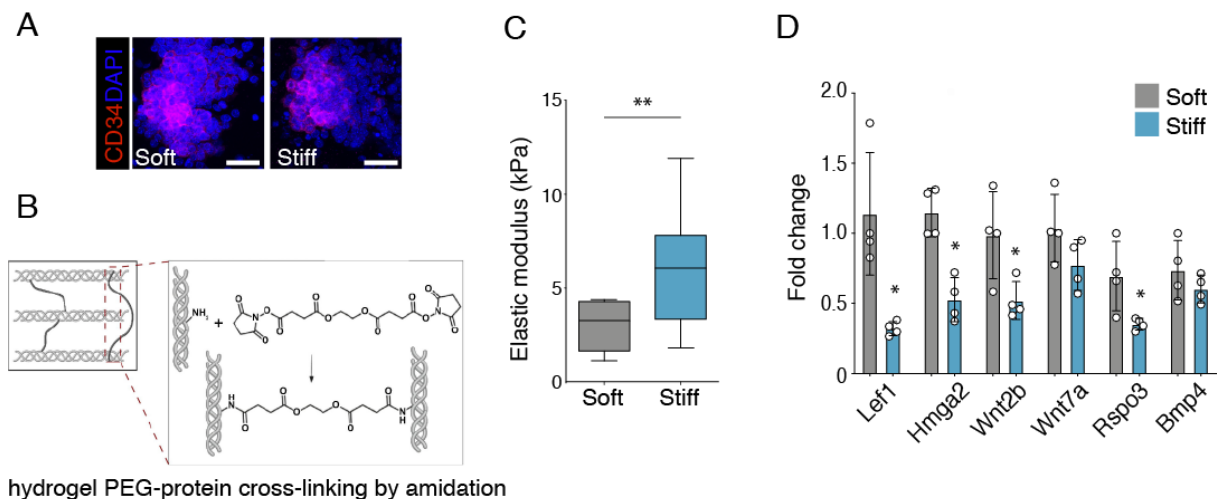


Fig. 19. Stiff environment reduces expression of bivalent genes

A. Representative images of HFSC organoids cultured in soft (~2.7 kPa) or stiff (~6 kPa) hydrogels and stained for CD34. Scale bars 30 μm . **B.** Collagen gels were formed by increasing the pH of the collagen solution to induce self-assembly of collagen molecules. Stiffness of the collagen gel was tuned by introducing covalent cross-links between collagen

*fibrils and PEG-diNHS. Modified from [396]. C. Box and whiskers plot of atomic force microscopy force indentation measurements of 3C organoid hydrogel stiffness (n=13 force curves pooled across 4 independent experiments; **p=0.0012, Kolmogorov-Smirnov). D. Quantitative RT-PCR of selected genes with poised promoter state and reduced accessibility in aged HFSCs in soft and stiff hydrogels. Note reduced expression in stiff hydrogels (mean \pm SEM; n=4 cultures/group; *p<0.05, Kolmogorov-Smirnov).*

4.13 BM stiffening induced HFSC loss can be recapitulated *in vivo*

Finally, we asked if increased BM stiffness was capable of compromising HFSC maintenance *in vivo*. To this end, we analyzed Tenascin X-deficient mice, which are a mouse model for the human Ehlers-Danlos Syndrome, characterized by defective organization of dermal collagen fibers and increased macroscopic hyperelasticity of the skin, indicative of altered mechanical properties of the dermis [341]. Surprisingly, despite this macroscopic hyperelasticity and disorganized dermo-epidermal junction collagen fibrils, one-year-old Tenascin X-deficient mice displayed a lack of apparent morphological abnormalities of the epidermis and the hair follicle (Fig. 20 A, B). However, similarly to aged mice, atomic force microscopy-based force indentation spectroscopy on skin sections displayed increased elastic moduli of the BM around the HF bulge, making these mice a suitable model for niche stiffening (Fig. 20 C). FACS-analyses of HFSCs showed a substantial HFSC loss in 1-y-old knockout mice (Fig. 20 D). This result was particularly intriguing as a subset of Ehler-Danlos Syndrome patients displays features of premature aging in their skin as hair loss, epidermal thinning, and translucency [397]. Collagen XIV, a member of the FACIT collagen family, interacts with TNX [398] and is likewise an important regulator of collagen fibrillogenesis in the skin [342]. Additionally, collagen XIV was among the most down-regulated proteins in aged skin (Fig. 16 B). Altered biomechanical properties of the skin, such as decreased tensile strength, have been previously reported as well [342]. Accordingly, when we compared 1-year old Col14 deficient to WT mice, we found increased BM stiffness (Fig. 20 E), as well as a reduction in HFSC percentage (Fig. 20 F).

Together these experiments showed that aging is accompanied by large-scale changes in the skin ECM and BM, associated with stiffening of the niche, loss of

accessibility, and thus activatability of poised SC genes leading to loss of HFSC self-renewing potential.

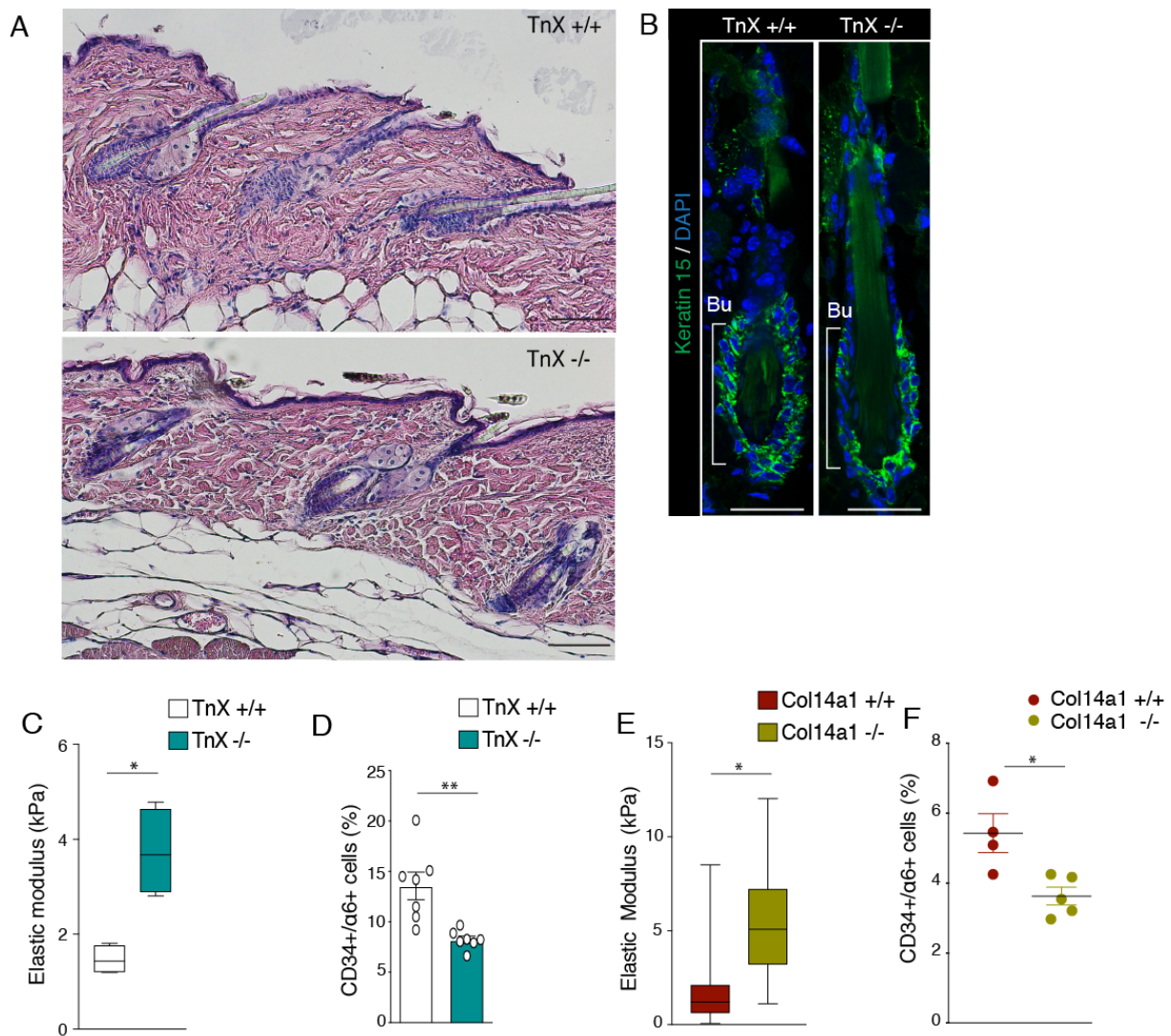


Fig. 20. Stiff BM influence HFSC potential in vivo

A. Representative Hematoxylin/Eosin staining from 1-year old *Tnx +/+* and *Tnx -/-* mice show overall normal skin morphology. Scale bars 100 μm . **B.** Representative immunofluorescence images of Keratin-15 staining to mark the bulge (bu) niche from 1-year old *Tnx +/+* and *Tnx -/-* mice show comparable hair follicle morphology. Scale bars 25 μm . **C.** Box and whiskers plot of atomic force microscopy force indentation measurements of BM stiffness in *TnX +/+* and *TnX -/-* mice. Note increased BM stiffness in *TnX -/-* mice ($n=23$ force maps pooled across 4 mice/genotype; $*p=0.0286$, Kolmogorov-Smirnov). **D.** Quantification of CD34+/ $\alpha 6$ integrin+ cells from 1 y-old *TnX +/+* and *TnX -/-* mouse epidermis shows decreased numbers of HFSCs in *TnX -/-* mice ($n=7$ mice/genotype; $**p=0.0026$, Student's *t*-test). **E.** Box and whiskers plot of atomic force microscopy force indentation measurements of BM stiffness in 1- y-old *Col14a1*

+/+ and *Col14a1 -/-* mice. Note increased BM stiffness in *Col14a1 -/-* mice ($n=20$ force maps pooled across 3 mice/genotype; $*p=0.028$, *t*-test with Welch's Correction). **F.** Quantification of *CD34+/ α 6 integrin+* cells from 1 y-old *Col14a1 +/+* and *Col14a1 -/-* mouse epidermis shows decreased numbers of HFSCs in *Col14a1 -/-* mice ($n=4$ *Col14a1 +/+*, 5 *Col14a1 -/-* mice; $*p=0.0157$, Student's *t*-test).

4.14 Niche stiffening triggers mechanical stress

Next, we tried to understand the molecular mechanisms by which age-induced niche stiffening could control promoter states and thereby HFSC potency. The hair follicle bulge niche is a semi-3D system as the HFSCs are sandwiched between the stiff BM and the stiff hair shaft, causing cells to be stretched/compressed. Indeed, quantification of nuclear deformation in young and aged HFSC niches revealed increased nuclear flattening and shape heterogeneity in aged HFSCs (Fig. 21 A). Also, cell contractility as quantified by the levels of Myosin II phosphorylation [399], was increased in aged HFSCs (Fig. 21 B), as an additional indication of increased mechanosignaling in aged HF and consistent with the observed upregulation of its kinase Rock1 in the proteomics data (Fig. 16 B).

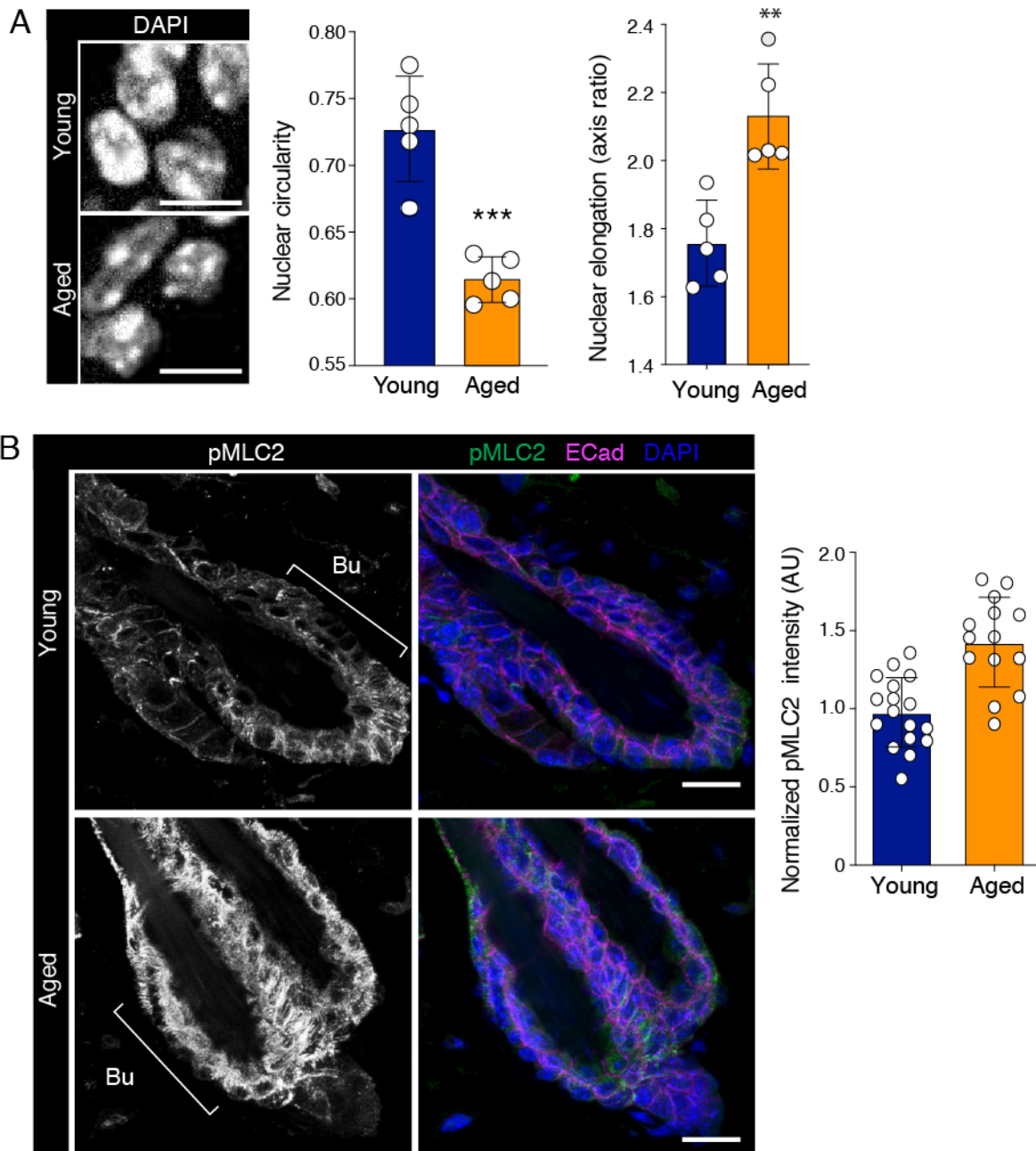


Fig. 21. Increased mechanical stress indications in aged HFSCs

A. Representative immunofluorescence images and quantification of nuclear circularity and nuclear aspect ratio in young and aged bulge HFSCs. Note decreased circularity and irregular shapes of aged nuclei ($n=5$ mice/group; $***p=0.0004$, Student's t -test). Scale bars $10\ \mu\text{m}$. Nuclear aspect ratio (major axis/minor axis) shows increased nuclear elongation of aged HFSCs (mean \pm SD; $n=5$ mice/group with >100 nuclei per mouse; $**p=0.0031$, Student's t -test).

B. Representative immunofluorescence images and quantification of phosphorylated myosin light chain 2 (pMLC2). Note increased pMLC2 indicating increased contractility in aged bulge HFSCs (14 images pooled across 3 mice/group).

4.15 Global transcription is reduced in HFSCs of aged- and TNX-deficient-mice

Previous work from our group demonstrated that mechanical stress leads to global transcriptional repression and decreased presence of the active, elongating form of RNA polymerase 2 (serine two phosphorylated form; RNAPII-S2P) [400]. Consistent with the increase in mechanical stress in the aged HFSCs, immunofluorescence staining showed a significant decrease in RNAPII-S2P levels in aged bulge HFSCs (Fig. 22 A). Importantly, a similar reduction in RNAPII-S2P was also detected in Tenascin-X-deficient mice (Fig. 22 B), confirming the role of niche mechanics in decreasing transcriptional elongation.

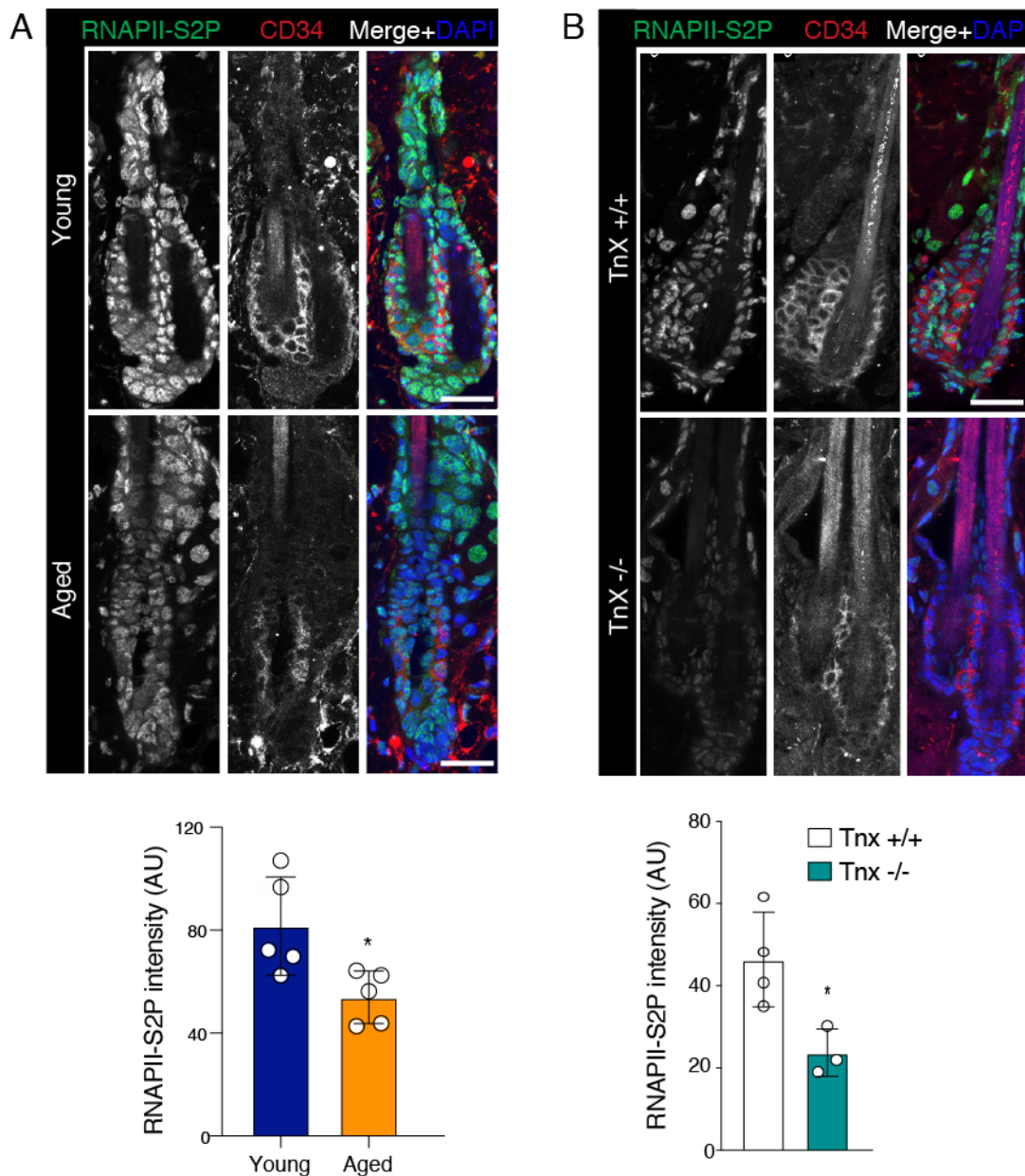


Fig. 22. RNAPII-S2P signal reduced in HFSCs of aged mice and TNX $-/-$ mice

A. Representative immunofluorescence images and quantification of RNAPII-S2P in young and aged bulge HFSCs shows decreased levels of RNAPII-S2P in aged HFSCs ($n=5$ mice/group; $*p=0.0213$, Student's *t*-test). Scale bars 25 μm . **B.** Representative immunofluorescence images and quantification of RNAPII-S2P in TnX $+/+$ and TnX $-/-$ mice shows decreased levels of RNAPII-S2P in TnX $-/-$ hair follicle bulges ($n=4$ (TnX $+/+$) /3 (TnX $-/-$) mice; $*p=0.0273$, Student's *t*-test). Scale bars 25 μm .

4.16 Reduction of global transcription leads to increased H3K27me3 occupancy at poised genes

Decreased transcription has been shown to enable increased H3K27me3 occupancy at CpG island-containing promoters [400, 401]. We thus hypothesized that genes with poised promoters might be particularly sensitive for the observed aging-driven global moderate transcriptional repression and increased H3K37me3, which could switch these promoters from poised into an H3K37me3-silenced state. To test this hypothesis, we inhibited transcription short-term (6 h) using the RNAPII inhibitor α -amanitin [402] (Fig. 23 A). α -amanitin is a small circular peptide that binds on the back side of the RNA polymerase, away from the active site and away from the binding site for the DNA and RNA. It jams the enzyme by blocking its essential motions and shape changes [403]. As expected, transcription of highly expressed genes as well as genes that were poised in the quiescent HFSCs were both substantially reduced, as quantified by the substantial reduction in nascent RNA, and became undetectable in several of the poised genes (Fig. 23 B). To understand if the transcriptional repression was sufficient to silence poised genes, we analyzed H3K27me3 occupancy at the promoters of the same set of genes using ChIP-qPCR. Whereas H3K27me3 was not increased on promoters of constitutively expressed CpG-island-containing genes, the promoters of poised genes accumulated H3K27me3 upon inhibition of transcription (Fig. 23 D). Collectively these analyses showed that the stiffening of the niche microenvironment reduces transcription, which leads to the silencing of particular genes with very low levels of transcription.

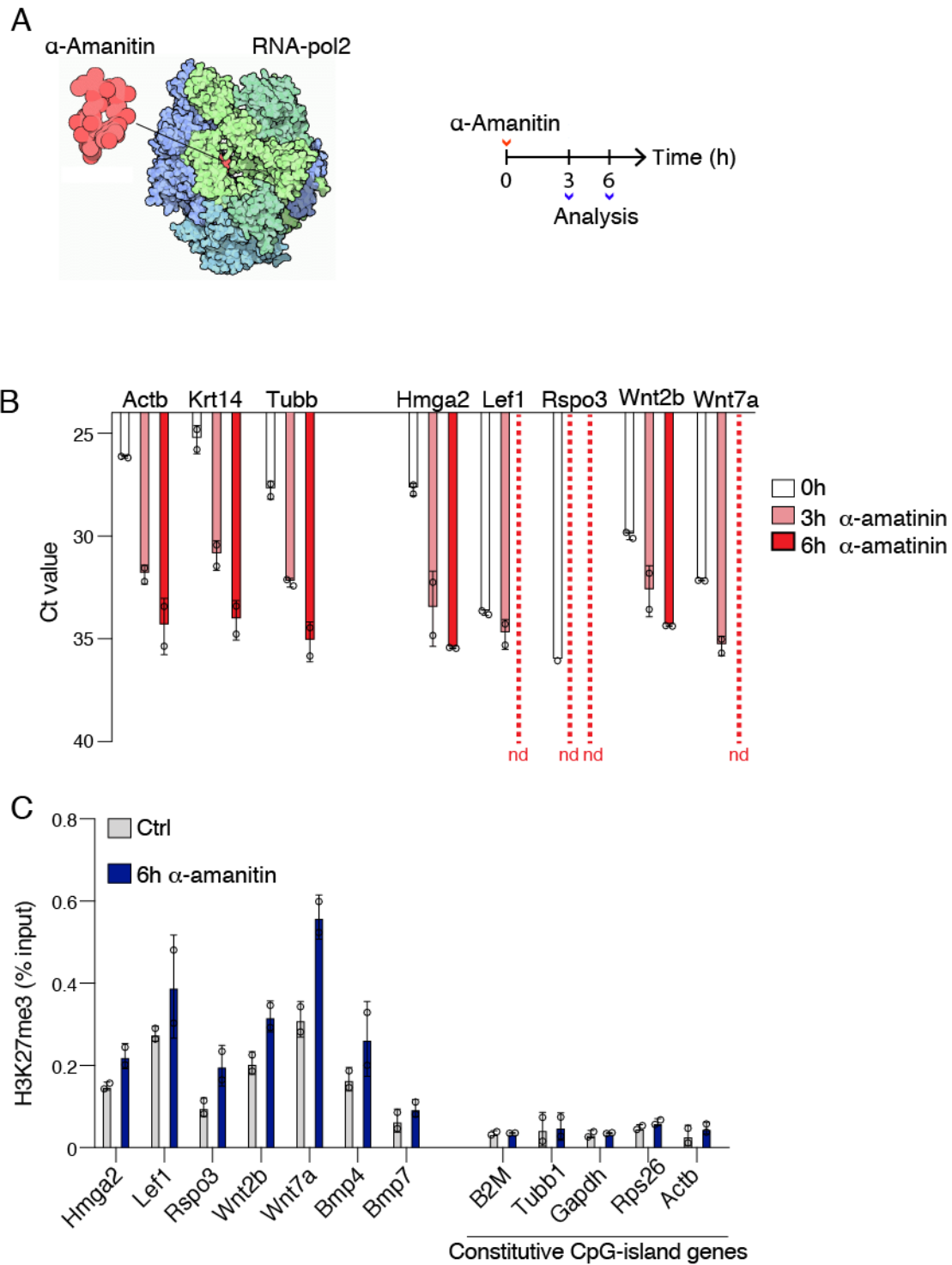


Fig. 23. α -amanitin inhibition of RNAPII leads to increased H3K27me3 occupancy at bivalent promoters

A. α -amanitin binds between two subunits of the RNAPII and blocks essential motions and shape changes of RNAPol2, thereby inhibiting the sequential steps of binding to DNA, unwinding it, and then building the RNA strand. Adapted from [403]. **B.** Quantitative RT-PCR of nascent RNA from selected highly transcribed genes and genes with poised promoter state

in quiescent HFSCs from HFSC cultures treated with α -amanitin for 3 or 6 h. Note decreased levels of nascent RNA in all genes as defined by high ct values (mean \pm SD; n=2 mice with 4 technical replicates each, n.d.=not detected). C. H3K7me3 chromatin immunoprecipitation and subsequent quantitative RT-PCR of promoters show increased H3K27me3 after α -amanitin treatment at poised genes (right), but not at constitutively expressed genes with CpG islands at their promoters (mean \pm SD; n=2 independent experiments with 4 technical replicates).

Collectively, our results indicate that aging results in reduced chromatin accessibility of HFSCs, particularly at poised lineage-specification genes. This specific chromatin state is determined by global levels of transcription, which are negatively impacted by the increased, niche-derived mechanical stress that acts on the aged HFSCs. The critical role of the niche, and in particular its ECM components, is consistent with recent studies showing compromised HFSC mobilization upon wound healing in aged mice, but not upon transplantation into young recipients [404]. Thus, the microenvironment and its mechanical properties play a critical role in regulating stem cell chromatin landscape and functionality during aging.

5 Discussion

Aging is a process characterized by the progressive loss of tissue and organ function. One of the seminal findings for the field of aging research was the observation made in 1939 that caloric restriction increased lifespan in mice and rats [405]. Since then, a lot of progress has been made, and many pathways have been discovered to influence lifespan, e.g., inhibition of IGF and mTOR, activation of AMPK, and sirtuins [406, 407]. Diet-based interventions and pharmacological interventions, such as dietary restriction or the mTOR inhibitor rapamycin, improve aspects of aging, even later in life [408-411]. However, the critical question, whether aging of cells, tissues, and organisms can be reversed or 'rejuvenated' rather than simply delayed, remains. It is essential to understand the drivers of the aging process to answer this question.

To consider rejuvenation, it is important to acknowledge that aging is a multifactorial condition. So far, aging has been linked, on the molecular level, with DNA damage, epigenetic alterations, telomere attrition, protein aggregation, and accumulation of aberrant mitochondria and lysosomes. At the cellular and organismal level, aging includes cellular senescence, deregulated nutrient sensing, and chronic low-grade inflammation [3, 4]. Loss in SC number and activity over time has been proposed to be another critical driver of aging [5]. Consistent with the SC aging hypothesis, SC aging phenotypes have been described for multiple tissues, including the hematopoietic system, intestine, muscle, brain, skin, and germline [369]. However, the mechanisms that lead to compromised adult SCs function and tissue maintenance are not clear.

The current thesis work unravels this question using HFSCs as a paradigm, which is interrogated with a panel of sequencing, quantitative imaging as well as biochemical methods. We show that the aged HFSC niche displays widespread alterations in extracellular matrix composition and mechanics, resulting in mechanical stress and concomitant transcriptional repression, triggering further silencing of bivalent promoters of key self-renewal and differentiation genes. This silencing of these specific promoters reduces self-renewing capacity and attenuated the ability to activate the expression of these bivalent genes upon regeneration. These functional defects were niche-dependent as transplantation of aged HFSCs into synthetic niches restored SC functions and transcription of poised genes. Tuning tissue mechanics *in vivo* and *in vitro* also recapitulated age-related SC changes, implicating niche mechanics as a

central regulator of chromatin state, which, when altered, leads to age-dependent SC exhaustion.

5.1 Age-induced HFSC exhaustion is associated with decreased chromatin accessibility

Building on findings from a previous study from our laboratory [370], we studied aging of the HF at a stage (24 months) in which the decline of HFSC numbers was initiated, as a sign of HFSC exhaustion and onset of aging, but where hair follicle morphology and the hair coat still appeared normal. Importantly, only skin areas in telogen were analyzed, and all mice housed together in the same animal facility room throughout their entire life span. We found that in old mice, the percentage of HFSCs to total epidermal cells is reduced to almost half compared to young mice. The previous study from our lab analyzed 3 independent young/aged mouse cohorts from 3 independent mouse facilities, showing that this decline of HFSCs is robust and reproducible, thus excluding extrinsic triggers such as facility-specific pathogens for HFSC reduction [370]. This finding is in line with the stem cell theory of aging that postulates that loss of stem cell number or activity causes a decline in tissue and organ function over time [87]. Several different stem cell lineages in other tissues show this decline: Among others, neural progenitors [88], melanocyte SCs [89, 90], hematopoietic SCs [91-93], and satellite cells [94-96]. In the skin, reduced potency of HFSCs has been reported, already at stages where HFSCs are still present at numbers comparable to young mice [327-329]. Later during aging, severe hair loss has been reported, which is associated with hair follicle destruction and reduced HFSC numbers [330]. However, studying the stage of HFSCs decline initiation allows us to identify the drivers behind this decline. We decided to use genome-wide sequencing approaches to identify drivers of stem cell exhaustion. First, we compared the transcriptome of young and old HFSCs. Perhaps surprisingly, we found minimal differences between the two groups. However, this finding is in line with a previous study, showing minor differences between young and old quiescent HFSCs by RNAseq [334]. Also, a recent publication utilizing scRNA-seq showed that aHFSCs maintain their identity and show no sign of shifting their fate [337]. However, the scRNA-seq analysis did identify changes in extracellular matrix genes, similar to our findings that processes like extracellular structure organization

and cytoskeleton organization are up-regulated in aHFSCs. The minor transcriptional changes we identified imply that the identity of old HFSCs becomes more diffuse, while translation and cell cycle genes are reduced. Collectively, these results along with the previous work suggest that the minor transcriptional changes alone cannot explain the loss of SC in aged HFs.

Thus, we used ATAC-seq [361] to determine changes in genome-wide chromatin accessibility landscape and investigated whether chromatin changes were linked to HFSC exhaustion. We discovered that young HFSCs showed significantly more accessible genomic regions than old (6745 in young/ 1104 in aged).

Reduced accessible regions in aHFSCs were enriched for promoters and CpG islands, suggesting that accessibility was specifically lost at promoters of coding genes in aged HFSCs. GO-term analyses implicated in particular genes involved in tissue development and cell differentiation. In contrast, the few regions that gained accessibility in aged HFSCs were enriched at transposable elements and intergenic areas, that are typically silenced by H3K9me3 [378]. Consistent with previous studies indicating loss of heterochromatinization upon aging [379], we also observed a reduction in overall constitutive heterochromatin marked by H3K9me3 in the aged HFSCs. Interestingly, in line with our findings, also aged CD8⁺ T cells lose chromatin accessibility at promoters [412]. These aged cells exhibited a chromatin openness pattern shift towards differentiated cells. Another study on aging T cells showed that reduced accessibility in old cells is associated with genes involved in T cell activation. In contrast, chromatin opening is associated with genes involved in myeloid leukocyte and osteoclast differentiation [413]. On the other hand, in aged human fibroblasts, promoter regions become progressively more accessible [414]. Similar to the previously discussed epigenetic factors of aging (s. 1.2.5), the extent or even the direction of chromatin accessibility changes induced by aging seems to differ between cells, organs, and species, thus highlighting the complexity of the epigenetic mechanisms underlying aging.

5.2 Decreased chromatin accessibility specifically at bivalent promoters

To understand the epigenetic landscape of the regions with reduced chromatin accessibility in aged HFSCs in more detail, we overlaid hypoaccessible regions with ChIPseq data for H3K4me3 and H3K27me3 from purified HFSCs [380], as well as our RNAseq data. Analysis of this data revealed that one main class of regions with reduced accessibility in aged HFSCs contained both H3K4me3 and H3K27me3 marks, together with absence of transcription. H3K4me3 is typically associated with activation, while H3K27me3 is associated with repression. Simultaneous occupancy of these histone methylation marks characterizes promoter bivalency [154]. Since these genes were not transcribed in either young or aged HFSCs, transcriptional heterogeneity as a cause for both active and silencing marks can be excluded. Further analysis revealed that this cluster was enriched for developmental and cell type-specification genes. Previous research has shown that the function of bivalent domains is to maintain the genomic loci in a state that is both rapidly responsive to developmental cues and, at the same time, refractory to subthreshold noise [154, 157]. Bivalent domains strongly correlate with CpG islands [159]. CpG islands thus appear to play a significant role in the establishment of bivalent domains. Also in our data, a large majority of the genes have CpG-island containing promoters (116 out of 131) and included key HFSC differentiation genes, as well as genes involved in SC self-renewal [105], which are under the control of the polycomb complex and H3K27me3 in HFSCs [380]. Studies of poised genes in other SCs likewise showed enrichment for developmental and cell type-specification genes [157].

Collectively these data indicate that aging decreased chromatin accessibility, specifically at crucial HFSC differentiation and self-renewal gene promoters, which are in a poised state. From our data, it is not clear if the change of accessibility is due to a change in the H3K4me3/H3K27me3 ratio. Removal of H3K27me3 can render bivalent promoters more amenable for transcription, in part due to the reduced compaction. In contrast, when PRCs establish a stronger foothold around promoters, H3K27me3 acts as a more substantial barrier for activation, forging repression [154, 160]. Therefore, a shift in balance towards H3K27me3 could render these poised regions less accessible. Another explanation could be an increase in DNA methylation. Bivalent promoters that lose both H3K4me3 and H3K27me3, have a high probability of becoming DNA-hypermethylated [161]. A recent publication confirms this notion and concurrently

reports a reduction in chromatin accessibility [415]. Interestingly, it has been previously proposed that aging may correlate with reduced plasticity in the expression of bivalent genes, instead of changing active gene transcription [177]. In line with this observation, bivalent gene promoters acquire DNA methylation in other aged tissues and are also methylated and stably silenced in cancer [171, 172, 178-180].

Future studies are required to test both of these hypotheses. ChIP-seq for H3K4me3 and H3K27me3 in old and young HFSCs along with DNA methylation analysis, e.g., through Reduced-representation bisulfite sequencing (RRBS-Seq) will be important next steps for resolving the epigenetic states of the promoters [416].

5.3 Aging leads to niche-dependent compromised activation of poised genes and loss of SC potential

Regardless of the precise epigenetic mechanism, we reasoned that loss of accessibility at bivalent promoters of self-renewal and differentiation genes would compromise activation of these genes, attenuating HFSC self-renewal as well as render aged HFSCs refractory to activation signals. To understand the functional significance of this reduced accessibility, we activated HFSC through inducing hair follicle anagen entry *in vivo* by depilation [394]. As expected, young HFSCs were efficiently activated and entered the cell cycle, whereas aged HFSCs responded less efficiently. Significantly, and in line with our hypothesis, bivalent genes were activated by depilation in young HFSCs but remained mostly silenced in old SCs. These results are consistent with previous work from our group, showing BrdU incorporation was reduced to less than half in aged HFSCs and thereby pointing to a reduction in the cycling of aHFSCs [370]. This compromised HFSC potency was also confirmed using a colony-forming assay in which aged HFSCs formed substantially fewer, but larger colonies than young HFSCs [370].

Age-dependent perturbed cell-cycle activity can be a sign of stem cell exhaustion and has also been reported in other SCs, like skeletal muscle stem cells, neural stem cells, and germline stem cells [417-420]. In muscle stem cells, SC activation appeared to be accompanied by an increase in H3K27me3 in a large number of bivalent nonmyogenic lineage genes, suggesting that these genes may be resolving to a thoroughly repressed state [421]. Interestingly, genes marked only by H3K4me3 in those SCs

became bivalent with age. During aging of HSCs, bivalent regions change as well, 335 bivalent domains disappeared in old HSCs, due to loss of H3K4me3, while 1245 emerged due to the gain of both H3K4me3 and H3K27me3, or H3K27me3 only [422]. However, in our study, we show, for the first time, a clear link between aging-reduced accessibility of bivalent genes and loss of SC potential.

In previous work, our lab also made the puzzling finding that aged HFSCs, transplanted into young nude mice, were as potent in regenerating hair as their young counterparts [370]. This is in contrast with the depilation experiments and thus suggested a role for the niche in the decline of SC potency in old mice. A stem cell niche is a local environment consisting of neighboring cells and ECM. It is involved in the regulation of SC behavior and function [105, 106]. To challenge our hypothesis of niche involvement, we cultured young and aged HFSCs using an *ex vivo* HFSC organoid culture system developed in our lab, which allows long-term maintenance of HFSCs [343]. In this synthetic niche system, aged HFSCs expanded and maintained their state comparable to young HFSCs, and bivalent gene transcription was activated equally both in young and aged HFSCs. When we blocked differentiation by inhibition of Shh, old SCs also showed similar self-renewal and maintenance capacity compared to young HFSCs. Together, these experiments show that *in vivo*, aged HFSCs display compromised self-renewal, activation potency, and reduced activation of poised genes. However, providing a young niche or a youthful synthetic niche, these compromised SC function can be restored.

In other tissues, the niche has been associated with stem cell aging, e.g., in SSCs [109, 110] or GSC [111-113]. Often the communication between niche cells and stem cells is affected in aging [116]. A recent study strengthened the causative role of the niche in epithelial stem cell aging [124]. A decrease in stemness-maintaining Wnt signaling caused a functional decline of ISC due to the production of Notum, an extracellular Wnt inhibitor, in aged niche cells, the Paneth cells, highlighting the role of soluble factors. While most research focused on changes in cell-cell communication, a recent study observed a stiffening of the central nervous system microenvironment with age. This mechanical change is sufficient to cause age-related loss of function of oligodendrocyte progenitor cells [125].

5.4 Widespread biochemical alterations in the extracellular matrix induce SC niche stiffening to control SC potential

We examined the whole skin proteome of young and aged mice to understand which changes in the old niche contribute to HFSC aging. Interestingly, we found changes that suggest aging alters the mechanical properties of the niche. The most up-regulated protein group terms in aged mice were linked to the ECM, BM, BM crosslinking, ECM expression, as well as cell adhesion and contractility. Accordingly, the group of Collagen biosynthesis and modifying enzymes was among the most down-regulated ones. ECM proteins and especially collagens are mainly produced by fibroblasts. A recent scRNAseq study of young (2 months) and aged fibroblasts (18 months) showed that old fibroblasts have a strong reduction in the expression of the main extracellular matrix genes, including collagens, e.g. Collagen XIV, Plod1, Sparc, and glycosaminoglycans, and of genes involved in their secretion [185]. Therefore, the decrease of Collagen XIV in aged skin is potentially connected to fibroblast aging. However, the transcription of other collagens, e.g. IV, VI, VII and XI, is not changed, but matrix metalloproteinases, such as MMP2, MMP3, and MMP14, are decreased in aged fibroblast [185]. This decrease in collagen degrading enzymes might explain our finding of elevated collagen levels in aged skin.

In line with these findings, previous research in our lab revealed thickening of the BM throughout the epidermis and HF by electron microscopy and stiffening of the BM by atomic force microscopy in aged skin [370]. Based on these findings, we measured and confirmed a stiffer BM also locally at the HFSC niche, using high-resolution atomic force microscopy-based force indentation spectroscopy on skin sections. Therefore, our results verify the age-induced stiffening of the HFSC niche.

Using cell-free mouse scaffolds of young and old skin, we next showed that an aged BM could contribute to the altered SC potency we observed. We cultured young, organoid-derived HFSCs on these young and old cell-free BMs and observed that young BMs promoted both significant HFSC proliferation and activation/differentiation. In contrast, old BMs failed to do so. These results show that altered BM composition, mechanics, or both influences HFSC potency.

For MSCs, substrate elasticity has been known to influence stem cell behavior. While soft matrices favor stem-like cellular phenotypes and differentiation of MSC into

neuronal-like cells, moderate elasticity promotes myogenic differentiation, and a rigid matrix stimulates osteogenic differentiation [213, 423]. We wondered, therefore, if matrix stiffness alone could change HFSC potency and the activation of poised self-renewal and differentiation genes. We were able to mimic the stiffness of young and aged BMs by modifying the HFSC organoid culture system and tuning the stiffness of these hydrogels. Interestingly, adjusting the hydrogel stiffness alone was sufficient to attenuate the activation of the poised SC self-renewal and differentiation genes.

Together these experiments showed that aging leads to large-scale changes in the skin ECM and BM, associated with stiffening of the niche. This stiffening is sufficient to attenuate the activatability of poised SC genes, leading to loss of HFSC self-renewing potential.

Next, we wondered if increased BM stiffness was capable of compromising HFSC maintenance in vivo as well. We used two different mouse models to investigate this hypothesis. Tenascin X-deficient mice are a model for the human Ehlers-Danlos Syndrome. These mice display defective organization of dermal collagen fibers and increased macroscopic hyperelasticity of the skin, indicative of altered mechanical properties of the dermis [341]. Furthermore, a subset of Ehler-Danlos Syndrome patients shows features of premature aging in their skin as hair loss, epidermal thinning, and translucency [397]. Collagen XIV, a member of the FACIT collagen family, interacts with TNX and is likewise involved in the regulation of fibrillogenesis [342]. Altered biomechanical properties of the skin, such as decreased tensile strength, have been previously reported as well [342]. Additionally, it was among the most down-regulated proteins in aged skin in our proteomics screen. In both mouse models, we observed an increase in BM stiffness, accompanied by a reduction of HFSCs. These results confirm that increased BM stiffness is capable of compromising HFSC maintenance in vivo as well. Yet, it remains unclear how both proteins are able to influence BM stiffness since Collagen XIV and TNX are mainly expressed throughout the dermis. One explanation could be that knock-out of either protein leads to changed mechanics in the dermis, to which the BM adapts. In accordance, a stiffer dermis has been observed in aged mice [370]. Also, the ECM is a complex network, thus, knock-out of one factor may change other proteins and, in the end, result in an altered BM composition. Mass spectrometry analysis of the skin of TNX-, collagen XIV- mice, or both, may help resolve this question.

Together these experiments showed that aging leads to large-scale changes in the skin ECM and BM, associated with stiffening of the niche, loss of accessibility, and thus, activatability of poised SC genes leading to loss of HFSC self-renewing potential. Our findings are also following the study mentioned above [125], which observed a stiffening of the niche of oligodendrocyte progenitor cells with age. Mechanical changes in the central nervous system microenvironment were enough to cause loss of function of these progenitor cells [125]. Therefore, it can be assumed that aging induced mechanical changes of the microenvironment may be a novel hallmark of aging and may affect other tissues as well. It will be interesting to analyze the premature aging phenotypes of the Ehlers-Danlos syndrome patients to see to what extent these mechanisms are also relevant to human disease.

5.5 Mechanical stress suppresses transcription to silence bivalent promoters

Since stiffening of the niche leads to loss of accessibility, and thus activatability of poised SC genes, we wondered which molecular mechanisms underlies this process. We hypothesized that in the aged hair follicle bulge niche, a semi-3D system, HFSCs are sandwiched between the stiff BM and the stiff hair shaft, causing cells to be stretched/compressed. Increased nuclear flattening, shape heterogeneity, and cell contractility in aged HFSCs indeed indicated higher mechanical stress. Furthermore, we observed a significant decrease in RNAPII-S2P levels, which is consistent with previous work from our lab [400], demonstrating that mechanical stress leads to global transcriptional repression and decreased presence of RNAPII-S2P.

A similar reduction in RNAPII-S2P was also detected in Tenascin-X-deficient mice, confirming the role of niche mechanics in decreasing transcriptional elongation.

Either the absence of transcription or transcription at levels below a certain threshold is sufficient to allow PRC2 recruitment to promoter CpG islands and increase H3K27me3 occupancy [154, 160, 400, 401]. Therefore, genes with poised promoters might be particularly sensitive for the observed aging-driven global moderate transcriptional repression and increase H3K37me3, which in turn could shift these promoters from poised to an H3K37me3-silenced state.

However, it is still unclear what leads to the reduction of global transcription. One possible explanation might be a change in nuclear actin. A study from our group revealed that mechanical strain leads to a reduction in the free nuclear G-actin pool, resulting in global transcriptional repression [216]. Another recent study observed a global reduction in transcription on stiff substrates linked to a reduction of active Cofilin-1 [424]. Cofilin-1 is involved in depolymerizing F-actin [425], in the nuclear transport of G-actin [426], and is required, in combination with G-actin, for RNA polymerase II-mediated transcription elongation [427]. This study proposes that mechanical force applied to cells via integrins causes Rho/ROCK/LIMK-dependent inhibition of Cofilin-1 [424]. In line with this hypothesis, we observed upregulation of Rock1 in the proteomics data, and phosphorylation of its target Myosin II in aHFSCs. These studies provide evidence for the direct coupling of cytoskeletal and global transcription in response to mechanical forces. However, the precise molecular mechanisms remain open for further studies.

Short-term inhibition of RNAPII in our HFSC hydrogel culture system reduced transcription of highly expressed genes as well as genes that were poised in the quiescent HFSCs both substantially, nascent RNA of several of the poised genes became undetectable. Simultaneously, the promoters of poised genes accumulated H3K27me3, whereas H3K27me3 occupancy on promoters of constitutively expressed CpG-island-containing genes did not increase. These results indicate that transcriptional repression is sufficient to silence poised genes. Together, these analyses showed that the stiffening of the niche microenvironment reduces transcription, which potentially leads to the silencing of particular genes with shallow levels of transcription.

The key open question of the thesis is the precise epigenetic state of the promoters, which should be addressed by performing ChIPs for H3K27me3, H3K4me3, and RNAPII. ChIPs for H3K27me3, H3K4me3, and Pol2. This data could confirm if indeed a shift in the H3K27me3/H3K4me3 ratio and a reduction of RNAPII occupancy are responsible for further silencing of the poised genes. Previous research has shown that bivalent promoters, which lose both H3K4me3 and H3K27me3, have a high probability of becoming DNA-hypermethylated [161, 415]. Hence, increased H3K27me3 might be an initial response to globally reduced transcription that is later on replaced by DNA methylation. Therefore, it will be interesting to investigate also

DNA methylation changes in aged HFSCs. Moreover, do the epigenetic changes occur in all cells or only in a subset of the HFSCs? Single-cell technologies such as scATAC-seq might help to answer this. Another key question is the mechanism by which niche stiffening leads to transcriptional repression and how this could be prevented, for example, by interfering with matrix cross-linking.

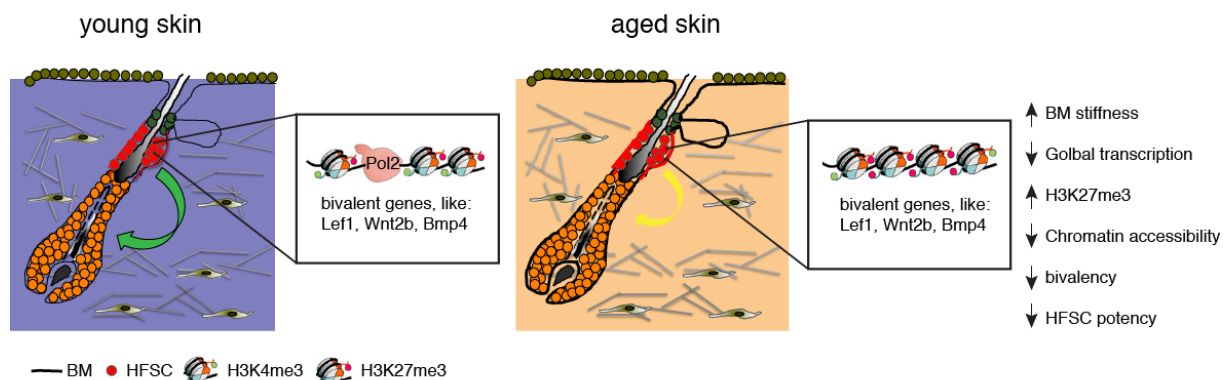


Fig. 24. Model of HFSC aging

In young skin, key differentiation genes, like Lef1, Wnt2b, and Bmp4, are in a bivalent state, preloaded with RNAP II. Upon sufficient signaling, these genes become robustly initiated, and HFSCs become activated (green arrow). During aging, changes in the ECM, such as downregulation of Col14, lead to increased BM stiffness, leading to global transcription downregulation. This downregulation is followed by an increase in H3K27me3 occupancy and less Chromatin accessibility, especially at bivalent genes. These bivalent genes are now more resistant to activation, also rendering HFSCs less activatable (yellow arrow). Consequently, HFSC potency and SC percentage are decreased.

In summary, this study reveals a mechanism explaining stem cell exhaustion in the HF (Fig. 24). Genome-wide analyses revealed that aged HFSCs displayed widespread reduction of chromatin accessibility, specifically at crucial self-renewal and differentiation genes that were characterized by bivalent promoters occupied by both active and repressive chromatin marks. Aged HFSCs showed reduced self-renewing capacity and attenuated ability to activate the expression of these bivalent genes upon regeneration. These functional defects were niche-dependent as transplantation of aged HFSCs into synthetic niches restored SC functions and transcription of poised

genes. Mechanistically, the old HFSC niche displayed widespread alterations in extracellular matrix composition and mechanics, resulting in mechanical stress and concomitant transcriptional repression, shifting these bivalent promoters to a silenced state. Tuning tissue mechanics *in vivo* and *in vitro* recapitulated age-related SC changes implicating niche mechanics as a central regulator of chromatin state, which, when altered, leads to age-dependent SC exhaustion. The critical role of the niche, and in particular its ECM component, is consistent with recent studies showing compromised HFSC mobilization upon wound healing in aged mice, but not upon transplantation into young recipients [404]. Thus, the microenvironment and its mechanical properties play a critical role in regulating stem cell chromatin landscape and functionality during aging, which might be relevant not only for the skin but other tissues as well.

References

1. Flatt, T., *A new definition of aging?* Front Genet, 2012. **3**: p. 148.
2. Klass, M.R., *A method for the isolation of longevity mutants in the nematode *Caenorhabditis elegans* and initial results.* Mech Ageing Dev, 1983. **22**(3-4): p. 279-86.
3. López-Otín, C., et al., *The hallmarks of aging.* Cell, 2013. **153**(6): p. 1194-1217.
4. Campisi, J., et al., *From discoveries in ageing research to therapeutics for healthy ageing.* Nature, 2019. **571**(7764): p. 183-192.
5. Lopez-Otin, C., et al., *The hallmarks of aging.* Cell, 2013. **153**(6): p. 1194-217.
6. Oh, S.-J., J.K. Lee, and O.S. Shin, *Ageing and the Immune System: the Impact of Immunosenescence on Viral Infection, Immunity and Vaccine Immunogenicity.* Immune Netw, 2019. **19**(6).
7. Beckman, K.B. and B.N. Ames, *The free radical theory of aging matures.* Physiol Rev, 1998. **78**(2): p. 547-81.
8. Pole, A., M. Dimri, and G.P. Dimri, *Oxidative stress, cellular senescence and ageing.* AIMS Molecular Science, 2016. **3**(3): p. 300-324.
9. Bárcena, C., P. Mayoral, and P.M. Quirós, *Mitohormesis, an Antiaging Paradigm.* Int Rev Cell Mol Biol, 2018. **340**: p. 35-77.
10. De la Fuente, M. and J. Miquel, *An update of the oxidation-inflammation theory of aging: the involvement of the immune system in oxi-inflamm-aging.* Curr Pharm Des, 2009. **15**(26): p. 3003-26.
11. Trifunovic, A., et al., *Premature ageing in mice expressing defective mitochondrial DNA polymerase.* Nature, 2004. **429**(6990): p. 417-423.
12. Kujoth, G.C., et al., *Mitochondrial DNA mutations, oxidative stress, and apoptosis in mammalian aging.* Science, 2005. **309**(5733): p. 481-484.
13. Alexeyev, M.F., *Is there more to aging than mitochondrial DNA and reactive oxygen species?* The FEBS journal, 2009. **276**(20): p. 5768-5787.
14. Kauppila, T.E.S., J.H.K. Kauppila, and N.-G. Larsson, *Mammalian Mitochondria and Aging: An Update.* Cell Metabolism, 2017. **25**(1): p. 57-71.
15. Park, C.B. and N.-G. Larsson, *Mitochondrial DNA mutations in disease and aging.* Journal of cell biology, 2011. **193**(5): p. 809-818.
16. Ameer, A., et al., *Ultra-deep sequencing of mouse mitochondrial DNA: mutational patterns and their origins.* PLoS Genet, 2011. **7**(3): p. e1002028.
17. Edgar, D., et al., *Random point mutations with major effects on protein-coding genes are the driving force behind premature aging in mtDNA mutator mice.* Cell metabolism, 2009. **10**(2): p. 131-138.
18. Fox, R.G., et al., *Mitochondrial DNA polymerase editing mutation, PolgD257A, disturbs stem-progenitor cell cycling in the small intestine and restricts excess fat absorption.* American Journal of Physiology-Gastrointestinal and Liver Physiology, 2012. **302**(9): p. G914-G924.
19. Ahlqvist, K.J., et al., *Somatic progenitor cell vulnerability to mitochondrial DNA mutagenesis underlies progeroid phenotypes in Polg mutator mice.* Cell metabolism, 2012. **15**(1): p. 100-109.
20. Drummond-Barbosa, D., *Stem cells, their niches and the systemic environment: an aging network.* Genetics, 2008. **180**(4): p. 1787-97.
21. Campisi, J., *Ageing, cellular senescence, and cancer.* Annu Rev Physiol, 2013. **75**: p. 685-705.

22. Chandrasekaran, A., M. Idelchik, and J.A. Melendez, *Redox control of senescence and age-related disease*. Redox Biol, 2017. **11**: p. 91-102.
23. Coppé, J.-P., et al., *The senescence-associated secretory phenotype: the dark side of tumor suppression*. Annual review of pathology, 2010. **5**: p. 99-118.
24. Collado, M., M.A. Blasco, and M. Serrano, *Cellular senescence in cancer and aging*. Cell, 2007. **130**(2): p. 223-33.
25. Chen, H., et al., *PDGF signalling controls age-dependent proliferation in pancreatic β -cells*. Nature, 2011. **478**(7369): p. 349-55.
26. Berent-Maoz, B., et al., *Fibroblast growth factor-7 partially reverses murine thymocyte progenitor aging by repression of *Ink4a**. Blood, 2012. **119**(24): p. 5715-21.
27. Blackburn, E.H., *Telomere states and cell fates*. Nature, 2000. **408**(6808): p. 53-6.
28. Sanders, J.L. and A.B. Newman, *Telomere length in epidemiology: a biomarker of aging, age-related disease, both, or neither?* Epidemiol Rev, 2013. **35**(1): p. 112-31.
29. Hayflick, L. and P.S. Moorhead, *The serial cultivation of human diploid cell strains*. Experimental cell research, 1961. **25**(3): p. 585-621.
30. Blasco, M.A., *Telomere length, stem cells and aging*. Nature chemical biology, 2007. **3**(10): p. 640-649.
31. Armanios, M., et al., *Short telomeres are sufficient to cause the degenerative defects associated with aging*. The American Journal of Human Genetics, 2009. **85**(6): p. 823-832.
32. Tomás-Loba, A., et al., *Telomerase reverse transcriptase delays aging in cancer-resistant mice*. Cell, 2008. **135**(4): p. 609-622.
33. Jaskelioff, M., et al., *Telomerase reactivation reverses tissue degeneration in aged telomerase-deficient mice*. Nature, 2011. **469**(7328): p. 102-106.
34. Bernardes de Jesus, B., et al., *Telomerase gene therapy in adult and old mice delays aging and increases longevity without increasing cancer*. EMBO molecular medicine, 2012. **4**(8): p. 691-704.
35. Boonekamp, J.J., et al., *Telomere length behaves as biomarker of somatic redundancy rather than biological age*. Aging cell, 2013. **12**(2): p. 330-332.
36. Breitling, L.P., et al., *Frailty is associated with the epigenetic clock but not with telomere length in a German cohort*. Clinical epigenetics, 2016. **8**(1): p. 21.
37. Marioni, R.E., et al., *The epigenetic clock and telomere length are independently associated with chronological age and mortality*. International journal of epidemiology, 2016. **45**(2): p. 424-432.
38. Bettedi, L. and L.C. Foukas, *Growth factor, energy and nutrient sensing signalling pathways in metabolic ageing*. Biogerontology, 2017. **18**(6): p. 913-929.
39. de Lucia, C., et al., *Lifestyle mediates the role of nutrient-sensing pathways in cognitive aging: cellular and epidemiological evidence*. Communications Biology, 2020. **3**(1): p. 157.
40. Fontana, L., L. Partridge, and V.D. Longo, *Extending healthy life span--from yeast to humans*. Science, 2010. **328**(5976): p. 321-6.
41. Kenyon, C.J., *The genetics of ageing*. Nature, 2010. **464**(7288): p. 504-12.
42. Milman, S., D.M. Huffman, and N. Barzilai, *The Somatotrophic Axis in Human Aging: Framework for the Current State of Knowledge and Future Research*. Cell Metab, 2016. **23**(6): p. 980-989.
43. Liu, G.Y. and D.M. Sabatini, *mTOR at the nexus of nutrition, growth, ageing and disease*. Nature Reviews Molecular Cell Biology, 2020. **21**(4): p. 183-203.

44. Kaeberlein, M. and B.K. Kennedy, *Ageing: A midlife longevity drug?* Nature, 2009. **460**(7253): p. 331-2.
45. Miller, R.A., et al., *Rapamycin-mediated lifespan increase in mice is dose and sex dependent and metabolically distinct from dietary restriction.* Aging Cell, 2014. **13**(3): p. 468-77.
46. Chang, H.C. and L. Guarente, *SIRT1 and other sirtuins in metabolism.* Trends Endocrinol Metab, 2014. **25**(3): p. 138-45.
47. Houtkooper, R.H., E. Pirinen, and J. Auwerx, *Sirtuins as regulators of metabolism and healthspan.* Nat Rev Mol Cell Biol, 2012. **13**(4): p. 225-238.
48. Guarente, L., *Sirtuins, aging, and metabolism.* Cold Spring Harb Symp Quant Biol, 2011. **76**: p. 81-90.
49. Garcia, D. and R.J. Shaw, *AMPK: mechanisms of cellular energy sensing and restoration of metabolic balance.* Molecular cell, 2017. **66**(6): p. 789-800.
50. Gwinn, D.M., et al., *AMPK phosphorylation of raptor mediates a metabolic checkpoint.* Molecular cell, 2008. **30**(2): p. 214-226.
51. Shaw, R.J., et al., *The LKB1 tumor suppressor negatively regulates mTOR signaling.* Cancer cell, 2004. **6**(1): p. 91-99.
52. Inoki, K., T. Zhu, and K.-L. Guan, *TSC2 mediates cellular energy response to control cell growth and survival.* Cell, 2003. **115**(5): p. 577-590.
53. Herzig, S. and R.J. Shaw, *AMPK: guardian of metabolism and mitochondrial homeostasis.* Nature reviews Molecular cell biology, 2018. **19**(2): p. 121.
54. Salminen, A. and K. Kaarniranta, *AMP-activated protein kinase (AMPK) controls the aging process via an integrated signaling network.* Ageing Res Rev, 2012. **11**(2): p. 230-41.
55. Hipp, M.S., P. Kasturi, and F.U. Hartl, *The proteostasis network and its decline in ageing.* Nature Reviews Molecular Cell Biology, 2019. **20**(7): p. 421-435.
56. Klaips, C.L., G.G. Jayaraj, and F.U. Hartl, *Pathways of cellular proteostasis in aging and disease.* Journal of Cell Biology, 2018. **217**(1): p. 51-63.
57. Hartl, F.U., A. Bracher, and M. Hayer-Hartl, *Molecular chaperones in protein folding and proteostasis.* Nature, 2011. **475**(7356): p. 324-332.
58. Brehme, M., et al., *A chaperome subnetwork safeguards proteostasis in aging and neurodegenerative disease.* Cell reports, 2014. **9**(3): p. 1135-1150.
59. Koga, H., S. Kaushik, and A.M. Cuervo, *Protein homeostasis and aging: The importance of exquisite quality control.* Ageing research reviews, 2011. **10**(2): p. 205-215.
60. Labbadia, J. and R.I. Morimoto, *The biology of proteostasis in aging and disease.* Annual review of biochemistry, 2015. **84**: p. 435-464.
61. Taylor, R.C. and A. Dillin, *Aging as an event of proteostasis collapse.* Cold Spring Harbor perspectives in biology, 2011. **3**(5): p. a004440.
62. Rubinsztein, D.C., G. Mariño, and G. Kroemer, *Autophagy and aging.* Cell, 2011. **146**(5): p. 682-695.
63. Min, J.-N., et al., *CHIP deficiency decreases longevity, with accelerated aging phenotypes accompanied by altered protein quality control.* Molecular and cellular biology, 2008. **28**(12): p. 4018-4025.
64. Sala, A.J., L.C. Bott, and R.I. Morimoto, *Shaping proteostasis at the cellular, tissue, and organismal level.* Journal of Cell Biology, 2017. **216**(5): p. 1231-1241.

65. Kundra, R., et al., *Protein homeostasis of a metastable subproteome associated with Alzheimer's disease*. Proceedings of the National Academy of Sciences, 2017. **114**(28): p. E5703-E5711.
66. Powers, E.T., et al., *Biological and chemical approaches to diseases of proteostasis deficiency*. Annual review of biochemistry, 2009. **78**: p. 959-991.
67. Vilchez, D., et al., *Increased proteasome activity in human embryonic stem cells is regulated by PSMD11*. Nature, 2012. **489**(7415): p. 304-308.
68. Noormohammadi, A., et al., *Somatic increase of CCT8 mimics proteostasis of human pluripotent stem cells and extends C. elegans lifespan*. Nature communications, 2016. **7**(1): p. 1-15.
69. Moore, D.L., et al., *A mechanism for the segregation of age in mammalian neural stem cells*. Science, 2015. **349**(6254): p. 1334-1338.
70. Bufalino, M.R., B. DeVeale, and D. van der Kooy, *The asymmetric segregation of damaged proteins is stem cell-type dependent*. Journal of Cell Biology, 2013. **201**(4): p. 523-530.
71. Hoeijmakers, J.H.J., *Genome maintenance mechanisms for preventing cancer*. nature, 2001. **411**(6835): p. 366-374.
72. Petr, M.A., et al., *Protecting the Aging Genome*. Trends Cell Biol, 2020. **30**(2): p. 117-132.
73. Jones, D.L. and T.A. Rando, *Emerging models and paradigms for stem cell ageing*. Nature cell biology, 2011. **13**(5): p. 506-512.
74. Rossi, D.J., C.H.M. Jamieson, and I.L. Weissman, *Stem cells and the pathways to aging and cancer*. Cell, 2008. **132**(4): p. 681-696.
75. Sedelnikova, O.A., et al., *Senescing human cells and ageing mice accumulate DNA lesions with unrepairable double-strand breaks*. Nat Cell Biol, 2004. **6**(2): p. 168-70.
76. Martínez-Ramírez, O.C., et al., *Association of the promoter methylation and the rs12917 polymorphism of MGMT with formation of DNA bulky adducts and the risk of lung cancer in Mexican mestizo population*. DNA and cell biology, 2019. **38**(4): p. 307-313.
77. Cetica, V., et al., *Pediatric brain tumors: mutations of two dioxygenases (hABH2 and hABH3) that directly repair alkylation damage*. Journal of neuro-oncology, 2009. **94**(2): p. 195-201.
78. Krokan, H.E. and M. Bjørås, *Base excision repair*. Cold Spring Harbor perspectives in biology, 2013. **5**(4): p. a012583.
79. Sinicrope, F.A., *Lynch syndrome—associated colorectal cancer*. New England Journal of Medicine, 2018. **379**(8): p. 764-773.
80. Cleaver, J.E., E.T. Lam, and I. Revet, *Disorders of nucleotide excision repair: the genetic and molecular basis of heterogeneity*. Nature Reviews Genetics, 2009. **10**(11): p. 756-768.
81. Hoeijmakers, J.H., *DNA damage, aging, and cancer*. N Engl J Med, 2009. **361**(15): p. 1475-85.
82. Keijzers, G., D. Bakula, and M. Scheibye-Knudsen, *Monogenic Diseases of DNA Repair*. N Engl J Med, 2017. **377**(19): p. 1868-1876.
83. Imam, S.Z., et al., *Mitochondrial and nuclear DNA-repair capacity of various brain regions in mouse is altered in an age-dependent manner*. Neurobiol Aging, 2006. **27**(8): p. 1129-36.
84. Krichevsky, S., et al., *Age related microsatellite instability in T cells from healthy individuals*. Exp Gerontol, 2004. **39**(4): p. 507-15.

85. White, M.C., et al., *Age and cancer risk: a potentially modifiable relationship*. Am J Prev Med, 2014. **46**(3 Suppl 1): p. S7-15.
86. Tower, J., *Programmed cell death in aging*. Ageing Res Rev, 2015. **23**(Pt A): p. 90-100.
87. Sharpless, N.E. and R.A. DePinho, *How stem cells age and why this makes us grow old*. Nat Rev Mol Cell Biol, 2007. **8**(9): p. 703-13.
88. Wong, K.K., et al., *Telomere dysfunction and Atm deficiency compromises organ homeostasis and accelerates ageing*. Nature, 2003. **421**(6923): p. 643-8.
89. Inomata, K., et al., *Genotoxic stress abrogates renewal of melanocyte stem cells by triggering their differentiation*. Cell, 2009. **137**(6): p. 1088-99.
90. Nishimura, E.K., S.R. Granter, and D.E. Fisher, *Mechanisms of hair graying: incomplete melanocyte stem cell maintenance in the niche*. Science, 2005. **307**(5710): p. 720-4.
91. Woolthuis, C.M., G. de Haan, and G. Huls, *Aging of hematopoietic stem cells: Intrinsic changes or micro-environmental effects?* Curr Opin Immunol, 2011. **23**(4): p. 512-7.
92. Wagner, W., et al., *Aging of hematopoietic stem cells is regulated by the stem cell niche*. Exp Gerontol, 2008. **43**(11): p. 974-80.
93. Jaiswal, S., et al., *Age-related clonal hematopoiesis associated with adverse outcomes*. N Engl J Med, 2014. **371**(26): p. 2488-98.
94. Brack, A.S., et al., *Increased Wnt signaling during aging alters muscle stem cell fate and increases fibrosis*. Science, 2007. **317**(5839): p. 807-10.
95. Conboy, M.J., I.M. Conboy, and T.A. Rando, *Heterochronic parabiosis: historical perspective and methodological considerations for studies of aging and longevity*. Aging Cell, 2013. **12**(3): p. 525-30.
96. Conboy, I.M. and T.A. Rando, *The regulation of Notch signaling controls satellite cell activation and cell fate determination in postnatal myogenesis*. Dev Cell, 2002. **3**(3): p. 397-409.
97. Molofsky, A.V., et al., *Increasing p16 INK4a expression decreases forebrain progenitors and neurogenesis during ageing*. Nature, 2006. **443**(7110): p. 448-452.
98. Gruber, R., et al., *Fracture healing in the elderly patient*. Experimental gerontology, 2006. **41**(11): p. 1080-1093.
99. Liu, G.-H., et al., *Recapitulation of premature ageing with iPSCs from Hutchinson–Gilford progeria syndrome*. Nature, 2011. **472**(7342): p. 221-225.
100. Zhang, W., et al., *A Werner syndrome stem cell model unveils heterochromatin alterations as a driver of human aging*. Science, 2015. **348**(6239): p. 1160-1163.
101. Liu, G.-H., et al., *Modelling Fanconi anemia pathogenesis and therapeutics using integration-free patient-derived iPSCs*. Nature communications, 2014. **5**(1): p. 1-17.
102. Liu, G.-H., et al., *Progressive degeneration of human neural stem cells caused by pathogenic LRRK2*. Nature, 2012. **491**(7425): p. 603-607.
103. Fu, L., et al., *Modeling xeroderma pigmentosum associated neurological pathologies with patients-derived iPSCs*. Protein & cell, 2016. **7**(3): p. 210-221.
104. Schofield, R., *The relationship between the spleen colony-forming cell and the haemopoietic stem cell*. Blood Cells, 1978. **4**(1-2): p. 7-25.
105. Hsu, Y.C., L. Li, and E. Fuchs, *Emerging interactions between skin stem cells and their niches*. Nat Med, 2014. **20**(8): p. 847-56.
106. Adams, G.B. and D.T. Scadden, *The hematopoietic stem cell in its place*. Nature immunology, 2006. **7**(4): p. 333-337.
107. Scadden, D.T., *Nice neighborhood: emerging concepts of the stem cell niche*. Cell, 2014. **157**(1): p. 41-50.

108. Chacón-Martínez, C.A., J. Koester, and S.A. Wickström, *Signaling in the stem cell niche: regulating cell fate, function and plasticity*. *Development*, 2018. **145**(15).
109. Ryu, B.Y., et al., *Effects of aging and niche microenvironment on spermatogonial stem cell self-renewal*. *Stem cells*, 2006. **24**(6): p. 1505-1511.
110. Schmidt, J.A., et al., *In vivo and in vitro aging is detrimental to mouse spermatogonial stem cell function*. *Biology of reproduction*, 2011. **84**(4): p. 698-706.
111. Toledano, H., et al., *The let-7–Imp axis regulates ageing of the Drosophila testis stem-cell niche*. *Nature*, 2012. **485**(7400): p. 605-610.
112. Zhao, R., et al., *Age-related changes of germline stem cell activity, niche signaling activity and egg production in Drosophila*. *Aging cell*, 2008. **7**(3): p. 344-354.
113. Boyle, M., et al., *Decline in self-renewal factors contributes to aging of the stem cell niche in the Drosophila testis*. *Cell stem cell*, 2007. **1**(4): p. 470-478.
114. Coppé, J.P., et al., *Senescence-associated secretory phenotypes reveal cell-nonautonomous functions of oncogenic RAS and the p53 tumor suppressor*. *PLoS Biol*, 2008. **6**(12): p. 2853-68.
115. Sinha, M., et al., *Restoring systemic GDF11 levels reverses age-related dysfunction in mouse skeletal muscle*. *Science*, 2014. **344**(6184): p. 649-652.
116. Chakkalakal, J.V., et al., *The aged niche disrupts muscle stem cell quiescence*. *Nature*, 2012. **490**(7420): p. 355-360.
117. Carlson, B.M. and J.A. Faulkner, *Muscle transplantation between young and old rats: age of host determines recovery*. *American Journal of Physiology-Cell Physiology*, 1989. **256**(6): p. C1262-C1266.
118. Katsimpardi, L., et al., *Vascular and neurogenic rejuvenation of the aging mouse brain by young systemic factors*. *Science*, 2014. **344**(6184): p. 630-634.
119. Villeda, S.A., et al., *The ageing systemic milieu negatively regulates neurogenesis and cognitive function*. *Nature*, 2011. **477**(7362): p. 90-94.
120. Doles, J., et al., *Age-associated inflammation inhibits epidermal stem cell function*. *Genes & development*, 2012. **26**(19): p. 2144-2153.
121. Ergen, A.V., N.C. Boles, and M.A. Goodell, *Rantes/Ccl5 influences hematopoietic stem cell subtypes and causes myeloid skewing*. *Blood*, 2012. **119**(11): p. 2500-2509.
122. Florian, M.C., et al., *A canonical to non-canonical Wnt signalling switch in haematopoietic stem-cell ageing*. *Nature*, 2013. **503**(7476): p. 392-6.
123. Geiger, H., G. de Haan, and M.C. Florian, *The ageing haematopoietic stem cell compartment*. *Nature Reviews Immunology*, 2013. **13**(5): p. 376-389.
124. Pentimikko, N., et al., *Notum produced by Paneth cells attenuates regeneration of aged intestinal epithelium*. *Nature*, 2019. **571**(7765): p. 398-402.
125. Segel, M., et al., *Niche stiffness underlies the ageing of central nervous system progenitor cells*. *Nature*, 2019. **573**(7772): p. 130-134.
126. Olins, D.E. and A.L. Olins, *Chromatin history: our view from the bridge*. *Nature reviews Molecular cell biology*, 2003. **4**(10): p. 809-814.
127. Allis, C.D. and T. Jenuwein, *The molecular hallmarks of epigenetic control*. *Nature Reviews Genetics*, 2016. **17**(8): p. 487.
128. Dann, G.P., et al., *ISWI chromatin remodellers sense nucleosome modifications to determine substrate preference*. *Nature*, 2017. **548**(7669): p. 607-611.
129. Szabo, Q., F. Bantignies, and G. Cavalli, *Principles of genome folding into topologically associating domains*. *Science advances*, 2019. **5**(4): p. eaaw1668.
130. Janssen, A., S.U. Colmenares, and G.H. Karpen, *Heterochromatin: Guardian of the Genome*. *Annual Review of Cell and Developmental Biology*, 2018. **34**(1): p. 265-288.

131. Allshire, R.C. and H.D. Madhani, *Ten principles of heterochromatin formation and function*. Nature Reviews Molecular Cell Biology, 2018. **19**(4): p. 229.
132. Lee, C.-K., et al., *Evidence for nucleosome depletion at active regulatory regions genome-wide*. Nature genetics, 2004. **36**(8): p. 900-905.
133. McBryant, S.J., V.H. Adams, and J.C. Hansen, *Chromatin architectural proteins*. Chromosome Research, 2006. **14**(1): p. 39-51.
134. Fyodorov, D.V., et al., *Emerging roles of linker histones in regulating chromatin structure and function*. Nature reviews Molecular cell biology, 2018. **19**(3): p. 192.
135. Izzo, A., et al., *Dynamic changes in H1 subtype composition during epigenetic reprogramming*. Journal of Cell Biology, 2017. **216**(10): p. 3017-3028.
136. Thurman, R.E., et al., *The accessible chromatin landscape of the human genome*. Nature, 2012. **489**(7414): p. 75-82.
137. Bannister, A.J. and T. Kouzarides, *Regulation of chromatin by histone modifications*. Cell Research, 2011. **21**(3): p. 381-395.
138. Campos, E.I. and D. Reinberg, *Histones: Annotating Chromatin*. Annual Review of Genetics, 2009. **43**(1): p. 559-599.
139. Jenuwein, T. and C.D. Allis, *Translating the Histone Code*. Science, 2001. **293**(5532): p. 1074.
140. Shema, E., et al., *Single-molecule decoding of combinatorially modified nucleosomes*. Science, 2016. **352**(6286): p. 717.
141. Klemm, S.L., Z. Shipony, and W.J. Greenleaf, *Chromatin accessibility and the regulatory epigenome*. Nature Reviews Genetics, 2019. **20**(4): p. 207-220.
142. Du, J., et al., *DNA methylation pathways and their crosstalk with histone methylation*. Nature Reviews Molecular Cell Biology, 2015. **16**(9): p. 519-532.
143. McAnena, P., J.A. Brown, and M.J. Kerin, *Circulating Nucleosomes and Nucleosome Modifications as Biomarkers in Cancer*. Cancers (Basel), 2017. **9**(1).
144. Suh, H., et al., *The C-terminal domain of Rpb1 functions on other RNA polymerase II subunits*. Molecular cell, 2013. **51**(6): p. 850-858.
145. Phatnani, H.P. and A.L. Greenleaf, *Phosphorylation and functions of the RNA polymerase II CTD*. Genes Dev, 2006. **20**(21): p. 2922-36.
146. Brookes, E. and A. Pombo, *Code breaking: the RNAPII modification code in pluripotency*. Cell Cycle, 2012. **11**(7): p. 1267-8.
147. Tietjen, J.R., et al., *Chemical-genomic dissection of the CTD code*. Nat Struct Mol Biol, 2010. **17**(9): p. 1154-61.
148. Hampsey, M., *Molecular genetics of the RNA polymerase II general transcriptional machinery*. Microbiol Mol Biol Rev, 1998. **62**(2): p. 465-503.
149. Black, J.C., et al., *A mechanism for coordinating chromatin modification and preinitiation complex assembly*. Molecular cell, 2006. **23**(6): p. 809-818.
150. Thomas, M.C. and C.-M. Chiang, *The general transcription machinery and general cofactors*. Critical reviews in biochemistry and molecular biology, 2006. **41**(3): p. 105-178.
151. Wasserman, W.W. and A. Sandelin, *Applied bioinformatics for the identification of regulatory elements*. Nature Reviews Genetics, 2004. **5**(4): p. 276-287.
152. Spitz, F. and E.E.M. Furlong, *Transcription factors: from enhancer binding to developmental control*. Nature reviews genetics, 2012. **13**(9): p. 613-626.
153. Zabidi, M.A. and A. Stark, *Regulatory enhancer–core-promoter communication via transcription factors and cofactors*. Trends in Genetics, 2016. **32**(12): p. 801-814.

154. Voigt, P., W.W. Tee, and D. Reinberg, *A double take on bivalent promoters*. *Genes Dev*, 2013. **27**(12): p. 1318-38.
155. Gaertner, B., et al., *Poised RNA polymerase II changes over developmental time and prepares genes for future expression*. *Cell reports*, 2012. **2**(6): p. 1670-1683.
156. Mikkelsen, T.S., et al., *Genome-wide maps of chromatin state in pluripotent and lineage-committed cells*. *Nature*, 2007. **448**(7153): p. 553-560.
157. Harikumar, A. and E. Meshorer, *Chromatin remodeling and bivalent histone modifications in embryonic stem cells*. *EMBO Rep*, 2015. **16**(12): p. 1609-19.
158. Blanco, E., et al., *The Bivalent Genome: Characterization, Structure, and Regulation*. *Trends Genet*, 2020. **36**(2): p. 118-131.
159. Bernstein, B.E., et al., *A bivalent chromatin structure marks key developmental genes in embryonic stem cells*. *Cell*, 2006. **125**(2): p. 315-326.
160. Ku, M., et al., *Genomewide analysis of PRC1 and PRC2 occupancy identifies two classes of bivalent domains*. *PLoS Genet*, 2008. **4**(10): p. e1000242.
161. Meissner, A., et al., *Genome-scale DNA methylation maps of pluripotent and differentiated cells*. *Nature*, 2008. **454**(7205): p. 766-770.
162. Lien, W.-H., et al., *Genome-wide maps of histone modifications unwind in vivo chromatin states of the hair follicle lineage*. *Cell stem cell*, 2011. **9**(3): p. 219-232.
163. Zhang, W., et al., *The ageing epigenome and its rejuvenation*. *Nature Reviews Molecular Cell Biology*, 2020. **21**(3): p. 137-150.
164. Rando, T.A. and H.Y. Chang, *Aging, rejuvenation, and epigenetic reprogramming: resetting the aging clock*. *Cell*, 2012. **148**(1-2): p. 46-57.
165. Booth, L.N. and A. Brunet, *The aging epigenome*. *Molecular cell*, 2016. **62**(5): p. 728-744.
166. Avgustinova, A. and S.A. Benitah, *Epigenetic control of adult stem cell function*. *Nature reviews Molecular cell biology*, 2016. **17**(10): p. 643.
167. Ermolaeva, M., et al., *Cellular and epigenetic drivers of stem cell ageing*. *Nature Reviews Molecular Cell Biology*, 2018. **19**(9): p. 594.
168. Benayoun, B.A., E.A. Pollina, and A. Brunet, *Epigenetic regulation of ageing: linking environmental inputs to genomic stability*. *Nat Rev Mol Cell Biol*, 2015. **16**(10): p. 593-610.
169. Sidler, C., O. Kovalchuk, and I. Kovalchuk, *Epigenetic regulation of cellular senescence and aging*. *Frontiers in genetics*, 2017. **8**: p. 138.
170. Bollati, V., et al., *Decline in genomic DNA methylation through aging in a cohort of elderly subjects*. *Mechanisms of ageing and development*, 2009. **130**(4): p. 234-239.
171. Rakyan, V.K., et al., *Human aging-associated DNA hypermethylation occurs preferentially at bivalent chromatin domains*. *Genome Res*, 2010. **20**(4): p. 434-9.
172. Teschendorff, A.E., et al., *Age-dependent DNA methylation of genes that are suppressed in stem cells is a hallmark of cancer*. *Genome Res*, 2010. **20**(4): p. 440-6.
173. Fernández, A.F., et al., *H3K4me1 marks DNA regions hypomethylated during aging in human stem and differentiated cells*. *Genome Res*, 2015. **25**(1): p. 27-40.
174. Day, K., et al., *Differential DNA methylation with age displays both common and dynamic features across human tissues that are influenced by CpG landscape*. *Genome Biol*, 2013. **14**(9): p. R102.
175. Heyn, H., et al., *Distinct DNA methylomes of newborns and centenarians*. *Proc Natl Acad Sci U S A*, 2012. **109**(26): p. 10522-7.
176. Ren, R., et al., *Regulation of stem cell aging by metabolism and epigenetics*. *Cell metabolism*, 2017. **26**(3): p. 460-474.

177. Horvath, S., *DNA methylation age of human tissues and cell types*. *Genome Biology*, 2013. **14**(10): p. 3156.
178. Ohm, J.E., et al., *A stem cell-like chromatin pattern may predispose tumor suppressor genes to DNA hypermethylation and heritable silencing*. *Nature genetics*, 2007. **39**(2): p. 237-242.
179. Schlesinger, Y., et al., *Polycomb-mediated methylation on Lys27 of histone H3 pre-marks genes for de novo methylation in cancer*. *Nature genetics*, 2007. **39**(2): p. 232-236.
180. Widschwendter, M., et al., *Epigenetic stem cell signature in cancer*. *Nature genetics*, 2007. **39**(2): p. 157-158.
181. Hernando-Herraez, I., et al., *Ageing affects DNA methylation drift and transcriptional cell-to-cell variability in mouse muscle stem cells*. *Nature communications*, 2019. **10**(1): p. 1-11.
182. Enge, M., et al., *Single-Cell Analysis of Human Pancreas Reveals Transcriptional Signatures of Aging and Somatic Mutation Patterns*. *Cell*, 2017. **171**(2): p. 321-330.e14.
183. Liu, P., et al., *Noise reduction as an emergent property of single-cell aging*. *Nat Commun*, 2017. **8**(1): p. 680.
184. Raser, J.M. and E.K. O'Shea, *Control of stochasticity in eukaryotic gene expression*. *Science*, 2004. **304**(5678): p. 1811-4.
185. Salzer, M.C., et al., *Identity Noise and Adipogenic Traits Characterize Dermal Fibroblast Aging*. *Cell*, 2018. **175**(6): p. 1575-1590.e22.
186. Swisa, A., K.H. Kaestner, and Y. Dor, *Transcriptional Noise and Somatic Mutations in the Aging Pancreas*. *Cell Metab*, 2017. **26**(6): p. 809-811.
187. Gravina, S., et al., *Single-cell genome-wide bisulfite sequencing uncovers extensive heterogeneity in the mouse liver methylome*. *Genome biology*, 2016. **17**(1): p. 1-8.
188. Jaalouk, D.E. and J. Lammerding, *Mechanotransduction gone awry*. *Nat Rev Mol Cell Biol*, 2009. **10**(1): p. 63-73.
189. Paluch, E.K., et al., *Mechanotransduction: use the force(s)*. *BMC Biol*, 2015. **13**: p. 47.
190. Sasai, Y., *Cytosystems dynamics in self-organization of tissue architecture*. *Nature*, 2013. **493**(7432): p. 318-26.
191. Thomson, J.A., *On Growth and Form*. *Nature*, 1917. **100**(2498): p. 21-22.
192. Ingber, D.E., *Cellular mechanotransduction: putting all the pieces together again*. *Faseb j*, 2006. **20**(7): p. 811-27.
193. Orr, A.W., et al., *Mechanisms of mechanotransduction*. *Dev Cell*, 2006. **10**(1): p. 11-20.
194. DuFort, C.C., M.J. Paszek, and V.M. Weaver, *Balancing forces: architectural control of mechanotransduction*. *Nat Rev Mol Cell Biol*, 2011. **12**(5): p. 308-19.
195. Reichelt, J., *Mechanotransduction of keratinocytes in culture and in the epidermis*. *Eur J Cell Biol*, 2007. **86**(11-12): p. 807-16.
196. Stutchbury, B., et al., *Distinct focal adhesion protein modules control different aspects of mechanotransduction*. *Journal of cell science*, 2017. **130**(9): p. 1612-1624.
197. Coste, B., et al., *Piezo proteins are pore-forming subunits of mechanically activated channels*. *Nature*, 2012. **483**(7388): p. 176-181.
198. Collins, C., et al., *Changes in E-cadherin rigidity sensing regulate cell adhesion*. *Proceedings of the National Academy of Sciences*, 2017. **114**(29): p. E5835-E5844.
199. Luca, V.C., et al., *Notch-Jagged complex structure implicates a catch bond in tuning ligand sensitivity*. *Science*, 2017. **355**(6331): p. 1320-1324.

200. Dupont, S., et al., *Role of YAP/TAZ in mechanotransduction*. Nature, 2011. **474**(7350): p. 179-183.
201. Miralles, F., et al., *Actin dynamics control SRF activity by regulation of its coactivator MAL*. Cell, 2003. **113**(3): p. 329-342.
202. Alam, S.G., et al., *The mammalian LINC complex regulates genome transcriptional responses to substrate rigidity*. Scientific Reports, 2016. **6**: p. 38063.
203. Crisp, M., et al., *Coupling of the nucleus and cytoplasm: role of the LINC complex*. The Journal of cell biology, 2006. **172**(1): p. 41-53.
204. Gruenbaum, Y. and R. Foisner, *Lamins: nuclear intermediate filament proteins with fundamental functions in nuclear mechanics and genome regulation*. Annual review of biochemistry, 2015. **84**: p. 131-164.
205. Thorpe, S.D. and D.A. Lee, *Dynamic regulation of nuclear architecture and mechanics—a rheostatic role for the nucleus in tailoring cellular mechanosensitivity*. Nucleus, 2017. **8**(3): p. 287-300.
206. Mazumder, A. and G.V. Shivashankar, *Gold-nanoparticle-assisted laser perturbation of chromatin assembly reveals unusual aspects of nuclear architecture within living cells*. Biophysical journal, 2007. **93**(6): p. 2209-2216.
207. Ramdas, N.M. and G.V. Shivashankar, *Cytoskeletal control of nuclear morphology and chromatin organization*. Journal of molecular biology, 2015. **427**(3): p. 695-706.
208. Buxboim, A., et al., *Matrix elasticity regulates lamin-A, C phosphorylation and turnover with feedback to actomyosin*. Current Biology, 2014. **24**(16): p. 1909-1917.
209. Swift, J., et al., *Nuclear lamin-A scales with tissue stiffness and enhances matrix-directed differentiation*. Science, 2013. **341**(6149).
210. Scaffidi, P. and T. Misteli, *Lamin A-dependent nuclear defects in human aging*. Science, 2006. **312**(5776): p. 1059-1063.
211. Heo, S.-J., et al., *Differentiation alters stem cell nuclear architecture, mechanics, and mechano-sensitivity*. Elife, 2016. **5**: p. e18207.
212. Uhler, C. and G.V. Shivashankar, *Regulation of genome organization and gene expression by nuclear mechanotransduction*. Nature Reviews Molecular Cell Biology, 2017. **18**(12): p. 717-727.
213. Engler, A.J., et al., *Matrix elasticity directs stem cell lineage specification*. Cell, 2006. **126**(4): p. 677-89.
214. Adamo, L., et al., *Biomechanical forces promote embryonic haematopoiesis*. Nature, 2009. **459**(7250): p. 1131-1135.
215. Przybyla, L., J.M. Muncie, and V.M. Weaver, *Mechanical control of epithelial-to-mesenchymal transitions in development and cancer*. Annual review of cell and developmental biology, 2016. **32**: p. 527-554.
216. Le, H.Q., et al., *Mechanical regulation of transcription controls Polycomb-mediated gene silencing during lineage commitment*. Nat Cell Biol, 2016. **18**(8): p. 864-75.
217. Miroshnikova, Y.A., M.M. Nava, and S.A. Wickström, *Emerging roles of mechanical forces in chromatin regulation*. J Cell Sci, 2017. **130**(14): p. 2243-2250.
218. Nava, M.M., et al., *Heterochromatin-Driven Nuclear Softening Protects the Genome against Mechanical Stress-Induced Damage*. Cell, 2020. **181**(4): p. 800-817.e22.
219. Argentati, C., et al., *Insight into Mechanobiology: How Stem Cells Feel Mechanical Forces and Orchestrate Biological Functions*. International journal of molecular sciences, 2019. **20**(21): p. 5337.

220. Potten, C.S., R. Saffhill, and H.I. Maibach, *Measurement of the transit time for cells through the epidermis and stratum corneum of the mouse and guinea-pig*. Cell Tissue Kinet, 1987. **20**(5): p. 461-72.
221. Reynolds, A.J. and C.A. Jahoda, *Hair follicle stem cells? A distinct germinative epidermal cell population is activated in vitro by the presence of hair dermal papilla cells*. J Cell Sci, 1991. **99 (Pt 2)**: p. 373-85.
222. Oshima, H., et al., *Morphogenesis and renewal of hair follicles from adult multipotent stem cells*. Cell, 2001. **104**(2): p. 233-45.
223. Muller-Rover, S., et al., *A comprehensive guide for the accurate classification of murine hair follicles in distinct hair cycle stages*. J Invest Dermatol, 2001. **117**(1): p. 3-15.
224. Gonzales, K.A.U. and E. Fuchs, *Skin and Its Regenerative Powers: An Alliance between Stem Cells and Their Niche*. Dev Cell, 2017. **43**(4): p. 387-401.
225. Sennett, R. and M. Rendl, *Mesenchymal-epithelial interactions during hair follicle morphogenesis and cycling*. Semin Cell Dev Biol, 2012. **23**(8): p. 917-27.
226. Botchkarev, V.A. and R. Paus, *Molecular biology of hair morphogenesis: development and cycling*. J Exp Zool B Mol Dev Evol, 2003. **298**(1): p. 164-80.
227. Schmidt-Ullrich, R. and R. Paus, *Molecular principles of hair follicle induction and morphogenesis*. Bioessays, 2005. **27**(3): p. 247-61.
228. Schneider, M.R., R. Schmidt-Ullrich, and R. Paus, *The hair follicle as a dynamic miniorgan*. Curr Biol, 2009. **19**(3): p. R132-42.
229. Stenn, K.S. and R. Paus, *Controls of hair follicle cycling*. Physiological reviews, 2001.
230. Hsu, Y.-C., H.A. Pasolli, and E. Fuchs, *Dynamics between stem cells, niche, and progeny in the hair follicle*. Cell, 2011. **144**(1): p. 92-105.
231. Rompolas, P., K.R. Mesa, and V. Greco, *Spatial organization within a niche as a determinant of stem-cell fate*. Nature, 2013. **502**(7472): p. 513-518.
232. Blanpain, C. and E. Fuchs, *Epidermal homeostasis: a balancing act of stem cells in the skin*. Nature Reviews Molecular Cell Biology, 2009. **10**(3): p. 207-217.
233. Yi, R., *Concise Review: Mechanisms of Quiescent Hair Follicle Stem Cell Regulation*. STEM CELLS, 2017. **35**(12): p. 2323-2330.
234. Veltri, A., C. Lang, and W.-H. Lien, *Concise Review: Wnt Signaling Pathways in Skin Development and Epidermal Stem Cells*. STEM CELLS, 2018. **36**(1): p. 22-35.
235. Cotsarelis, G., T.T. Sun, and R.M. Lavker, *Label-retaining cells reside in the bulge area of pilosebaceous unit: implications for follicular stem cells, hair cycle, and skin carcinogenesis*. Cell, 1990. **61**(7): p. 1329-37.
236. Greco, V., et al., *A two-step mechanism for stem cell activation during hair regeneration*. Cell Stem Cell, 2009. **4**(2): p. 155-69.
237. Rahmani, W., et al., *Hair follicle dermal stem cells regenerate the dermal sheath, repopulate the dermal papilla, and modulate hair type*. Dev Cell, 2014. **31**(5): p. 543-58.
238. Biernaskie, J., et al., *SKPs derive from hair follicle precursors and exhibit properties of adult dermal stem cells*. Cell Stem Cell, 2009. **5**(6): p. 610-23.
239. Nishimura, E.K., et al., *Dominant role of the niche in melanocyte stem-cell fate determination*. Nature, 2002. **416**(6883): p. 854-60.
240. Festa, E., et al., *Adipocyte lineage cells contribute to the skin stem cell niche to drive hair cycling*. Cell, 2011. **146**(5): p. 761-71.
241. Plikus, M.V., et al., *Cyclic dermal BMP signalling regulates stem cell activation during hair regeneration*. Nature, 2008. **451**(7176): p. 340-4.

242. Mecklenburg, L., et al., *Active hair growth (anagen) is associated with angiogenesis*. J Invest Dermatol, 2000. **114**(5): p. 909-16.
243. Gur-Cohen, S., et al., *Stem cell-driven lymphatic remodeling coordinates tissue regeneration*. Science, 2019. **366**(6470): p. 1218-1225.
244. Brownell, I., et al., *Nerve-derived sonic hedgehog defines a niche for hair follicle stem cells capable of becoming epidermal stem cells*. Cell Stem Cell, 2011. **8**(5): p. 552-65.
245. Plikus, M.V., *New activators and inhibitors in the hair cycle clock: targeting stem cells' state of competence*. J Invest Dermatol, 2012. **132**(5): p. 1321-4.
246. Murray, P.J., et al., *Modelling hair follicle growth dynamics as an excitable medium*. PLoS Comput Biol, 2012. **8**(12): p. e1002804.
247. Plikus, M.V., et al., *Self-organizing and stochastic behaviors during the regeneration of hair stem cells*. Science, 2011. **332**(6029): p. 586-9.
248. Plikus, M.V., et al., *Cyclic dermal BMP signalling regulates stem cell activation during hair regeneration*. Nature, 2008. **451**(7176): p. 340-344.
249. Myung, P.S., et al., *Epithelial Wnt ligand secretion is required for adult hair follicle growth and regeneration*. Journal of Investigative Dermatology, 2013. **133**(1): p. 31-41.
250. Choi, Y.S., et al., *Distinct functions for Wnt/ β -catenin in hair follicle stem cell proliferation and survival and interfollicular epidermal homeostasis*. Cell stem cell, 2013. **13**(6): p. 720-733.
251. Oshimori, N. and E. Fuchs, *Paracrine TGF- β signaling counterbalances BMP-mediated repression in hair follicle stem cell activation*. Cell stem cell, 2012. **10**(1): p. 63-75.
252. Wang, E.C.E., et al., *A subset of TREM2+ dermal macrophages secretes Oncostatin M to maintain hair follicle stem cell quiescence and inhibit hair growth*. Cell Stem Cell, 2019. **24**(4): p. 654-669.
253. Leishman, E., et al., *Foxp1 maintains hair follicle stem cell quiescence through regulation of Fgf18*. Development, 2013. **140**(18): p. 3809-3818.
254. Chen, C.-L., et al., *Functional complexity of hair follicle stem cell niche and therapeutic targeting of niche dysfunction for hair regeneration*. Journal of Biomedical Science, 2020. **27**(1): p. 43.
255. Lowry, W.E., et al., *Defining the impact of beta-catenin/Tcf transactivation on epithelial stem cells*. Genes Dev, 2005. **19**(13): p. 1596-611.
256. Deschene, E.R., et al., *β -Catenin activation regulates tissue growth non-cell autonomously in the hair stem cell niche*. Science, 2014. **343**(6177): p. 1353-6.
257. Lim, X., et al., *Axin2 marks quiescent hair follicle bulge stem cells that are maintained by autocrine Wnt/ β -catenin signaling*. Proc Natl Acad Sci U S A, 2016. **113**(11): p. E1498-505.
258. Clevers, H. and R. Nusse, *Wnt/ β -catenin signaling and disease*. Cell, 2012. **149**(6): p. 1192-205.
259. Huelsken, J., et al., *beta-Catenin controls hair follicle morphogenesis and stem cell differentiation in the skin*. Cell, 2001. **105**(4): p. 533-45.
260. van Genderen, C., et al., *Development of several organs that require inductive epithelial-mesenchymal interactions is impaired in LEF-1-deficient mice*. Genes Dev, 1994. **8**(22): p. 2691-703.
261. Lien, W.-H., et al., *In vivo transcriptional governance of hair follicle stem cells by canonical Wnt regulators*. Nature cell biology, 2014. **16**(2): p. 179-190.
262. Ito, M., et al., *Wnt-dependent de novo hair follicle regeneration in adult mouse skin after wounding*. Nature, 2007. **447**(7142): p. 316-20.

263. Gay, D., et al., *Fgf9 from dermal $\gamma\delta$ T cells induces hair follicle neogenesis after wounding*. Nat Med, 2013. **19**(7): p. 916-23.
264. Owens, P., et al., *The role of Smads in skin development*. J Invest Dermatol, 2008. **128**(4): p. 783-90.
265. Kobiela, K., et al., *Loss of a quiescent niche but not follicle stem cells in the absence of bone morphogenetic protein signaling*. Proc Natl Acad Sci U S A, 2007. **104**(24): p. 10063-8.
266. Rendl, M., L. Polak, and E. Fuchs, *BMP signaling in dermal papilla cells is required for their hair follicle-inductive properties*. Genes Dev, 2008. **22**(4): p. 543-57.
267. Kimura-Ueki, M., et al., *Hair cycle resting phase is regulated by cyclic epithelial FGF18 signaling*. Journal of Investigative Dermatology, 2012. **132**(5): p. 1338-1345.
268. Zhang, X., et al., *Receptor specificity of the fibroblast growth factor family. The complete mammalian FGF family*. J Biol Chem, 2006. **281**(23): p. 15694-700.
269. Brewer, J.R., P. Mazot, and P. Soriano, *Genetic insights into the mechanisms of Fgf signaling*. Genes Dev, 2016. **30**(7): p. 751-71.
270. Hsu, Y.C., L. Li, and E. Fuchs, *Transit-amplifying cells orchestrate stem cell activity and tissue regeneration*. Cell, 2014. **157**(4): p. 935-49.
271. Ezhkova, E., et al., *EZH1 and EZH2 cogovern histone H3K27 trimethylation and are essential for hair follicle homeostasis and wound repair*. Genes & development, 2011. **25**(5): p. 485-498.
272. Li, J., et al., *Progressive alopecia reveals decreasing stem cell activation probability during aging of mice with epidermal deletion of DNA methyltransferase 1*. Journal of Investigative Dermatology, 2012. **132**(12): p. 2681-2690.
273. Frantz, C., K.M. Stewart, and V.M. Weaver, *The extracellular matrix at a glance*. Journal of cell science, 2010. **123**(24): p. 4195-4200.
274. Hubmacher, D. and S.S. Apte, *The biology of the extracellular matrix: novel insights*. Current opinion in rheumatology, 2013. **25**(1): p. 65.
275. Gattazzo, F., A. Urciuolo, and P. Bonaldo, *Extracellular matrix: a dynamic microenvironment for stem cell niche*. Biochim Biophys Acta, 2014. **1840**(8): p. 2506-19.
276. Watt, F.M. and H. Fujiwara, *Cell-extracellular matrix interactions in normal and diseased skin*. Cold Spring Harb Perspect Biol, 2011. **3**(4).
277. Schultz, G.S., et al., *Dynamic reciprocity in the wound microenvironment*. Wound Repair and Regeneration, 2011. **19**(2): p. 134-148.
278. Bissell, M.J., H.G. Hall, and G. Parry, *How does the extracellular matrix direct gene expression?* Journal of theoretical biology, 1982. **99**(1): p. 31-68.
279. Yue, B., *Biology of the extracellular matrix: an overview*. Journal of glaucoma, 2014: p. S20.
280. Mecham, R.P., *Overview of extracellular matrix*. Current protocols in cell biology, 2012. **57**(1): p. 10-1.
281. Jiang, D., et al., *Efficacy of tendon stem cells in fibroblast-derived matrix for tendon tissue engineering*. Cytotherapy, 2014. **16**(5): p. 662-73.
282. Ng, C.P., et al., *Enhanced ex vivo expansion of adult mesenchymal stem cells by fetal mesenchymal stem cell ECM*. Biomaterials, 2014. **35**(13): p. 4046-57.
283. Peng, Y., et al., *Human fibroblast matrices bio-assembled under macromolecular crowding support stable propagation of human embryonic stem cells*. J Tissue Eng Regen Med, 2012. **6**(10): p. e74-86.

284. Zhou, Y., et al., *Effects of Human Fibroblast-Derived Extracellular Matrix on Mesenchymal Stem Cells*. Stem Cell Rev Rep, 2016. **12**(5): p. 560-572.
285. Bruckner, P., *Suprastructures of extracellular matrices: paradigms of functions controlled by aggregates rather than molecules*. Cell Tissue Res, 2010. **339**(1): p. 7-18.
286. Kadler, K.E., et al., *Collagens at a glance*. J Cell Sci, 2007. **120**(Pt 12): p. 1955-8.
287. Ricard-Blum, S., *The collagen family*. Cold Spring Harbor perspectives in biology, 2011. **3**(1): p. a004978-a004978.
288. Gordon, M.K. and R.A. Hahn, *Collagens*. Cell Tissue Res, 2010. **339**(1): p. 247-57.
289. Naba, A., et al., *The matrisome: in silico definition and in vivo characterization by proteomics of normal and tumor extracellular matrices*. Mol Cell Proteomics, 2012. **11**(4): p. M111.014647.
290. Ramirez, F. and H.C. Dietz, *Fibrillin-rich microfibrils: Structural determinants of morphogenetic and homeostatic events*. J Cell Physiol, 2007. **213**(2): p. 326-30.
291. Schwarzbauer, J.E. and D.W. DeSimone, *Fibronectins, their fibrillogenesis, and in vivo functions*. Cold Spring Harb Perspect Biol, 2011. **3**(7).
292. Sakai, T., M. Larsen, and K.M. Yamada, *Fibronectin requirement in branching morphogenesis*. Nature, 2003. **423**(6942): p. 876-81.
293. Gesslbauer, B., et al., *Exploring the glycosaminoglycan-protein interaction network by glycan-mediated pull-down proteomics*. Electrophoresis, 2016. **37**(11): p. 1437-47.
294. Murphy-Ullrich, J.E. and E.H. Sage, *Revisiting the matricellular concept*. Matrix Biology, 2014. **37**: p. 1-14.
295. Stanton, A.E., X. Tong, and F. Yang, *Extracellular matrix type modulates mechanotransduction of stem cells*. Acta biomaterialia, 2019. **96**: p. 310-320.
296. Yang, Y., et al., *Biophysical Regulation of Cell Behavior—Cross Talk between Substrate Stiffness and Nanotopography*. Engineering, 2017. **3**(1): p. 36-54.
297. Humphrey, J.D., E.R. Dufresne, and M.A. Schwartz, *Mechanotransduction and extracellular matrix homeostasis*. Nature reviews Molecular cell biology, 2014. **15**(12): p. 802-812.
298. Eckes, B. and T. Krieg, *Regulation of connective tissue homeostasis in the skin by mechanical forces*. Clin Exp Rheumatol, 2004. **22**(3 Suppl 33): p. S73-6.
299. Aumailley, M. and B. Gayraud, *Structure and biological activity of the extracellular matrix*. J Mol Med (Berl), 1998. **76**(3-4): p. 253-65.
300. Krieg, T. and M. Aumailley, *The extracellular matrix of the dermis: flexible structures with dynamic functions*. Exp Dermatol, 2011. **20**(8): p. 689-95.
301. Behrens, D.T., et al., *The epidermal basement membrane is a composite of separate laminin- or collagen IV-containing networks connected by aggregated perlecan, but not by nidogens*. The Journal of biological chemistry, 2012. **287**(22): p. 18700-18709.
302. Mokkalapati, S., et al., *Basement membranes in skin are differently affected by lack of nidogen 1 and 2*. J Invest Dermatol, 2008. **128**(9): p. 2259-67.
303. Breitreutz, D., et al., *Skin basement membrane: the foundation of epidermal integrity--BM functions and diverse roles of bridging molecules nidogen and perlecan*. Biomed Res Int, 2013. **2013**: p. 179784.
304. Marinkovich, M.P., et al., *Cellular origin of the dermal-epidermal basement membrane*. Dev Dyn, 1993. **197**(4): p. 255-67.
305. Sugawara, K., et al., *Spatial and temporal control of laminin-332 (5) and -511 (10) expression during induction of anagen hair growth*. The journal of histochemistry and cytochemistry : official journal of the Histochemistry Society, 2007. **55**(1): p. 43-55.

306. Tateishi, C., et al., *Spatial and temporal control of laminin-511 and -332 expressions during catagen*. J Dermatol Sci, 2010. **58**(1): p. 55-63.
307. Nishiuchi, R., et al., *Characterization of the ligand-binding specificities of integrin alpha3beta1 and alpha6beta1 using a panel of purified laminin isoforms containing distinct alpha chains*. J Biochem, 2003. **134**(4): p. 497-504.
308. Wickström, S.A., K. Radovanac, and R. Fässler, *Genetic analyses of integrin signaling*. Cold Spring Harbor perspectives in biology, 2011. **3**(2): p. a005116.
309. Makrantonaki, E. and C.C. Zouboulis, *Molecular mechanisms of skin aging: state of the art*. Ann N Y Acad Sci, 2007. **1119**: p. 40-50.
310. Makrantonaki, E. and C.C. Zouboulis, *William J. Cunliffe Scientific Awards. Characteristics and pathomechanisms of endogenously aged skin*. Dermatology, 2007. **214**(4): p. 352-60.
311. Lock-Andersen, J., et al., *Epidermal thickness, skin pigmentation and constitutive photosensitivity*. Photodermatol Photoimmunol Photomed, 1997. **13**(4): p. 153-8.
312. Moragas, A., C. Castells, and M. Sans, *Mathematical morphologic analysis of aging-related epidermal changes*. Anal Quant Cytol Histol, 1993. **15**(2): p. 75-82.
313. Brégégère, F., et al., *Cellular senescence in human keratinocytes: unchanged proteolytic capacity and increased protein load*. Exp Gerontol, 2003. **38**(6): p. 619-29.
314. Lavker, R.M., *Structural alterations in exposed and unexposed aged skin*. J Invest Dermatol, 1979. **73**(1): p. 59-66.
315. Gilchrest, B.A., F.B. Blog, and G. Szabo, *Effects of aging and chronic sun exposure on melanocytes in human skin*. J Invest Dermatol, 1979. **73**(2): p. 141-3.
316. Ortonne, J.P., *Pigmentary changes of the ageing skin*. Br J Dermatol, 1990. **122 Suppl 35**: p. 21-8.
317. Uitto, J., *Connective tissue biochemistry of the aging dermis. Age-related alterations in collagen and elastin*. Dermatol Clin, 1986. **4**(3): p. 433-46.
318. Kligman, L.H., *Photoaging. Manifestations, prevention, and treatment*. Clin Geriatr Med, 1989. **5**(1): p. 235-51.
319. Watson, R.E., et al., *A short-term screening protocol, using fibrillin-1 as a reporter molecule, for photoaging repair agents*. J Invest Dermatol, 2001. **116**(5): p. 672-8.
320. Bernstein, E.F., et al., *Long-term sun exposure alters the collagen of the papillary dermis. Comparison of sun-protected and photoaged skin by northern analysis, immunohistochemical staining, and confocal laser scanning microscopy*. J Am Acad Dermatol, 1996. **34**(2 Pt 1): p. 209-18.
321. Brenneisen, P., et al., *Ultraviolet B wavelength dependence for the regulation of two major matrix-metalloproteinases and their inhibitor TIMP-1 in human dermal fibroblasts*. Photochem Photobiol, 1996. **64**(5): p. 877-85.
322. Ashcroft, G.S., S.J. Mills, and J.J. Ashworth, *Ageing and wound healing*. Biogerontology, 2002. **3**(6): p. 337-45.
323. Wu, S., et al., *Optical features for chronological aging and photoaging skin by optical coherence tomography*. Lasers Med Sci, 2013. **28**(2): p. 445-50.
324. Boyer, B., et al., *Age-dependent variations of the biosyntheses of fibronectin and fibrous collagens in mouse skin*. Exp Gerontol, 1991. **26**(4): p. 375-83.
325. Yamashita, K., et al., *Klotho mice: a novel wound model of aged skin*. Plastic and reconstructive surgery. Global open, 2014. **2**(1): p. e101-e101.
326. Yanai, H., et al., *Is rate of skin wound healing associated with aging or longevity phenotype?* Biogerontology, 2011. **12**(6): p. 591-7.

327. Doles, J., et al., *Age-associated inflammation inhibits epidermal stem cell function*. *Genes Dev*, 2012. **26**(19): p. 2144-53.
328. Giangreco, A., et al., *Epidermal stem cells are retained in vivo throughout skin aging*. *Aging Cell*, 2008. **7**(2): p. 250-9.
329. Keyes, B.E., et al., *Nfatc1 orchestrates aging in hair follicle stem cells*. *Proc Natl Acad Sci U S A*, 2013. **110**(51): p. E4950-9.
330. Matsumura, H., et al., *Hair follicle aging is driven by transepidermal elimination of stem cells via COL17A1 proteolysis*. *Science*, 2016. **351**(6273): p. aad4395.
331. Solanas, G., et al., *Aged Stem Cells Reprogram Their Daily Rhythmic Functions to Adapt to Stress*. *Cell*, 2017. **170**(4): p. 678-692.e20.
332. Giangreco, A., et al., *Epidermal stem cells are retained in vivo throughout skin aging*. *Aging cell*, 2008. **7**(2): p. 250-259.
333. Castilho, R.M., et al., *mTOR mediates Wnt-induced epidermal stem cell exhaustion and aging*. *Cell stem cell*, 2009. **5**(3): p. 279-289.
334. Keyes, B.E., et al., *Nfatc1 orchestrates aging in hair follicle stem cells*. *Proceedings of the National Academy of Sciences*, 2013. **110**(51): p. E4950-E4959.
335. Chen, C.-C., et al., *Regenerative hair waves in aging mice and extra-follicular modulators follistatin, dkk1, and sfrp4*. *Journal of Investigative Dermatology*, 2014. **134**(8): p. 2086-2096.
336. Matsumura, H., et al., *Hair follicle aging is driven by transepidermal elimination of stem cells via COL17A1 proteolysis*. *Science*, 2016. **351**(6273).
337. Ge, Y., et al., *The aging skin microenvironment dictates stem cell behavior*. *Proceedings of the National Academy of Sciences*, 2020. **117**(10): p. 5339.
338. Keyes, B.E., et al., *Impaired Epidermal to Dendritic T Cell Signaling Slows Wound Repair in Aged Skin*. *Cell*, 2016. **167**(5): p. 1323-1338.e14.
339. Marsh, E., et al., *Positional stability and membrane occupancy define skin fibroblast homeostasis in vivo*. *Cell*, 2018. **175**(6): p. 1620-1633.
340. Mahmoudi, S., et al., *Heterogeneity in old fibroblasts is linked to variability in reprogramming and wound healing*. *Nature*, 2019. **574**(7779): p. 553-558.
341. Mao, J.R., et al., *Tenascin-X deficiency mimics Ehlers-Danlos syndrome in mice through alteration of collagen deposition*. *Nat Genet*, 2002. **30**(4): p. 421-5.
342. Ansorge, H.L., et al., *Type XIV Collagen Regulates Fibrillogenesis: PREMATURE COLLAGEN FIBRIL GROWTH AND TISSUE DYSFUNCTION IN NULL MICE*. *J Biol Chem*, 2009. **284**(13): p. 8427-38.
343. Chacon-Martinez, C.A., et al., *Hair follicle stem cell cultures reveal self-organizing plasticity of stem cells and their progeny*. *EMBO J*, 2017. **36**(2): p. 151-164.
344. Liang, Y., et al., *A cell-instructive hydrogel to regulate malignancy of 3D tumor spheroids with matrix rigidity*. *Biomaterials*, 2011. **32**(35): p. 9308-15.
345. Cho, S.H., et al., *Review Article: Recent advancements in optofluidic flow cytometer*. *Biomicrofluidics*, 2010. **4**(4): p. 43001.
346. Pawley, J.B., *Handbook of biological confocal microscopy*. 3rd ed. 2006, New York, NY: Springer. xxviii, 985 p.
347. Marinkovich, M.P., G.P. Lunstrum, and R.E. Burgeson, *The anchoring filament protein kalinin is synthesized and secreted as a high molecular weight precursor*. *J Biol Chem*, 1992. **267**(25): p. 17900-6.
348. Sorokin, L.M., et al., *Laminin alpha4 and integrin alpha6 are upregulated in regenerating dy/dy skeletal muscle: comparative expression of laminin and integrin*

- isoforms in muscles regenerating after crush injury*. Exp Cell Res, 2000. **256**(2): p. 500-14.
349. Schindelin, J., et al., *Fiji: an open-source platform for biological-image analysis*. Nat Methods, 2012. **9**(7): p. 676-82.
350. Hermanowicz, P., et al., *AtomicJ: an open source software for analysis of force curves*. Rev Sci Instrum, 2014. **85**(6): p. 063703.
351. Brown, J., M. Pirrung, and L.A. McCue, *FQC Dashboard: integrates FastQC results into a web-based, interactive, and extensible FASTQ quality control tool*. Bioinformatics, 2017. **33**(19): p. 3137-3139.
352. Dodt, M., et al., *FLEXBAR-Flexible Barcode and Adapter Processing for Next-Generation Sequencing Platforms*. Biology (Basel), 2012. **1**(3): p. 895-905.
353. Dobin, A., et al., *STAR: ultrafast universal RNA-seq aligner*. Bioinformatics, 2013. **29**(1): p. 15-21.
354. Liao, Y., G.K. Smyth, and W. Shi, *featureCounts: an efficient general purpose program for assigning sequence reads to genomic features*. Bioinformatics, 2014. **30**(7): p. 923-30.
355. Love, M.I., W. Huber, and S. Anders, *Moderated estimation of fold change and dispersion for RNA-seq data with DESeq2*. Genome Biol, 2014. **15**(12): p. 550.
356. Subramanian, A., et al., *Gene set enrichment analysis: a knowledge-based approach for interpreting genome-wide expression profiles*. Proc Natl Acad Sci U S A, 2005. **102**(43): p. 15545-50.
357. Heinz, S., et al., *Simple combinations of lineage-determining transcription factors prime cis-regulatory elements required for macrophage and B cell identities*. Mol Cell, 2010. **38**(4): p. 576-89.
358. Zhou, Y., et al., *Metascape provides a biologist-oriented resource for the analysis of systems-level datasets*. Nat Commun, 2019. **10**(1): p. 1523.
359. Ramirez, F., et al., *deepTools2: a next generation web server for deep-sequencing data analysis*. Nucleic Acids Res, 2016. **44**(W1): p. W160-5.
360. Robinson, J.T., et al., *Integrative genomics viewer*. Nat Biotechnol, 2011. **29**(1): p. 24-6.
361. Buenrostro, J.D., et al., *Transposition of native chromatin for fast and sensitive epigenomic profiling of open chromatin, DNA-binding proteins and nucleosome position*. Nat Methods, 2013. **10**(12): p. 1213-8.
362. Li, H., *Aligning sequence reads, clone sequences and assembly contigs with BWA-MEM*. arXiv preprint arXiv:1303.3997, 2013.
363. Allhoff, M., et al., *Differential peak calling of ChIP-seq signals with replicates with THOR*. Nucleic Acids Res, 2016. **44**(20): p. e153.
364. Yu, G., L.G. Wang, and Q.Y. He, *ChIPseeker: an R/Bioconductor package for ChIP peak annotation, comparison and visualization*. Bioinformatics, 2015. **31**(14): p. 2382-3.
365. Rappsilber, J., Y. Ishihama, and M. Mann, *Stop and go extraction tips for matrix-assisted laser desorption/ionization, nanoelectrospray, and LC/MS sample pretreatment in proteomics*. Anal Chem, 2003. **75**(3): p. 663-70.
366. Cox, J. and M. Mann, *MaxQuant enables high peptide identification rates, individualized p.p.b.-range mass accuracies and proteome-wide protein quantification*. Nat Biotechnol, 2008. **26**(12): p. 1367-72.
367. Ritchie, M.E., et al., *limma powers differential expression analyses for RNA-sequencing and microarray studies*. Nucleic Acids Res, 2015. **43**(7): p. e47.

368. Perez-Riverol, Y., et al., *The PRIDE database and related tools and resources in 2019: improving support for quantification data*. Nucleic Acids Res, 2019. **47**(D1): p. D442-D450.
369. Signer, R.A. and S.J. Morrison, *Mechanisms that regulate stem cell aging and life span*. Cell Stem Cell, 2013. **12**(2): p. 152-65.
370. Ghatak, S., *Characterization of the extracellular matrix niche and stem cell homeostasis during skin aging*. PhD thesis, 2015.
371. Sun, Y., N. Miao, and T. Sun, *Detect accessible chromatin using ATAC-sequencing, from principle to applications*. Hereditas, 2019. **156**(1): p. 29.
372. Adam, R.C., et al., *NFI transcription factors provide chromatin access to maintain stem cell identity while preventing unintended lineage fate choices*. Nature Cell Biology, 2020. **22**(6): p. 640-650.
373. Zhang, Y., et al., *Activation of beta-catenin signaling programs embryonic epidermis to hair follicle fate*. Development, 2008. **135**(12): p. 2161-72.
374. Huggins, I.J., et al., *The WNT target SP5 negatively regulates WNT transcriptional programs in human pluripotent stem cells*. Nature Communications, 2017. **8**(1): p. 1034.
375. Mayer, S.I., et al., *Epidermal-growth-factor-induced proliferation of astrocytes requires Egr transcription factors*. Journal of cell science, 2009. **122**(18): p. 3340-3350.
376. Tarcic, G., et al., *EGR1 and the ERK-ERF axis drive mammary cell migration in response to EGF*. The FASEB Journal, 2012. **26**(4): p. 1582-1592.
377. Gaut, L., et al., *EGR1 Regulates Transcription Downstream of Mechanical Signals during Tendon Formation and Healing*. PLOS ONE, 2016. **11**(11): p. e0166237.
378. Saha, P. and R.K. Mishra, *Heterochromatic hues of transcription-the diverse roles of noncoding transcripts from constitutive heterochromatin*. FEBS J, 2019. **286**(23): p. 4626-4641.
379. Brunet, A. and T.A. Rando, *Interaction between epigenetic and metabolism in aging stem cells*. Curr Opin Cell Biol, 2017. **45**: p. 1-7.
380. Lien, W.H., et al., *Genome-wide maps of histone modifications unwind in vivo chromatin states of the hair follicle lineage*. Cell Stem Cell, 2011. **9**(3): p. 219-32.
381. Rada-Iglesias, A., *Is H3K4me1 at enhancers correlative or causative?* Nature Genetics, 2018. **50**(1): p. 4-5.
382. Karwacz, K., et al., *Critical role of IRF1 and BATF in forming chromatin landscape during type 1 regulatory cell differentiation*. Nature immunology, 2017. **18**(4): p. 412-421.
383. Miraldi, E.R., et al., *Leveraging chromatin accessibility for transcriptional regulatory network inference in T Helper 17 Cells*. Genome research, 2019. **29**(3): p. 449-463.
384. Ramirez, R.N., et al., *Dynamic gene regulatory networks of human myeloid differentiation*. Cell systems, 2017. **4**(4): p. 416-429.
385. Kim, S., N.-K. Yu, and B.-K. Kaang, *CTCF as a multifunctional protein in genome regulation and gene expression*. Experimental & Molecular Medicine, 2015. **47**(6): p. e166-e166.
386. Folgueras, Alicia R., et al., *Architectural Niche Organization by LHX2 Is Linked to Hair Follicle Stem Cell Function*. Cell Stem Cell, 2013. **13**(3): p. 314-327.
387. Hwang, J., et al., *Dlx3 is a crucial regulator of hair follicle differentiation and cycling*. Development, 2008. **135**(18): p. 3149-59.

388. Rorke, E.A., et al., *Structural and biochemical changes underlying a keratoderma-like phenotype in mice lacking suprabasal AP1 transcription factor function*. *Cell Death & Disease*, 2015. **6**(2): p. e1647-e1647.
389. Barski, A., et al., *High-resolution profiling of histone methylations in the human genome*. *Cell*, 2007. **129**(4): p. 823-37.
390. Creyghton, M.P., et al., *Histone H3K27ac separates active from poised enhancers and predicts developmental state*. *Proceedings of the National Academy of Sciences*, 2010. **107**(50): p. 21931.
391. Morris, R.J., et al., *Capturing and profiling adult hair follicle stem cells*. *Nat Biotechnol*, 2004. **22**(4): p. 411-7.
392. Sur, I., et al., *Epidermal and craniofacial defects in mice overexpressing Klf5 in the basal layer of the epidermis*. *Journal of Cell Science*, 2006. **119**(17): p. 3593.
393. Romano, R.-A., et al., *Abnormal hair follicle development and altered cell fate of follicular keratinocytes in transgenic mice expressing $\Delta Np63\alpha$* . *Development*, 2010. **137**(9): p. 1431.
394. Ito, M., et al., *Hair follicle stem cells in the lower bulge form the secondary germ, a biochemically distinct but functionally equivalent progenitor cell population, at the termination of catagen*. *Differentiation*, 2004. **72**(9-10): p. 548-57.
395. Segura-Valdez, M.L., et al., *Visualization of internal in situ cell structure by atomic force microscopy*. *Histochemistry and Cell Biology*, 2018. **150**(5): p. 521-527.
396. Liang, Y., et al., *A cell-instructive hydrogel to regulate malignancy of 3D tumor spheroids with matrix rigidity*. *Biomaterials*, 2011. **32**(35): p. 9308-9315.
397. Sarbacher, C.A. and J.T. Halper, *Connective Tissue and Age-Related Diseases*. *Subcell Biochem*, 2019. **91**: p. 281-310.
398. Lethias, C., et al., *A model of tenascin-X integration within the collagenous network*. *FEBS Letters*, 2006. **580**(26): p. 6281-6285.
399. Murrell, M., et al., *Forcing cells into shape: the mechanics of actomyosin contractility*. *Nat Rev Mol Cell Biol*, 2015. **16**(8): p. 486-98.
400. Le, H.Q., et al., *Mechanical regulation of transcription controls Polycomb-mediated gene silencing during lineage commitment*. *Nat Cell Biol*, 2016. **18**(8): p. 864-75.
401. Riising, E.M., et al., *Gene silencing triggers polycomb repressive complex 2 recruitment to CpG islands genome wide*. *Mol Cell*, 2014. **55**(3): p. 347-60.
402. Liu, X., et al., *Cryo-EM structure of a mammalian RNA polymerase II elongation complex inhibited by alpha-amanitin*. *J Biol Chem*, 2018. **293**(19): p. 7189-7194.
403. Bushnell, D.A., P. Cramer, and R.D. Kornberg, *Structural basis of transcription: α -Amanitin-RNA polymerase II cocystal at 2.8 Å resolution*. *Proceedings of the National Academy of Sciences*, 2002. **99**(3): p. 1218.
404. Ge, Y., et al., *The aging skin microenvironment dictates stem cell behavior*. *Proc Natl Acad Sci U S A*, 2020. **117**(10): p. 5339-5350.
405. McCay, C.M., et al., *Retarded growth, life span, ultimate body size and age changes in the albino rat after feeding diets restricted in calories: four figures*. *The Journal of Nutrition*, 1939. **18**(1): p. 1-13.
406. Gems, D. and L. Partridge, *Genetics of longevity in model organisms: debates and paradigm shifts*. *Annual review of physiology*, 2013. **75**: p. 621-644.
407. Kenyon, C.J., *The genetics of ageing*. *Nature*, 2010. **464**(7288): p. 504-512.
408. Harrison, D.E., et al., *Rapamycin fed late in life extends lifespan in genetically heterogeneous mice*. *nature*, 2009. **460**(7253): p. 392-395.

409. Roberts, M.N., et al., *A ketogenic diet extends longevity and healthspan in adult mice*. Cell metabolism, 2017. **26**(3): p. 539-546.
410. Newman, J.C., et al., *Ketogenic diet reduces midlife mortality and improves memory in aging mice*. Cell metabolism, 2017. **26**(3): p. 547-557.
411. Cheng, C.-W., et al., *Fasting-mimicking diet promotes Ngn3-driven β -cell regeneration to reverse diabetes*. Cell, 2017. **168**(5): p. 775-788.
412. Moskowitz, D.M., et al., *Epigenomics of human CD8 T cell differentiation and aging*. Science Immunology, 2017. **2**(8): p. eaag0192.
413. Ucar, D., et al., *The chromatin accessibility signature of human immune aging stems from CD8+ T cells*. Journal of Experimental Medicine, 2017. **214**(10): p. 3123-3144.
414. Shan, X., et al., *Age Alters Chromatin Structure and Expression of SUMO Proteins under Stress Conditions in Human Adipose-Derived Stem Cells*. Sci Rep, 2018. **8**(1): p. 11502.
415. Eckersley-Maslin, M.A., et al., *Epigenetic priming by Dppa2 and 4 in pluripotency facilitates multi-lineage commitment*. Nature Structural & Molecular Biology, 2020. **27**(8): p. 696-705.
416. Meissner, A., et al., *Reduced representation bisulfite sequencing for comparative high-resolution DNA methylation analysis*. Nucleic acids research, 2005. **33**(18): p. 5868-5877.
417. Rera, M., et al., *Modulation of longevity and tissue homeostasis by the Drosophila PGC-1 homolog*. Cell Metab, 2011. **14**(5): p. 623-34.
418. Sousa-Victor, P., et al., *Geriatric muscle stem cells switch reversible quiescence into senescence*. Nature, 2014. **506**(7488): p. 316-21.
419. Molofsky, A.V., et al., *Increasing p16INK4a expression decreases forebrain progenitors and neurogenesis during ageing*. Nature, 2006. **443**(7110): p. 448-52.
420. Boyle, M., et al., *Decline in self-renewal factors contributes to aging of the stem cell niche in the Drosophila testis*. Cell Stem Cell, 2007. **1**(4): p. 470-8.
421. Liu, L., et al., *Chromatin modifications as determinants of muscle stem cell quiescence and chronological aging*. Cell reports, 2013. **4**(1): p. 189-204.
422. Sun, D., et al., *Epigenomic profiling of young and aged HSCs reveals concerted changes during aging that reinforce self-renewal*. Cell stem cell, 2014. **14**(5): p. 673-688.
423. Gerardo, H., et al., *Soft culture substrates favor stem-like cellular phenotype and facilitate reprogramming of human mesenchymal stem/stromal cells (hMSCs) through mechanotransduction*. Scientific Reports, 2019. **9**(1): p. 9086.
424. Domingues, C., et al., *Cofilin-1 Is a Mechanosensitive Regulator of Transcription*. Frontiers in Cell and Developmental Biology, 2020. **8**(678).
425. Yang, N., et al., *Cofilin phosphorylation by LIM-kinase 1 and its role in Rac-mediated actin reorganization*. Nature, 1998. **393**(6687): p. 809-812.
426. Dopie, J., et al., *Active maintenance of nuclear actin by importin 9 supports transcription*. Proceedings of the National Academy of Sciences, 2012. **109**(9): p. E544-E552.
427. Obrdlik, A. and P. Percipalle, *The F-actin severing protein cofilin-1 is required for RNA polymerase II transcription elongation*. Nucleus, 2011. **2**(1): p. 72-79.

Abbreviations

7-AAD	7-aminoactinomycin D
ACN	acetonitrile
ACTB	beta actin
ADP	adenosine diphosphate
AFM	Atomic force microscope
aHFSCs	aged HFSCs
AMP	adenosine monophosphate
AMPK	AMP-activated kinase
ATAC-seq	genome-wide transposase-accessible chromatin sequencing
B2M	Beta-2-Microglobulin
BM	basement membrane
BMPs	Bone Morphogenetic Proteins
bp	base-pairs
ChIP	chromatin immunoprecipitation
Chr	chromosome
CTD	carboxyl-terminal domain
DMSO	dimethyl sulfoxide
DNA	Deoxyribonucleic acid
DP	dermal papilla
E	embryonic day
ECM	extracellular matrix
EdU	5-ethynyl-2'-deoxyuridine
EGF	epidermal growth factor
EU	5-ethynyl uridine
FA	formic acid
FACS	fluorescence-activated cell sorting
FCS	fetal calf serum
FN	fibronectin
GAPDH	Glyceraldehyde 3-phosphate dehydrogenase
GO	Gene ontology
GSC	germline stem cell
H&E	Hematoxylin and Eosin

H3K4me1	mono-methylation of lysine 4 on histone 3
H3K4me3	trimethylation of lysine 4 on histone 3
H3K27ac	acetylation of lysine 27 on histone 3
H3K27me3	trimethylation of lysine 27 on histone 3
H3K9me3	trimethylation of lysine 9 on histone 3
HF	hair follicle
HFSCs	hair follicle stem cells
HG	hair germ
HSCs	Hematopoietic SCs
IF	immunofluorescence
IFE	interfollicular epidermis
IGF-1	Insulin-like growth factor
IRS	inner root sheath
K	keratins
KGM	Keratinocyte Growth Medium
LCSM	Laser confocal scanning microscopy
LEF	lymphoid enhancer-binding factor
Lgr5	Leucine-rich repeat-containing G protein-coupled receptor 5
LN	laminin
MMPs	matrix metalloproteases
MSCs	mesenchymal stem cells
mtDNA	mitochondrial DNA
mTOR	mechanistic Target Of Rapamycin
NAD ⁺	nicotinamide adenine dinucleotide
NGS	Next-generation sequencing
NSCs	Neural stem cells
ORS	outer root sheath
P	postnatal day
PBS	phosphate-buffered saline
pMLC2	phosphorylated myosin light chain 2
q-PCR	Quantitative real-time polymerase chain reaction
RNAPII	RNA polymerase II
RNAPII-S2p	RNA polymerase II – serine 2 phosphorylation

ROCK	Rho-associated protein kinase
ROS	reactive oxygen species
RONS	reactive oxygen and nitrogen species
Rpm	rounds per minute
RRBS-Seq	Reduced-representation bisulfite sequencing
RT	room temperature
SASP	senescence-associated secretory phenotype
SC	stem cell
seq	sequencing
SG	sebaceous gland
siRNA	small interfering RNA
Sox 9	(sex determining region Y)-box 9
SSCs	spermatogonial stem cells
TACs	transit-amplifying cells
TADs	topologically associating domains
TF	transcription factor
TGF- β	transforming growth factor β
TSS	transcription start site
Wnt	wingless-type MMTV integration site family member
yHFSCs	young HFSCs

Acknowledgements

Undertaking this Ph.D. has been a truly life-changing experience for me, and it would not have been possible to do without the support and guidance that I received from many people.

Firstly, I would like to thank Dr. Sara Wickström for the continuous support of my Ph.D. study, for her patience, motivation, and immense knowledge. Her guidance helped me in all the time of research and writing of this thesis. Thank you for all the fruitful and inspiring discussions and for being so patient with me.

Besides my advisor, I would like to thank the rest of my thesis committee: Prof. Mirka Uhlirova, Prof. Ulrich Baumann, and Dr. Matthias Rübsam.

I would also like to say a huge thank you to Prof. Carien Niessen for “adopting” me and allowing me to finish my thesis in her lab, for the great support, and awesome garden parties.

My sincere thanks also go to Nadine Hachenberg and Anu Luoto for expert technical assistance, Marko Loparic, and David Schneider for initial AFM measurements, Lydia Sorokin for laminin antibodies, the FACS & Imaging Facility of MPI for Biology of Ageing, Imaging Facility of CECAD Cologne, and the Biomedicum Helsinki Imaging Unit for imaging support, and Cologne Center for Genomics for sequencing.

I want to thank Tessarz lab, Denzel lab, Iden lab, Hoeijmakers lab, Bazzi lab, Rada-Iglesias lab, Larsson Department, MPI-AGE, and CECAD core facilities for sharing techniques, reagents, equipment as well as for their tremendous support during my Ph.D.

I want to express my gratitude to all former and current Wickström and Niessen lab members for being great colleagues and for such an excellent atmosphere in both labs. Sushmita Ghatak for setting up this project at the beginning. Huy Le Quang for giving me a very warm welcome to the lab. Carlos Andrés Chacón-Martínez for being a great friend. Christine Kim for always having a bottle of wine ready. Kate Miroshnikova for

that crazy positive attitude. Emmi Wachsmuth for being an awesome bench mate. Matthias Rübsam for great discussions about science and cars. Thank you and all others for sharing good and bad moments during such a long and challenging journey and your great support inside and outside the lab.

Finally, I would like to express my deepest gratitude to my parents, my brother, and Armaghan for always being there whenever I need them.

Publication

Chacón-Martínez CA*, **Koester J***, Wickström SA. “Signaling in the stem cell niche: regulating cell fate, function and plasticity” Review, Development 2018

Erklärung

Ich versichere, dass ich die von mir vorgelegte Dissertation selbständig angefertigt, die benutzten Quellen und Hilfsmittel vollständig angegeben und die Stellen der Arbeit – einschließlich Tabellen, Karten und Abbildungen –, die anderen Werken im Wortlaut oder dem Sinn nach entnommen sind, in jedem Einzelfall als Entlehnung kenntlich gemacht habe; dass diese Dissertation noch keiner anderen Fakultät oder Universität zur Prüfung vorgelegen hat; dass sie – abgesehen von unten angegebenen Teilpublikationen – noch nicht veröffentlicht worden ist sowie, dass ich eine solche Veröffentlichung vor Abschluss des Promotionsverfahrens nicht vornehmen werde. Die Bestimmungen der Promotionsordnung sind mir bekannt. Die von mir vorgelegte Dissertation ist von Frau Dr. Sara A. Wickström betreut worden.

Köln, 20. September 2020



Janis Koester

Lebenslauf

Persönliche Angaben

Name: Janis Koester
Geburtsort/ Geburtstag: Leverkusen, den 14. Dezember 1986
Nationalität: deutsch

Akademische Ausbildung und Studium

- 08/2015 bis heute **Doktorarbeit**
Max Planck Institut für Biologie des Alterns unter der
Anleitung von Dr. Sara A. Wickström
Thema: „Mechanisms of aging-mediated loss of stem cell
potency through changes in niche architecture and
chromatin accessibility“
- 04/2013 – 07/2015 **Studium der Technischen Biologie (Master of
Science), Universität Stuttgart**
Gesamtnote: “sehr gut” (1,3)
Schwerpunkte: Molekulare Zellbiologie, Immunologie,
Tissue Engineering

Master-Thesis am Department of Microbiology and
Immunology, University of California San Francisco, USA:
Immature B-cell Selection in Lupus
- 10/2009 – 03/2013 **Studium der Technischen Biologie (Bachelor of
Science), Universität Stuttgart**
Gesamtnote: “gut” (2,4)

Bachelor-Thesis am Department of Pathology and
Laboratory Medicine Emory University School of Medicine,
Atlanta, USA: Characterization of the FPR1 receptor in
human intestinal epithelial cells (SK CO-15)
- 08/1997 – 04/2006 Nicolaus-Cusanus-Gymnasium, Bergisch Gladbach
Abitur

Berufliche Erfahrungen

- 04/2014 – 10/2014 **Praktikum bei Boehringer Ingelheim**
im Bereich BioPharmaceuticals – Zelllinienentwicklung
- 08/2013 – 03/2014 **wissenschaftliche Hilfskraft** am Institut für Zellbiologie
und Immunologie
Analysierung der Resistenzmechanismen von
dreidimensionalen Tumorzellkulturen
- 02/2012 – 06/2012 **wissenschaftliche Hilfskraft** am Institut für Zellbiologie
und Immunologie
Charakterisierung der Tumortoxizität von Varianten des
Death Receptor Liganden TRAIL
- 05/2011 – 01/2012 **wissenschaftliche Hilfskraft** am Institut für
Systemtheorie und Regelungstechnik
Erforschung und Modellierung der Interaktion von
Caspase 3 und XIAP beim Auslösen von Apoptose
- 07/2009 – 09/2009 Vermessungstechniker bei der Stadt Bergisch Gladbach
- 08/2006 – 06/2009 Ausbildung zum Vermessungstechniker bei der Stadt
Bergisch Gladbach

Präsentationen und Publikationen

Koester J, Ghatak S., Morgner J, Chacón-Martínez CA, Schneider D, Brinckmann J, Bloch W, Koch M, Rada-Iglesias A, Wickström SA. *Poster Presentation at "The stem cell niche conference", Copenhagen, 2018.* "Ageing leads to alterations in chromatin accessibility and depletion of quiescent stem cells in the skin"

Chacón-Martínez CA*, **Koester J***, Wickström SA. "Signaling in the stem cell niche: regulating cell fate, function and plasticity" Review, Development 2018